INFLUENCE OF BEDROCK TYPE AND DEPTH

ON ROAD DEFLECTIONS

by

Jeffrey G. Paine, Principal Investigator
Bureau of Economic Geology
The University of Texas at Austin
University Station, Box X
Austin, Texas 78713-8924
painej@begv.beg.utexas.edu

Interim Report, Project 7-2990

Michael Murphy, Project Director
Texas Department of Transportation
Design Division, Pavements Section

February 1999

CONTENTS

Figures

v

Tables

Plate

SUMMARY

Geologic maps provide much information about the distribution of rock types at and near the land surface. Deflections of Texas highways measured with the Falling-Weight Deflectometer (FWD) appear to be correlated to bedrock type, particularly at the most distant FWD sensors. To examine this apparent bedrock influence, we compared FWD data with mapped geologic units from six roadway segments in four physiographic regions of Texas. This analysis revealed differences in FWD responses among regions that are likely to be related to systematic differences in either bedrock depths or physical properties of geologic units that range from Precambrian to Holocene in age and include many different sedimentary, igneous, and metamorphic rocks. At the W7 detector (6-ft [1.8-m] offset), average normalized deflections are highest for areas where roads are underlain by siliciclastic sedimentary rocks (sandstones, mudstones, and shales) and unconsolidated alluvial sediments. Lowest normalized W7 deflections are measured in areas underlain by Precambrian igneous and metamorphic rocks that include granites, schists, and gneisses and in areas underlain by chemically precipitated sedimentary rocks such as limestone.

Better rock-type discrimination is obtained from ratios calculated from deflections measured at the W2 (1-ft [0.3-m] offset) and W7 detectors than from W7 deflections alone. W2:W7 ratios vary regionally, but observed ratios are highest for rigid rock types such as granites, gneisses, and schists (ratios of 17 to 40), are intermediate for limestones (10 to 27), and are relatively low for sandstones, mudstones, and unconsolidated sediments (6 to 14). These results suggest that (1) existing geologic maps can be used to estimate outermost FWD sensor response for highway segments, and (2) rock type might be predicted from FWD data, allowing the FWD to be used in such applications as geologic mapping and sinkhole detection.

From FWD data alone, it is difficult to determine whether the relationship between rock type and road deflections is caused by differences in rock properties or bedrock depth. To resolve

this ambiguity, we employed the FWD and a modified soil-probe hammer as impulsive sources for seismic-refraction experiments at two test sites in north and central Texas. These tests showed that (1) the FWD can be used as a seismic source for refraction data, but the detectors need to extend farther from the source, and (2) refraction data sufficient to calculate bedrock depths can be acquired with sources and detectors either on road shoulders or directly on pavement. The success of these refraction experiments suggests that combined FWD–refraction systems could be used along roads to aid deflection analysis by estimating bedrock depth and assist in rock-type identification by measuring compressional velocities for bedrock and overburden.

INTRODUCTION

The purposes of this study, conducted by the Bureau of Economic Geology (BEG) on behalf of the Texas Department of Transportation (TxDOT), are to examine whether (1) existing geologic information can be used to help interpret roadway-deflection data collected with TxDOT's Falling Weight Deflectometers (FWD's), and (2) seismic-refraction data, perhaps collected in conjunction with FWD data, can be used along with geologic information to estimate bedrock depths and consequently improve FWD analyses. This interim report summarizes results from the first 2 years of a 3-year project, in which we examined the relationship between bedrock type and FWD response and assessed the feasibility of collecting seismic-refraction data on and adjacent to roads. A final report at the end of the third year will address the implementation of seismic-refraction methods in FWD analysis.

Trailer-mounted FWD's consist of a falling weight and a series of seven calibrated detectors at distances of 0, 1, 2, 3, 4, 5, and 6 ft (0, 0.3, 0.6, 0.9, 1.2, 1.5, and 1.8 m) from the falling weight. The height of the weight drop can be selected to produce seismic impulses of varying strength. The vertical detectors, in contact with the pavement as the weight falls, measure pavement deflection following weight impact. The most commonly used FWD data are the maximum deflections at each detector, normalized for drop load. In general, deflections measured close to the source are most affected by pavement condition, and deflections measured at the longest offsets are more affected by deeper layers such as fill, soil, and bedrock (M. Murphy, personal communication, 1997). Physical properties of roadway layers that can be calculated from FWD data also depend on depth to bedrock (depth to "rigid" layer), which is generally not known. Rather than drilling boreholes to measure bedrock depth directly, we wish to determine the precision with which geological and geomorphological information can be used to estimate bedrock depth. We also want to examine whether existing geophysical methods, such as seismic refraction, can be adapted to rapidly and accurately estimate bedrock depths beneath roads.

1

There is an empirical relationship between rock type and FWD deflections, particularly at the longest offsets. Average W7 deflections (6-ft- [1.8-m-] source-to-detector distance) calculated by county (fig. 1) resemble a simplified geologic map of the state (fig. 2; plate 1). The largest W7 deflections are observed along the coast and in the Panhandle, where the geologic units are relatively young; the smallest W7 deflections are observed in central Texas, where old igneous and metamorphic rocks and younger limestones are mapped. Outcrop trends of individual geologic units match average W7 deflection trends visible over many counties, including (1) the increased average deflections in east Texas on the Miocene Fleming and Oakville Formations and the Pliocene Willis Formation; (2) low deflections on the Cretaceous Trinity, Fredericksburg, and Lower Washita Groups in Texas; and (3) increased deflections that follow the Cretaceous Austin, Eagle Ford, Woodbine, Upper Washita, Navarro, and Taylor Groups in northeast Texas (figs. 1 and 2). Our goals are to determine why this relationship exists, how well it translates to the local scale, and how it might be exploited to both aid road-deflection analyses and establish geologic uses of the FWD. We also want to determine whether there is sufficient justification to acquire refraction data along with FWD data.

Physiographic Regions and Bedrock Types

The relationship between far-offset FWD data and geologic units supports the subdivision of Texas into regions that have similar FWD response. Many earth scientists have recognized physiographic regions that reflect differences in elevation, topography, geologic structure, and bedrock types (fig. 3; table 1). These seven principal physiographic regions (Gulf Coastal Plains, Edwards Plateau, Central Texas Uplift, Grand Prairie, Basin and Range, North-Central Plains, and High Plains) provide a framework for grouping rock types that influence FWD response.

Bedrock types differ in each of the seven principal physiographic regions (figs. 2 and 3; table 1). On the Gulf Coastal Plains, unconsolidated and semiconsolidated sands, silts, and clays deposited along rivers and shorelines in the Cenozoic era (within the last 66 million years [Ma]) form relatively weak highway substrates. Relatively young bedrock is also found in the High

2
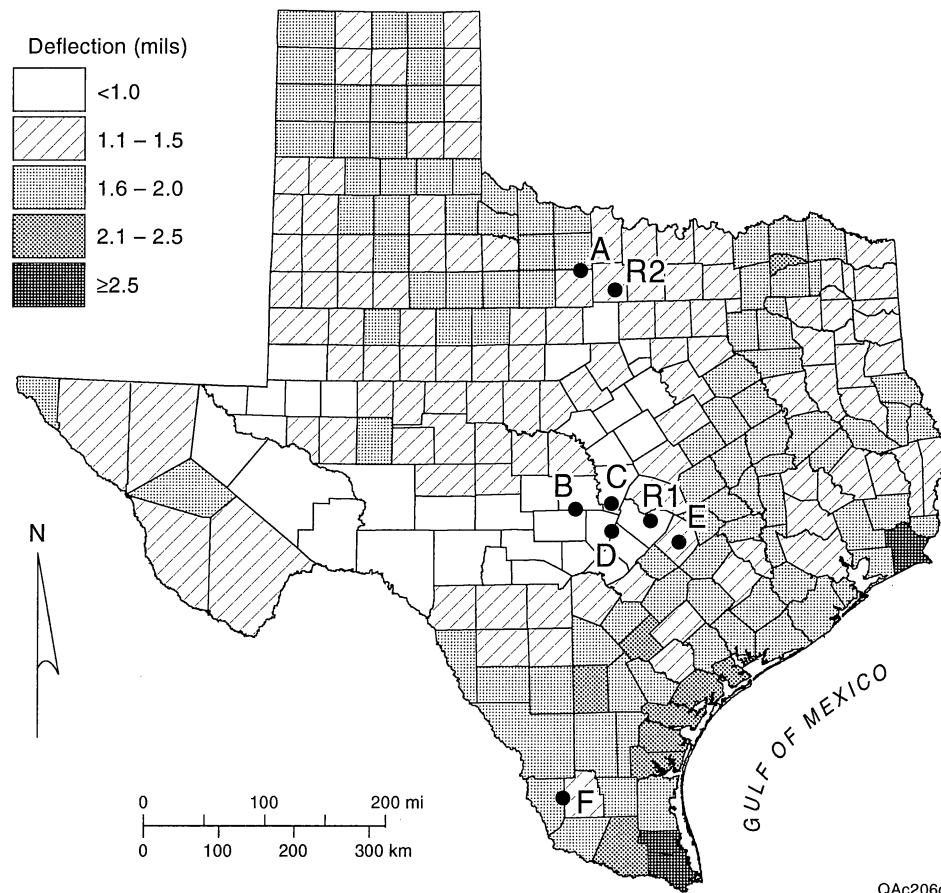
Figure 1. Average roadway deflection by county measured at Falling Weight Deflectometer detector W7. Also shown are locations of study areas A though F and refraction test sites R1 (Road D, Pickle Research Campus) and R2 (U.S. Highway 281 near Jacksboro).
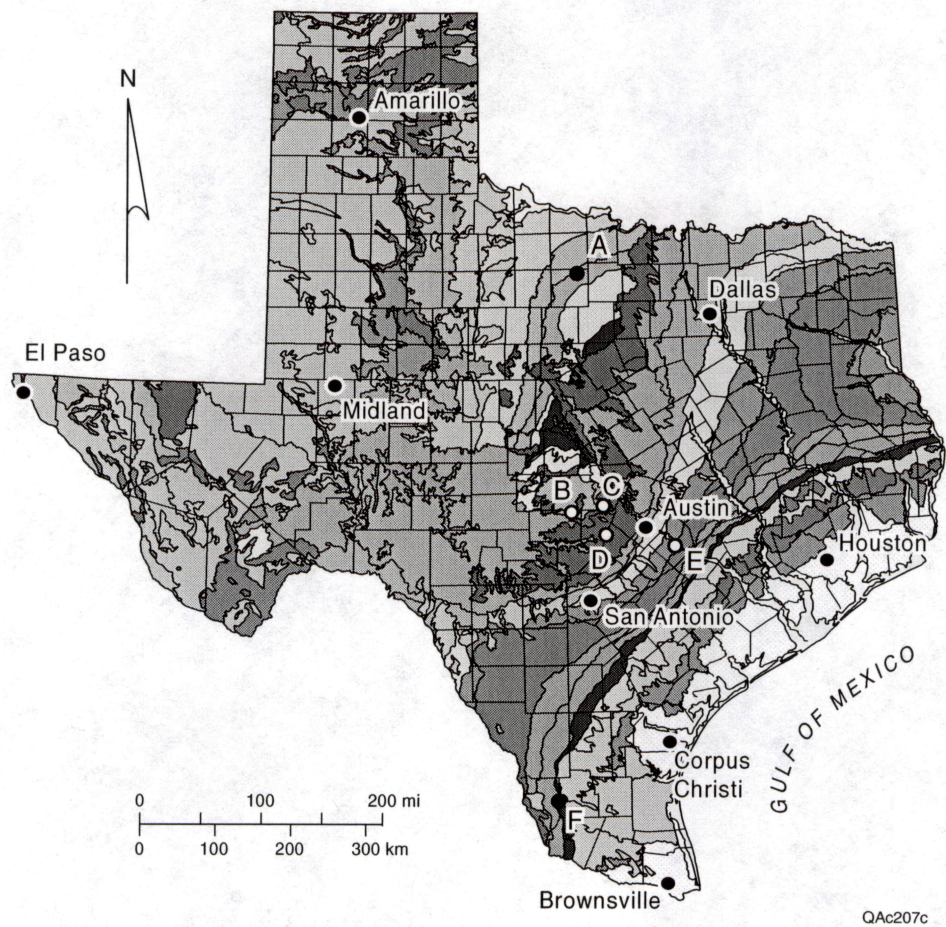
Figure 2. Geologic map of Texas. Refer to plate 1 for more detailed version with a key to geologic units. Adapted from Bureau of Economic Geology (1992).

4
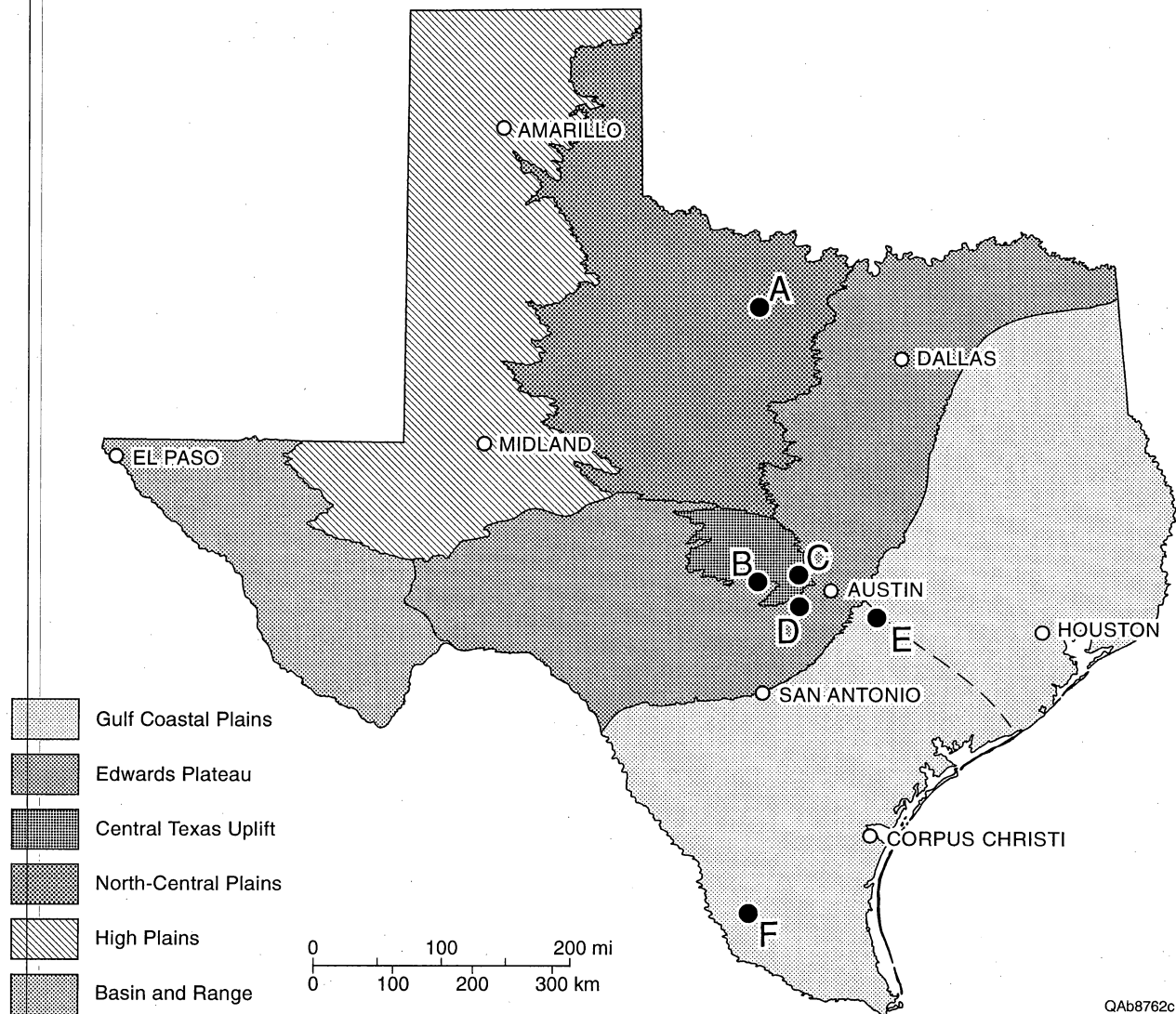
Figure 3. Physiographic regions of Texas. Adapted from Wermund (1996).

Table 1. Principal physiographic regions of Texas. Adapted from Wermund (1996).

Region	Elevation range (ft)	Topography	Geologic structure	Bedrock type
Gulf Coastal Plains	0–100	Nearly flat to low rolling terrain	Nearly flat strata	Unconsolidated deltaic sands and muds; chalks and marls
Grand Prairie	450–1,250	Plains to low stair-step hills	Eastward dip	Calcareous to sandy
Edwards Plateau	450–3,000	Flat upper surface with box canyons	Southward dip	Limestones and dolomites
Central Texas Uplift	800–2,000	Knobby plain	Outward dip; faulted	Igneous and metamorphic rocks
North-Central Plains	900–3,000	Low north-south ridges	Westward dip	Limestones, sandstones, shales
High Plains	2,200–4,750	Southeastward-sloping prairies	Gentle southeastward dip	Windblown silt and fine sand
Basin and Range	1,700–8,750	North-south mountains and basins	Complex folding and faulting	Igneous, metamorphic, and sedimentary rocks

Plains, where unconsolidated to moderately cemented eolian (windblown) and alluvial (river-borne) sand and silt formed the Blackwater Draw Formation during the Quaternary period (less than 2 Ma) and the Ogallala Formation during the Miocene to Pliocene periods (24 to 2 Ma). Limestone and dolomite deposited during the Cretaceous period (144 to 66 Ma) underlie the Edwards Plateau in central Texas, forming strong substrates that are resistant to erosion. Sandier, calcareous deposits of similar age underlie the Grand Prairie, the northern extension of the Edwards Plateau. Westward-dipping limestone, sandstone, and shale dating to the late Paleozoic Era (320 to 245 Ma) are found in the North-Central Plains. The oldest rocks in Texas are found in the Central Texas Uplift and the Basin and Range regions. In the Central Texas Uplift, mechanically strong, late Precambrian-era (2,000 to 1,200 Ma) igneous and metamorphic rocks and Paleozoic-era (570 to 245 Ma) sandstone, limestone, and shale crop out. In the Basin and Range, faulting formed a series of basins and ranges. The ranges, cored by strong igneous and metamorphic rocks, are separated by basins that have been filled by younger sedimentary deposits that are generally weaker than the range-forming rocks.

More detailed information on the distribution of geologic units is obtained from geologic maps produced at various scales. The most useful map series for a statewide study is the Geologic Atlas of Texas. This series consists of 38 maps that cover the entire state at a scale of 1:250,000 and have been compiled, published, and updated over the last several decades by BEG. Soil surveys, published by the Natural Resources Conservation Service of the U.S. Department of Agriculture, exist for most Texas counties. The information on soil distribution, grain size, soil depth, and surface slope contained in the maps and tables that make up these surveys, more detailed than that shown on geologic maps, may also be useful in the interpretation of FWD data. Soil maps, published at a scale of 1:20,000, show many more units and subdivisions than do most geologic maps, but are difficult to place in a statewide or regional context that would lend itself well to FWD analysis.

Investigative Approach

Our approach to understanding the relationship between FWD response and bedrock type and depth was to examine in detail several road segments in different physiographic regions. The six highway segments analyzed are located in the (1) North-Central Plains, (2) Central Texas Uplift, (3) Edwards Plateau, and (4) southern and interior Gulf Coastal Plains. In the first project year, we examined the relationship between existing TxDOT FWD data and mapped geologic units along the highway segments. In year 2, we collected seismic-refraction data along selected roadway segments to investigate the effectiveness of this proven method in directly determining bedrock depths to anticipated maximum depths of about 6 m.

METHODS

Methods employed in this study include those that were used to investigate the relationship between existing information on bedrock type and FWD response, and those that were used to augment FWD data with additional geophysical measurements.

Bedrock Type and FWD Response

To determine whether there is a quantifiable relationship between bedrock and FWD response beyond what is apparent from the similarity of the geologic map of Texas and the county average W7 deflection, we selected six highway segments in different parts of the state. For each highway segment, we (1) obtained FWD deflections and locations from TxDOT, (2) normalized FWD response to a common 9,000-lb (4,082-kg) load, (3) plotted FWD locations on U.S. Geological Survey 7.5-minute quadrangle maps (appendix A), (4) determined elevations for each FWD site, and (5) determined what geologic unit underlies the highway at each FWD site from 1:250,000-scale geologic maps published by BEG (appendix A). These data were entered into a data base that

includes highway name, reference marker, geologic unit, elevation, and normalized deflection for each FWD site.

We then analyzed the data base to understand better how bedrock influences FWD response. Plots of elevation, rock type, and deflection versus distance along the highway show how deflections relate to different geologic units beneath the highway and to changes in elevation and relief. When the deflection data are sorted by rock type, we can calculate the average deflection bowl for a given bedrock type, determine how the deflection bowls vary, and decide whether bedrock types have distinctive deflection bowls. If deflection bowls have different slopes, we can calculate deflection ratios for near- and far-offset detectors to further discriminate rock types.

Seismic Refraction

Seismic refraction is a well-established geophysical method (Telford and others, 1976; Milsom, 1989) to determine compressional-wave velocity structure at depths as shallow as tens of centimeters to as deep as several kilometers. In the shallow subsurface, seismic refraction is commonly used to measure depth to the water table or to bedrock (rigid layer beneath soil and weathered bedrock). Compressional-wave velocities increase downward in most geologic settings, where relatively dry soil (compressional-wave velocities ranging from 300 to 700 m/s) is underlain by saturated soil at the water table (compressional velocities of about 1,500 m/s) or by unweathered bedrock (compressional velocities commonly more than 2,000 m/s, depending on rock type). These typically abrupt, downward increases in wave velocity refract surface-generated seismic waves along the interface between the units. The refracted waves generate wavefronts that propagate back to the surface, where they are detected by motion sensors (geophones). The time delay between seismic-source impact and first seismic arrivals at known geophone distances allows us to calculate compressional velocities and thicknesses of near-surface layers, which in turn allows us to estimate a depth to the water table or to bedrock. In general, exploration depth increases with distance between the source and detector. For shallow investigations, the detector spread should extend from within a short distance of the source to four or more times the desired

9

maximum exploration depth. This allows one to measure enough arrivals of both the direct wave (traveling in the surface layer only) and the critically refracted wave (traveling along the water table or at the interface between the surface layer and bedrock) to calculate accurate compressional-wave velocities for these layers.

We recorded seismic-refraction data using 48 40-Hz geophones, a 48-channel seismograph, and 2 seismic sources (the FWD and a modified soil-probe hammer) at the J. J. Pickle Research Campus at The University of Texas at Austin (PRC) and on U.S. Highway 281 southbound at TxDOT's Mobile Load Simulator (MLS) site in north-central Texas (table 2). Spread length, geophone spacing, and seismic-source selection depend on target depths, ambient seismic noise, ground conditions, and desired lateral resolution. For typical highway settings, a sledge hammer, a modified soil-probe hammer, or the FWD itself can be suitable sources. We picked the first compressional-wave arrivals using the Seismic Processing Workshop software package. We calculated true seismic velocities, layer thicknesses, and apparent dip angles using the slope-intercept method (Palmer, 1986).

At the Pickle Research Campus site along Road D, geophones were mounted on 10-cm-long spikes that were driven into the south shoulder near the edge of the pavement. Geophones were spaced at 0.3-m intervals along an east–west recording spread for a total distance of 14.3 m (fig. 4; table 2). The FWD was operated on the pavement, offset north of the recording spread 1.1 to 1.2 m. The soil-probe hammer was operated on the edge of the pavement 0.4 m north of the recording spread, and on the shoulder inline with the recording spread. Seismic pulses from the FWD and the soil-probe hammer were recorded with the sources located at the center and at the east and west ends of the recording spread (fig. 4).

At the Jacksboro MLS site (fig. 1), the spikeless geophones were threaded onto steel plates that were laid on the pavement surface at 0.5-m intervals (fig. 5; table 2). The north–south recording spread, covering a distance of 23.5 m, was laid out on the inside, southbound lane of U.S. Highway 281 on the footprint of the MLS. FWD seismic pulses were recorded from source locations offset 0.9 m west of the recording spread; soil-probe hammer pulses were recorded from

Table 2. Acquisition parameters for seismic-refraction data collected on Road D at the Pickle Research Center in Austin, Texas, and on U. S. Highway 281 southbound at the Mobile Load Simulator site south of Jacksboro, Texas.

	Pickle Research Campus	Jacksboro MLS site
Date acquired	September 23, 1997	May 28, 1998
Seismic sources	FWD (on pavement) Soil-probe hammer (on pavement and shoulder)	FWD (on pavement) Soil-probe hammer (on pavement)
Source geometry	Center and ends of sensor spread	Center and ends of sensor spread
Sensors	Mark Products L-40A (on shoulder)	Mark Products L-40A (on pavement)
Number of sensors	48	48
Sensor spacing (m)	0.3	0.5
Recording spread (m)	14.3	23.5
Seismograph	Bison 9048	Bison 9048
Recording channels	48	48
Sample interval (s)	0.0001	0.0001
Record length (s)	0.2	0.2
Analog filters	4 Hz (low cut) 1,000 Hz (high cut)	4 Hz (low cut) 1,000 Hz (high cut)

Road D

Geophone 1

Geophone 48

N

| 0 | | | | | 20 ft |
| 0 | | | | 5 m | |

⊠ FWD source point

⊠ Soil-probe hammer source point

○ Geophone

QAc4612c
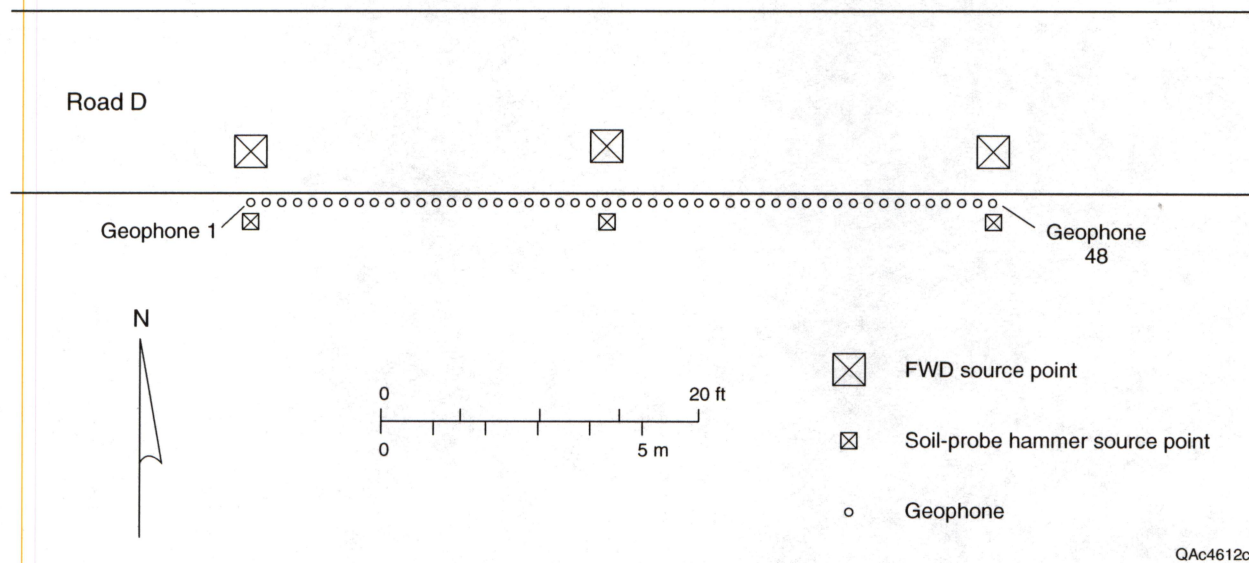
Figure 4. Map of the seismic-refraction test site along Road D at the J. J. Pickle Research Center (PRC), The University of Texas at Austin.

Geophone 48

U.S. Highway 281 South

N

Geophone 1

⊠ FWD source point

⊠ Soil-probe hammer source point

∘ Geophone

0   10 ft

0   5 m
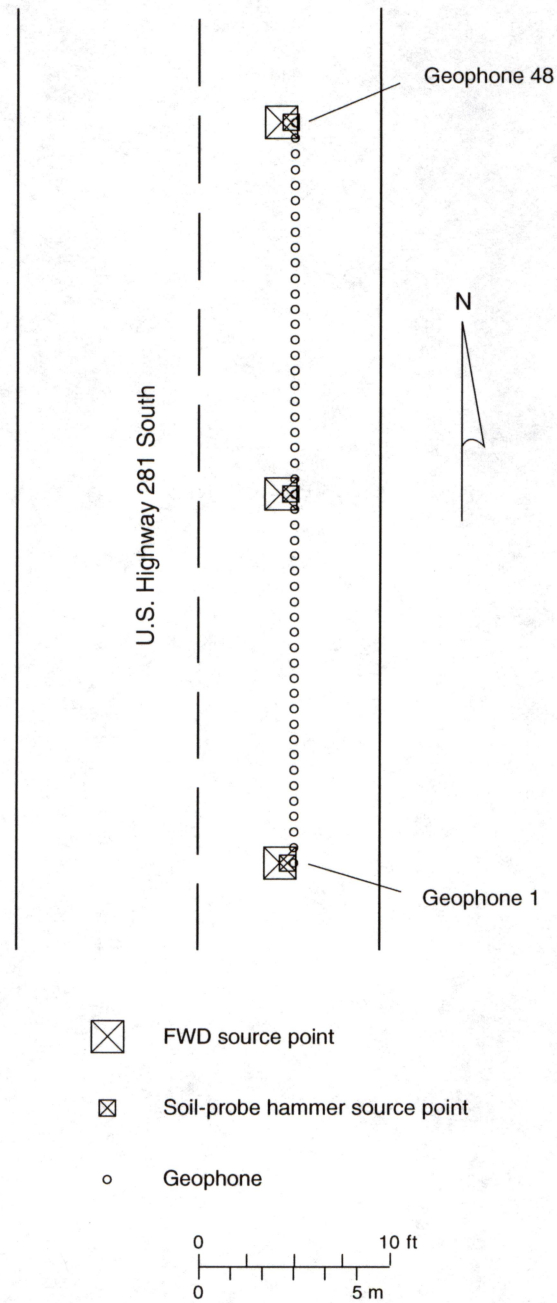
QAc4613c

Figure 5. Map of the seismic-refraction test site on southbound U.S. Highway 281 at the Texas Department of Transportation's Mobile Load Simulator site south of Jacksboro, Texas.

locations along the recording spread. For both sources, source points were at the center and north and south ends of the recording spread (fig. 5).

At both sites, a short seismograph sample interval of 0.0001 s (table 2) allowed precise first-arrival times to be picked. At a propagation velocity of 500 m/s, a seismic pulse travels 5 cm in 0.0001 s. A longer sample interval, such as 0.001 s, typical of many refraction surveys, translates to 0.5 m of wave propagation between samples. Sample intervals this long may cause unacceptable errors in arrival-time picks, which in turn cause erroneous layer depth calculations. Spatial aliasing of the recorded seismic pulse was prevented by having the detector spacing (0.3 to 0.5 m) be much shorter than the compressional-wave wavelengths of 5 to 30 m at a 100-Hz dominant frequency. Recording was initiated by an electronic switch mounted to the seismic source, which was activated when the source struck pavement or the ground. Seismic data were recorded for 0.2 s after source impact.

RELATIONSHIP BETWEEN BEDROCK TYPE AND FWD RESPONSE

Bedrock units are one of three major rock types: igneous (solidified from molten rock), sedimentary (particles deposited by wind, water, or gravity flow), and metamorphic (plastically deformed igneous or sedimentary rock). Physical properties for these major rock types, including density, wave-propagation velocities, and elastic parameters, have been shown in numerous field and laboratory experiments to vary widely (Press, 1966). For geologic maps to be useful in the interpretation of FWD data, FWD deflections should show some relationship to mapped rock type. From the similarity of county deflection averages to a simplified map of Texas, we infer that bedrock type and FWD response are related (figs. 1 and 2). Whether this relationship is caused by a similarity in bedrock depths for a given bedrock type or by a similarity in physical properties of a given bedrock type is unknown.

To determine whether existing maps of bedrock can help interpret FWD data at a local scale, we examined the relationship between bedrock type and FWD response along six highway segments in four physiographic regions (fig. 3). These regions include Precambrian rocks as old

14

as 2 billion years and Holocene sediments deposited at the present, as well as examples of sedimentary, igneous, and metamorphic rocks. Sedimentary bedrock types include (1) unconsolidated gravel, silt, sand, and clay along streams in each of the regions studied, (2) chemically precipitated limestones and dolomites in the Edwards Plateau, Central Texas Uplift, and North-Central Plains, and (3) lithified to semiconsolidated sandstone and shale in each region. Igneous bedrock types include granites that crop out in the Central Texas Uplift. Metamorphic rocks, including gneisses and schists, are also mapped in the Central Texas Uplift.

North-Central Plains Site

Compared to the rest of Texas, county average deflections in the North-Central Plains physiographic region are moderate, ranging from 1.1 to 2.0 mils (fig. 1). Lithified sedimentary bedrock types common in this region include Paleozoic limestone, sandstone, and shale (table 1). Land-surface elevation increases from 900 ft (274 m) in the southeast part of the region to 3,000 ft (914 m) in the northwest part. Unconsolidated sediments are common along the major rivers (Colorado, Brazos, Trinity, and Red Rivers) and numerous smaller streams that cross the region. FWD data and bedrock-type information were analyzed for one site in the North-Central Plains.

Site A: Texas 16, Archer and Young Counties

Site A extends along Texas 16 between reference markers 220 and 264 in Archer and Young Counties. Average W7 deflections are between 1.6 and 2.0 mils for Archer County and 1.1 and 1.5 mils for Young County (fig. 1). Geologic units mapped along this roadway segment include lithified Paleozoic sandstones, limestones, and mudstones and unconsolidated Quaternary stream deposits (fig. 6; appendix B).

FWD data for 87 locations along this highway segment (appendix C) show a wide range of deflections for each detector (fig. 6). W7 deflections average 0.99 mils (table 3), which is lower than the reported deflection average for Archer and Young Counties. The calculated average for

15
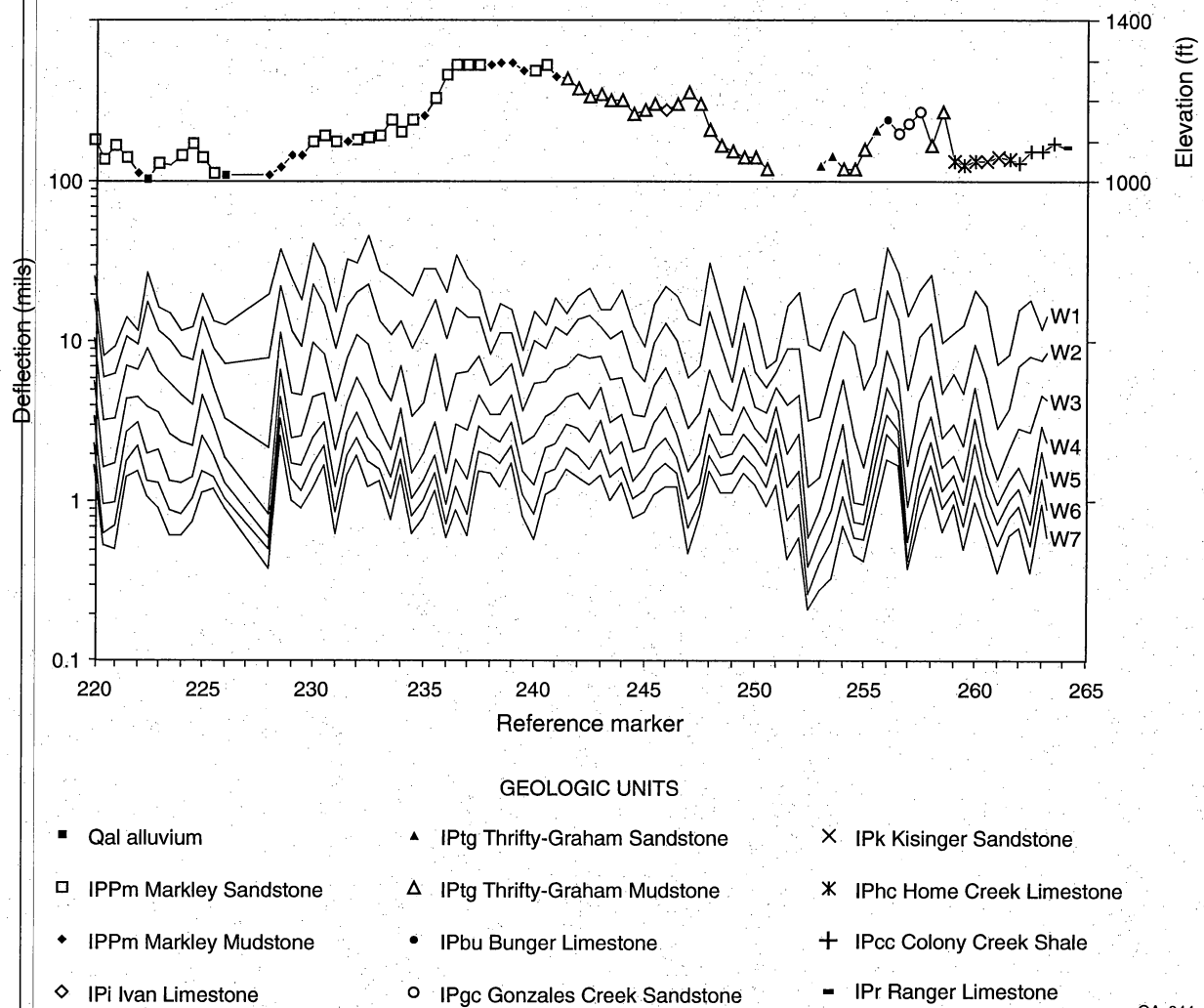
Figure 6. Geologic units, elevation, and W1 through W7 deflections along Texas 16 between reference markers 220 and 265, Archer and Young Counties, north Texas.

16

Table 3. Deflection statistics (normalized to 9,000-lb [4,082-kg] load) for sites A through F (fig. 1).

Site A: Texas 16, Archer and Young Counties, n=87.

Statistic	W1	W2	W3	W4	W5	W6	W7
Average	18.68	10.48	5.22	2.89	1.87	1.33	0.99
Standard Deviation	8.07	4.60	2.38	1.30	0.83	0.59	0.45
Maximum	46.12	22.96	11.43	6.57	4.45	3.29	2.56
Minimum	6.87	2.86	1.23	0.59	0.39	0.26	0.21

Site B: Texas 16, Llano and Gillespie Counties, n=69.

Statistic	W1	W2	W3	W4	W5	W6	W7
Average	34.72	15.19	5.31	2.73	1.71	1.23	0.93
Standard Deviation	13.73	6.52	2.34	1.20	0.73	0.53	0.41
Maximum	79.12	30.76	12.00	6.05	3.80	2.65	1.96
Minimum	4.67	2.11	0.85	0.77	0.48	0.32	0.23

Site C: Texas 71, Burnet County, n=30.

Statistic	W1	W2	W3	W4	W5	W6	W7
Average	16.09	7.08	2.94	1.61	1.03	0.76	0.57
Standard Deviation	6.20	3.56	1.68	1.02	0.68	0.51	0.41
Maximum	35.96	16.85	7.51	4.34	2.94	2.06	1.59
Minimum	7.56	2.47	1.03	0.48	0.30	0.18	0.09

Site D: U.S. 290, Blanco and Hays Counties, n=52.

Statistic	W1	W2	W3	W4	W5	W6	W7
Average	11.02	5.30	2.20	1.15	0.72	0.52	0.40
Standard Deviation	3.39	1.63	0.80	0.50	0.36	0.28	0.22
Maximum	20.19	9.47	4.27	2.55	1.67	1.26	1.04
Minimum	4.45	2.30	0.70	0.34	0.13	0.06	0.05

Site E: Texas 71, Bastrop County, n=34.

Statistic	W1	W2	W3	W4	W5	W6	W7
Average	21.25	12.07	6.37	3.77	2.51	1.88	1.49
Standard Deviation	6.71	5.29	3.37	2.07	1.32	0.95	0.74
Maximum	38.57	23.83	14.35	9.07	6.04	4.52	3.49
Minimum	13.49	5.11	2.20	0.78	0.46	0.40	0.32

Site F: Texas 16, Jim Hogg and Zapata Counties, n=89.

Statistic	W1	W2	W3	W4	W5	W6	W7
Average	34.28	15.24	5.90	3.32	2.32	1.77	1.41
Standard Deviation	16.90	6.77	2.47	1.37	0.94	0.71	0.54
Maximum	84.44	36.97	13.51	6.92	4.80	3.53	2.69
Minimum	6.66	4.00	1.58	1.00	0.79	0.61	0.46

Texas 16 is higher than average deflections calculated for sites in the Central Texas Uplift and Edwards Plateau regions and lower than calculated averages for the Gulf Coastal Plains sites (table 3), in agreement with the map of county-wide average deflections.

For many of the 11 geologic units mapped along this highway segment, FWD data show considerable overlap in observed deflection ranges (fig. 7). For example, W7 deflections over the Markley Mudstone range from 0.8 to more than 2.0 mils; Markley Sandstone deflections range from 0.5 to 2.0 mils (fig. 7b and c). Other rock units with more than a few measured deflections have similarly broad ranges.

Deflection averages calculated for the geologic units mapped at site A decrease from 10 to 40 mils at W1 to between 0.5 and 2 mils at W7 (figs. 7 and 8). Deflection series that have high near-offset deflections also tend to have high far-offset deflections. Geologic units over which relatively small average W7 deflections (<1.0 mil) were measured are the Thrifty-Graham and Kisinger Sandstones at 0.5 mils, the Ranger and Home Creek Limestones at 0.6 to 0.8 mils, and the Gonzales Creek Sandstone at 0.9 mils (fig. 9a). Relatively large average W7 deflections were measured over the Bunger Limestone (1.8 mils), the Markley Mudstone (1.3 mils), and the Ivan Limestone (1.2 mils).

Ratios calculated for average deflections at different detectors can help remove the covariance of near- and far-offset deflections and better reveal bedrock effects. We calculated the W2:W7 ratio (fig. 9b) because W2 should have the largest source- and pavement-related deflection component and W7 should have the largest bedrock-related deflection. Ratios calculated for the North-Central Plains geologic units range from 7.96 to 14.01, increasing for units that have large W2 deflections for a given W7 deflection. With all other factors equal, rigid geologic units should have higher W2:W7 ratios than less rigid ones. In this analysis, the Home Creek Limestone, Kisinger Sandstone, and Thrifty-Graham Mudstone have low ratios (less rigid); the Markley Sandstone, Ranger Limestone, and Thrifty-Graham Sandstone have relatively high ratios (more rigid). When compared to geologic units at other sites in other physiographic regions, these ratios are lower than

18

those calculated for the Central Texas Uplift and Edwards Plateau, but are higher than those in the Gulf Coastal Plains.

Central Texas Uplift Sites

The Central Texas Uplift, underlain by Precambrian igneous and metamorphic rocks, Paleozoic and Mesozoic sedimentary rocks, and unconsolidated Quaternary sediments (table 1), covers the smallest area of any physiographic region (fig. 3). County average deflections in this region of typically rigid bedrock types are the lowest in the state, ranging from less than 1 to 1.5 mils (fig. 1). Two study sites, B and C, are located in this region (fig. 3).

Site B: Texas 16, Llano and Gillespie Counties

This segment of Texas 16 begins at reference marker 450 south of Llano and extends about 38 mi (61 km) to reference marker 488 north of Fredericksburg. It is mostly underlain by Precambrian metamorphic (Packsaddle Schist and Valley Spring Gneiss) and igneous (Town Mountain Granite) rocks and the Cretaceous Hensell Sand (fig. 10). A few occurrences of younger granites, Cambrian Hickory Sandstone, Cretaceous Ft. Terrett Limestone, and Quaternary stream deposits are mapped along the highway (fig. 10; appendix B). Younger geologic units are found at the relatively high elevations on the south part of the segment; older igneous and metamorphic rocks are found at relatively low elevations on the north part of the segment (fig. 10). Average W7 deflections for both Llano and Gillespie Counties are less than 1.0 mil (fig. 1), reflecting the abundance of rigid bedrock in the Central Texas Uplift.

We analyzed FWD data from 69 sites along this highway segment (table 3; appendix C). This segment has the highest average W1 deflection of any of the study sites (34.7 mils), but the third-lowest average W7 deflection (0.93 mils). When the data are grouped by geologic unit (fig. 11), they show that (1) sites with large near-offset deflections generally also have large far-offset deflections, and (2) there is more variation within a geologic unit than there is between average

19
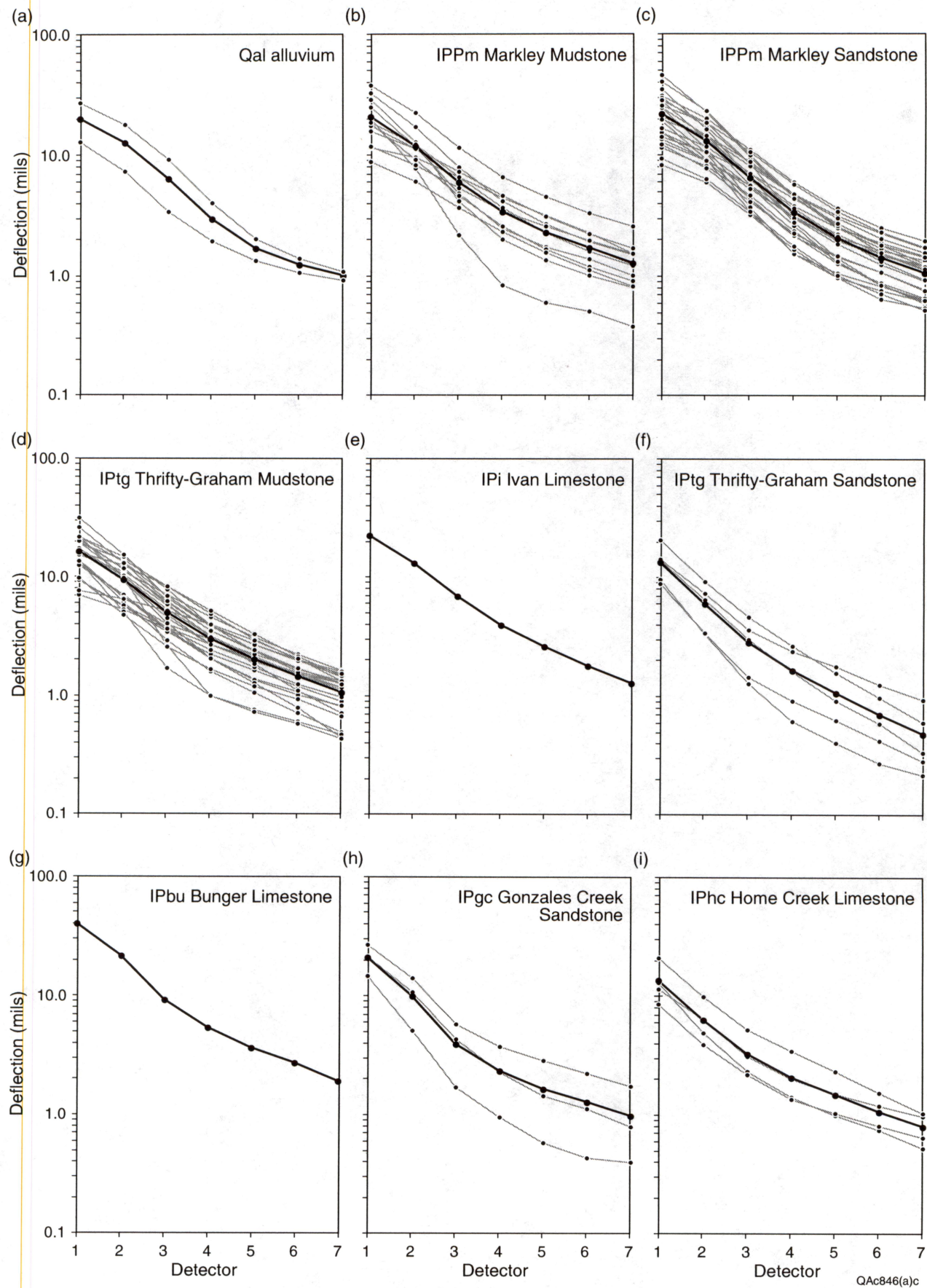
Figure 7. Average and individual deflections for rock types mapped along Texas 16 in Archer and Young Counties.

20

(j)

IPk Kisinger Sandstone

(k)

IPr Ranger Limestone

Deflection (mils)

Detector

Detector

QAc846(b)c

Figure 7 (cont.)

Figure 8. Average deflections for all rock units mapped along Texas 16 in Archer and Young Counties.

The chart legend contains the following entries:
- Qal alluvium
- IPPm Markley Mudstone
- IPPm Markley Sandstone
- IPPtg Thrifty-Graham Mudstone
- IPPtg Thrifty-Graham Sandstone
- IPi Ivan Limestone
- IPbu Bunger Limestone
- IPgc Gonzales Creek Sandstone
- IPhc Home Creek Limestone
- IPk Kisinger Sandstone
- IPr Ranger Limestone
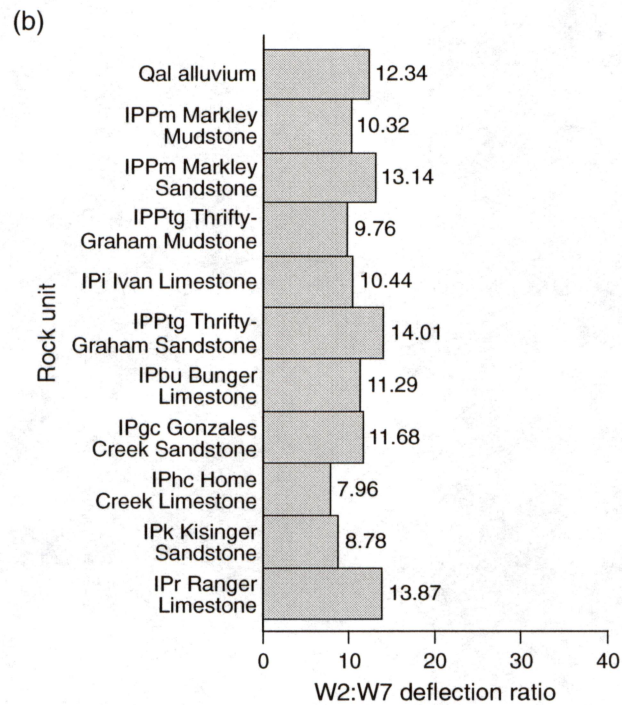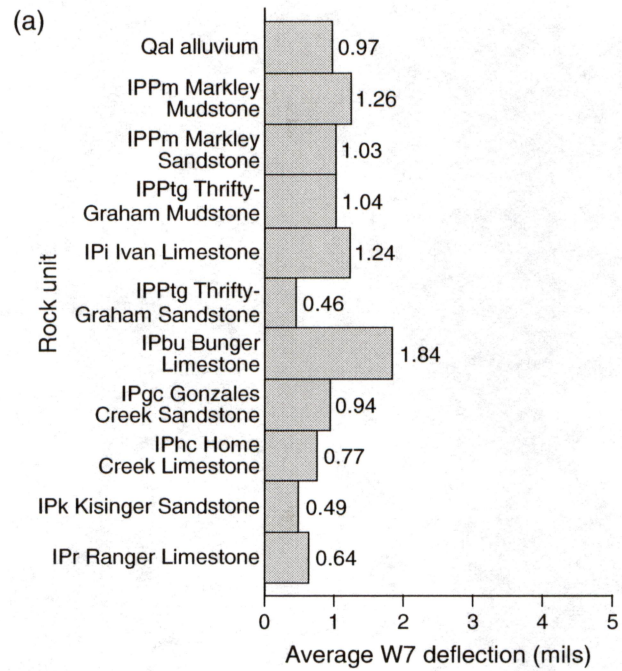
QAc845c

Figure 9. (a) Average W7 deflection and (b) W2:W7 deflection ratio by rock type along Texas 16, Archer and Young Counties.
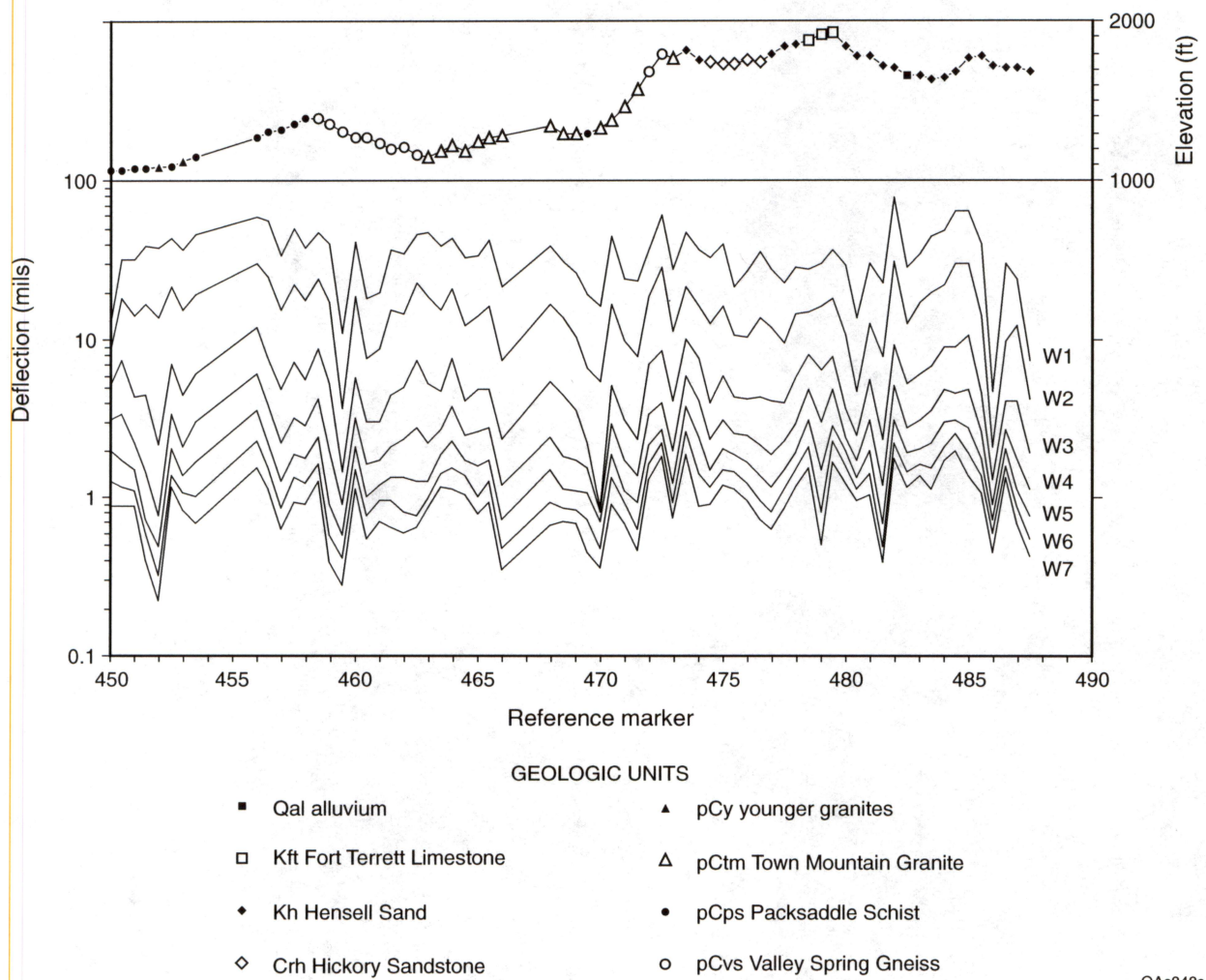
Figure 10. Geologic units, elevation, and W1 through W7 deflections along Texas 16 between reference markers 450 and 490, Llano and Gillespie Counties, central Texas.

24
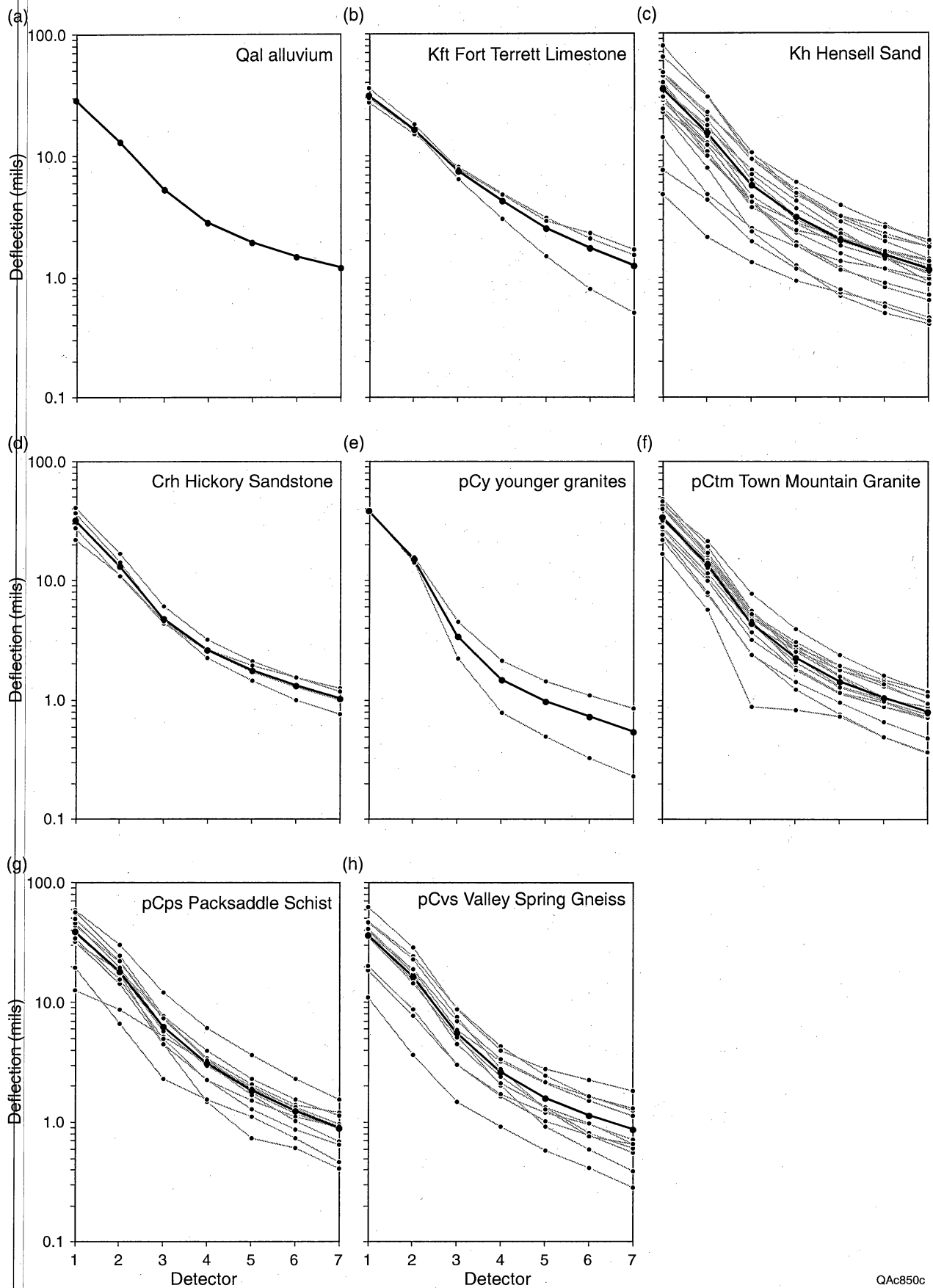
Figure 11. Average and individual deflections for rock types mapped along Texas 16 in Llano and Gillespie Counties.

25

deflections of each rock type. Although average W7 deflections calculated for the Hensell Sand are higher than those for the Town Mountain Granite and the Valley Spring Gneiss, the range in individual W7 deflections observed for these rock types is similar: 0.4 to 2 mils for the Hensell Sand, 0.3 to 1.1 mils for the Town Mountain Granite, and 0.3 to 1.8 mils for the Valley Spring Gneiss (fig. 11).

Statistically, Precambrian igneous and metamorphic rocks have low average W7 deflections that range from 0.53 mils for younger granites to 0.87 mils for the Packsaddle Schist (figs. 12 and 13a). Higher average W7 deflections, ranging from 1.11 to 1.24 mils, are calculated for Cretaceous and younger sedimentary units. W7 averages for geologic units at site B are similar to those calculated for geologic units in the North-Central Plains.

The W2:W7 ratio provides better discrimination of rock type for site B. Very high ratios are calculated for the rigid rock units (fig. 13b): between 17 and 40 for granites, metamorphic rocks, and the Fort Terrett Limestone. Lower ratios are calculated for the younger sedimentary units, ranging from 13 to 14 for the Hickory Sandstone and Hensell Sand, and 11 for Quaternary stream deposits. Ratios for the most common units encountered along Texas 16 are higher than those observed in the North-Central Plains and Gulf Coastal Plains and are similar to ratios calculated for the Edwards Plateau.

Site C: Texas 71, Burnet County

This 14-mi- (23-km-) long segment extends from reference markers 528 to 542 in eastern Burnet County. Along the west part of this segment, Paleozoic limestones are mapped that are extensively exposed within the Central Texas Uplift (fig. 14). Cretaceous sands and limestones are common along the east part of this segment, which represents a transitional zone from typical Central Texas Uplift units to typical Edwards Plateau units. Average W7 deflection for Burnet County is less than 1 mil, the lowest category (fig. 1).

FWD data from 30 locations along this highway segment (table 3; appendix C) indicate that average deflections at each offset are the second-lowest of the 6 study sites. Average W7 deflection

Figure 12. Average deflections for all rock units mapped along Texas 16 in Llano and Gillespie Counties.

(a)

Rock unit

Qal alluvium	1.18
Kft Fort Terrett Limestone	1.24
Kh Hensell Sand	1.11
Crh Hickory Sandstone	0.99
pCy younger granites	0.53
pCtm Town Mountain Granite	0.76
pCps Packsaddle Schist	0.87
pCvs Valley Spring Gneiss	0.85

Average W7 deflection (mils)

(b)

Rock unit

Qal alluvium	10.80
Kft Fort Terrett Limestone	17.44
Kh Hensell Sand	13.52
Crh Hickory Sandstone	13.38
pCy younger granites	39.86
pCtm Town Mountain Granite	17.53
pCps Packsaddle Schist	21.51
pCvs Valley Spring Gneiss	21.01

W2:W7 deflection ratio

QAc851c

Figure 13. (a) Average W7 deflection and (b) W2:W7 deflection ratio by rock type along Texas 16, Llano and Gillespie Counties.

28

Figure 14. Geologic units, elevation, and W1 through W7 deflections along Texas 71 between reference markers 528 and 542, Burnet County, central Texas.

is 0.57 mils, which falls within the indicated county-average category (fig. 1). Most of the FWD measurements were acquired over the Ordovician Honeycut Limestone, for which individual W7 deflections ranged from less than 0.1 to 0.8 mils (fig. 15). The average W7 deflections for all but two rock types fall within this range, including Quaternary stream deposits, Cretaceous Upper Glen Rose Limestone and Hensell Sand, and Ordovician Gorman Limestone (figs. 16 and 17a). Two units that had higher average W7 deflections than the range observed for the Honeycut Limestone were the Cretaceous Sycamore Sand (1.5 mils) and the Pennsylvanian–Permian Marble Falls Limestone (1.1 mils). Average W7 values for all other units were below 0.7 mils.

W2:W7 ratios (fig. 17b) proved to be a better discriminant of rock types than W7 values alone. High ratios (between 13 and 27), indicating a rapid decrease in deflection as offset increases and probably a relatively stiff or shallow bedrock, were calculated for the Honeycut Limestone, the Upper Glen Rose Limestone, and the Gorman Limestone. Intermediate ratios (9 to 10) were calculated for the small number of examples over the Marble Falls Limestone, the Sycamore and Hensell Sands, and Quaternary stream deposits. A low ratio of about 5 was calculated for the one example of Lower Glen Rose Limestone mapped along the segment. The most common geologic unit along the highway, the Honeycut Limestone, has a ratio that is similar to that of other rigid units in the Central Texas Uplift and Edwards Plateau regions and is higher than those in the North-Central and Gulf Coastal Plains regions.

Edwards Plateau Site

Average W7 deflections for counties within the Edwards Plateau region are below 1.5 mils (figs. 1 and 3), similar to those in the Central Texas Uplift counties and the lowest in the state. Relatively rigid Cretaceous limestones and dolomites are the most common bedrock types across the Edwards Plateau (table 1). Young, unconsolidated gravel, sand, and clay are common along numerous streams and rivers that dissect the plateau (fig. 2; plate 1). One study site is located in the central part of the Edwards Plateau.
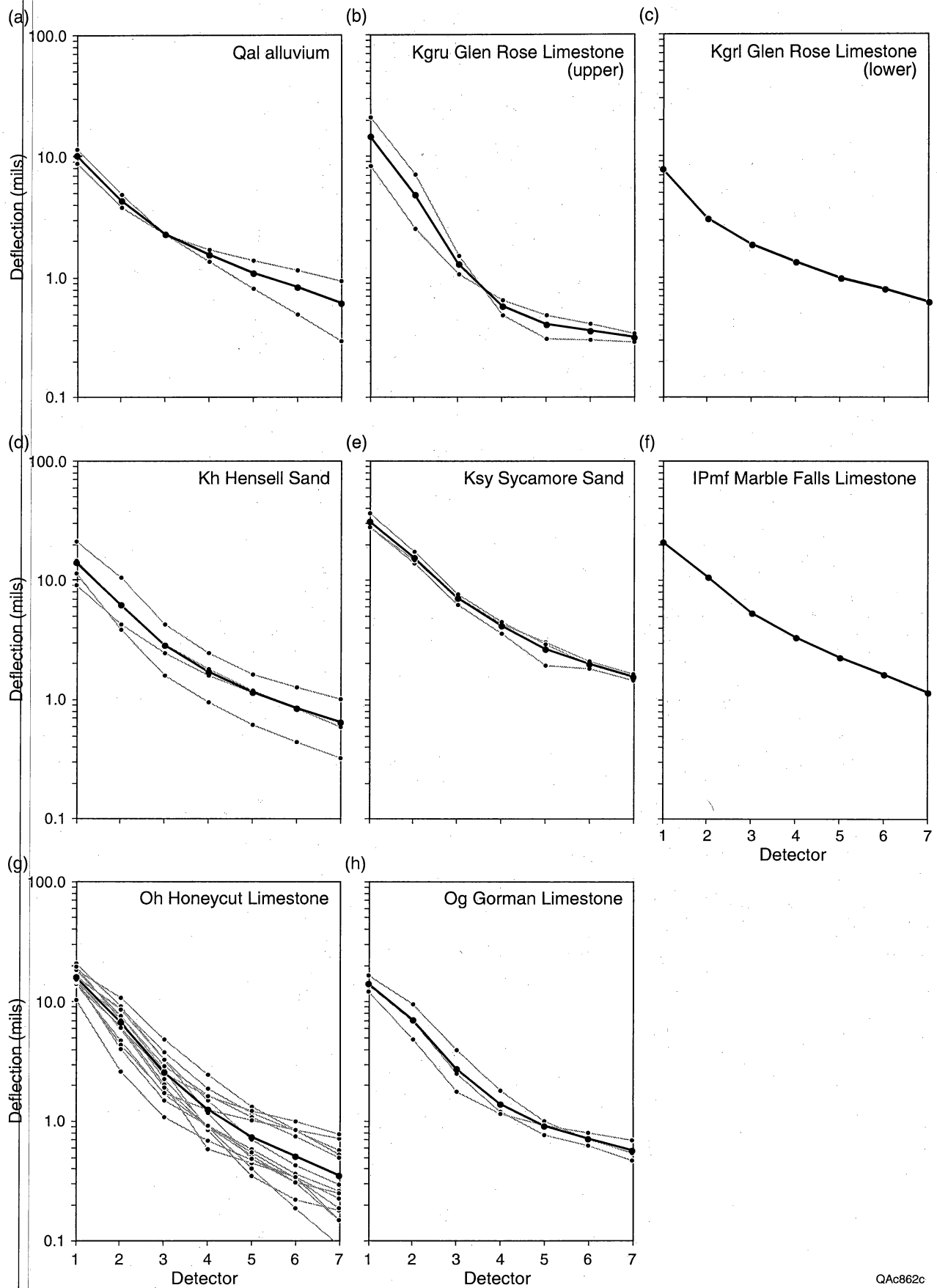
Figure 15. Average and individual deflections for rock types mapped along Texas 71 in Burnet County.
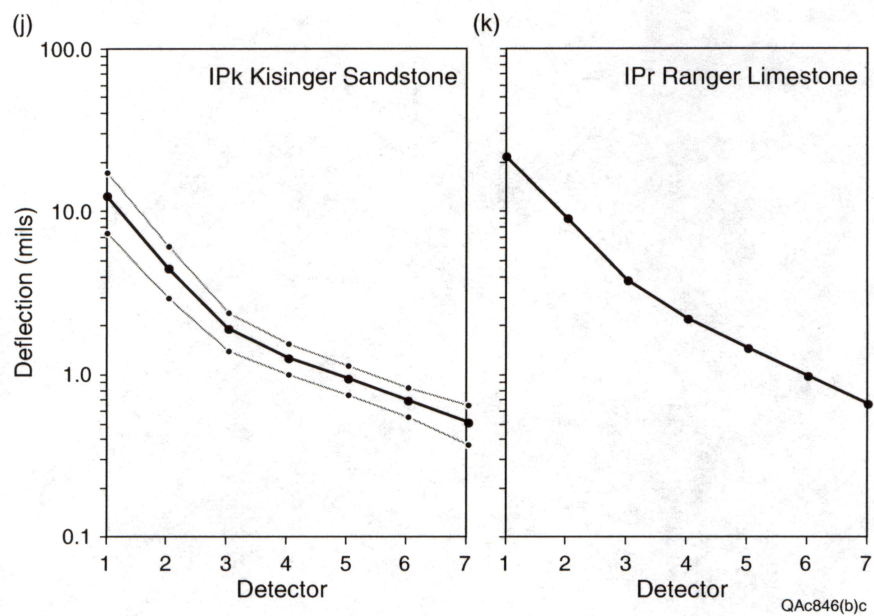
31
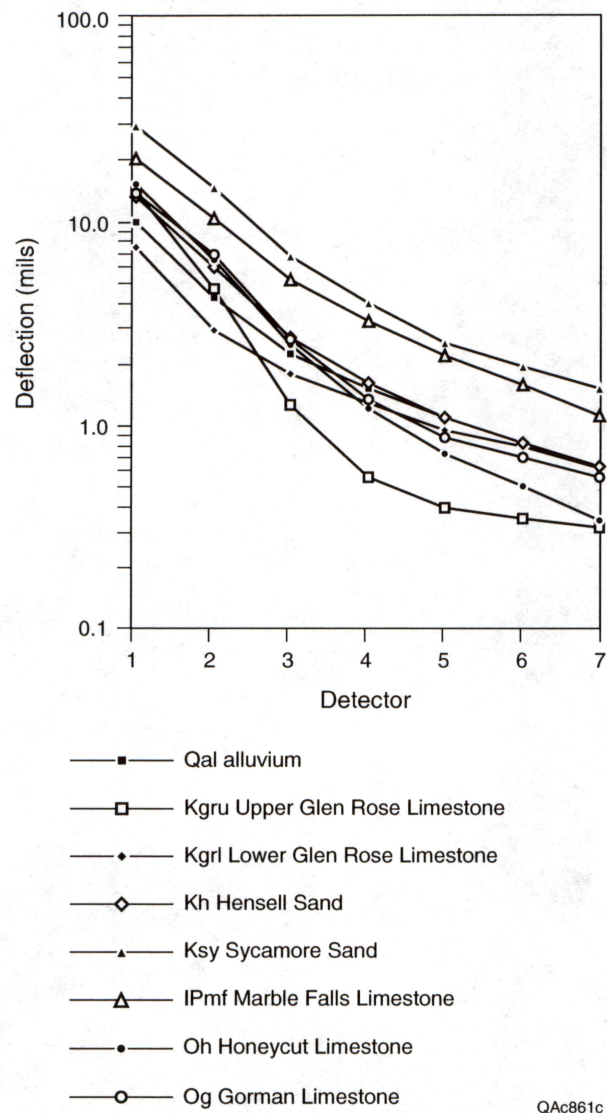
Figure 16. Average deflections for all rock units mapped along Texas 71 in Burnet County.

32

(a)

(b)
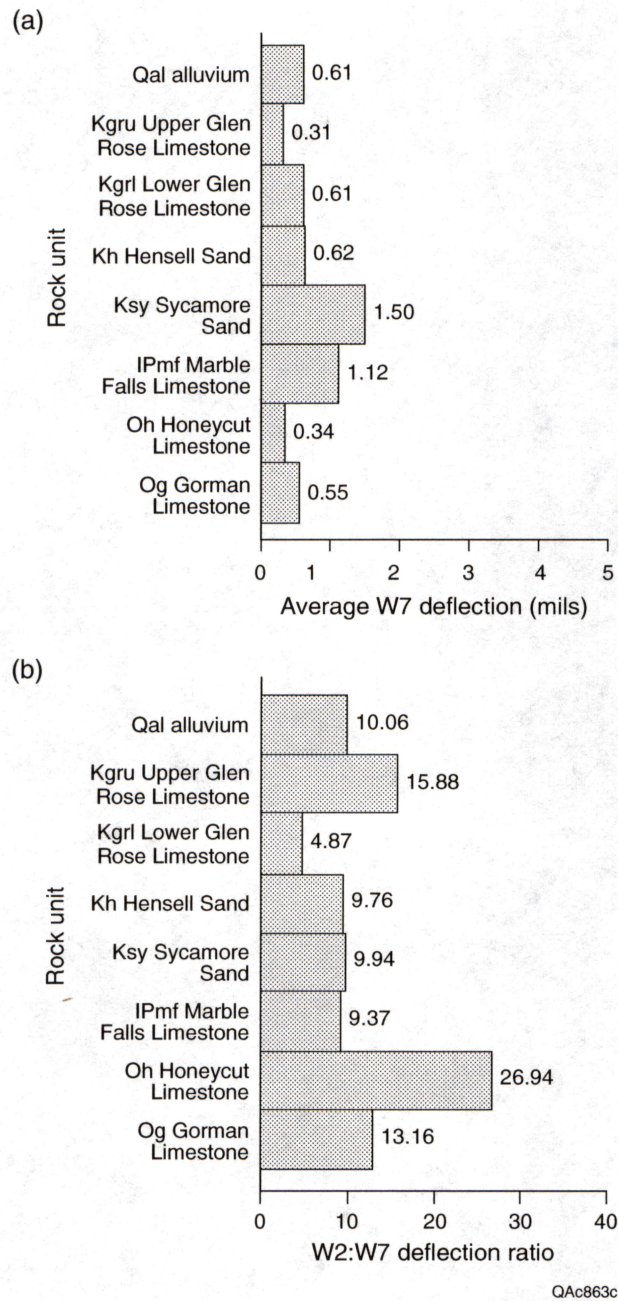
Figure 17. (a) Average W7 deflection and (b) W2:W7 deflection ratio by rock type along Texas 71, Burnet County.

Site D: U.S. 290, Blanco and Hays Counties

This segment of U.S. 290 extends about 27 mi (43 km) across eastern Blanco and northern Hays Counties between reference markers 536 and 563. Average W7 deflections for these counties are very low (each is below 1.0 mils, fig. 1). Only four geologic units are mapped: Cretaceous lithified sedimentary rocks that include the Upper and Lower Glen Rose and Fort Terrett Limestones and unconsolidated Quaternary stream deposits (appendix B). Upper and Lower Glen Rose Limestones are the most common geologic units; the Lower Glen Rose is found in the west part of the segment (reference markers 526 to 541, fig. 18) and the Upper Glen Rose crops out at the higher elevations common in the east part of the segment (reference markers 542 to 563). Younger, unconsolidated deposits are found in local topographic lows.

FWD measurements acquired at 52 sites have the lowest average deflections of the 6 sites at all offsets (table 3; appendix C). Average deflections for the W5, W6, and W7 detectors are each below 1.0 mil. Deflections observed at detector W7 for the Upper Glen Rose Limestone, the most common geologic unit along this segment, range from less than 0.1 to 0.9 mils. This range matches Blanco and Hays County averages and includes W7 deflections for each of the other geologic units (fig. 19).

Upper and Lower Glen Rose Limestones have similar deflection averages for each offset (fig. 20) and have very low W7 averages (0.36 to 0.38 mils, fig. 21a). Deflections for the one Fort Terrett Limestone example are even lower than the Glen Rose units for detectors W5, W6, and W7. Highest deflections are observed for the Quaternary stream deposits, although W7 values for this unit are quite low (0.6 mils) relative to similar deposits in other regions, perhaps because of roadway stiffness.

Calculations of W2:W7 ratios for these geologic units appear to remove the road-stiffness effect (fig. 21b). The Fort Terrett and Upper and Lower Glen Rose Limestones all have high ratios (19 to 24) that are comparable to rigid geologic units in the Central Texas Uplift. The W2:W7 ratio

34
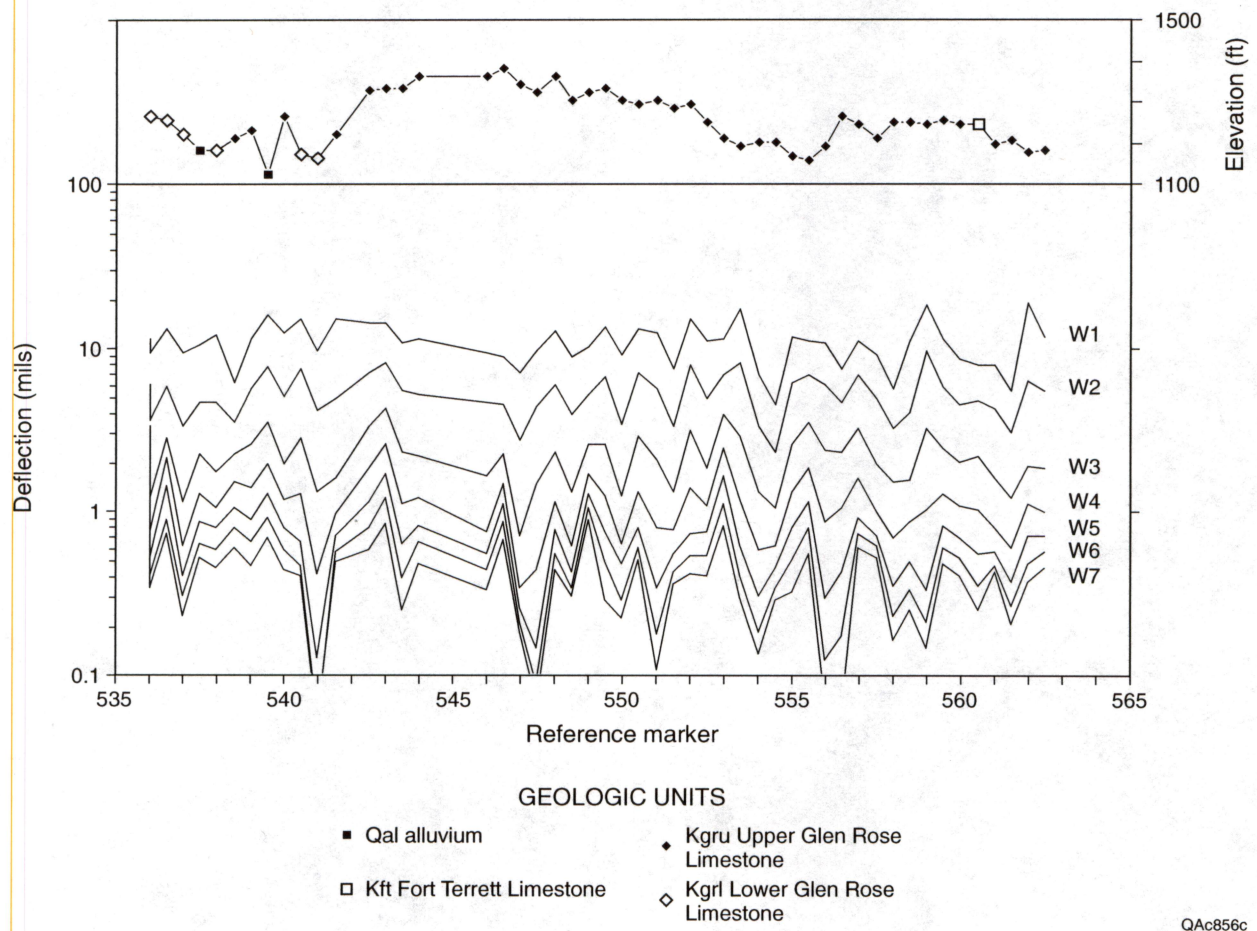
Figure 18. Geologic units, elevation, and W1 through W7 deflections along U.S. 290 between reference markers 536 and 563, Blanco and Hays Counties, central Texas.
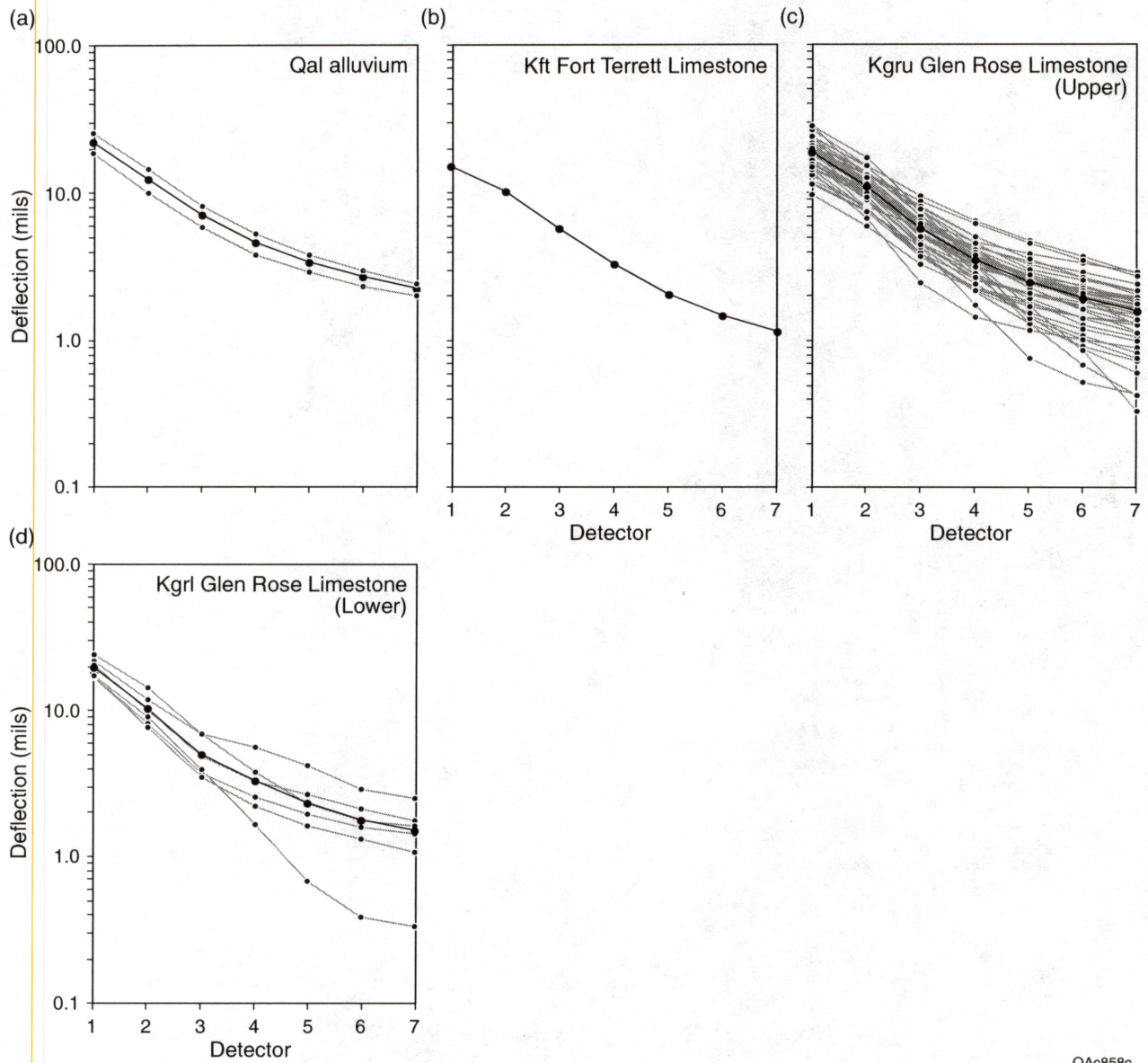
Figure 19. Average and individual deflections for rock types mapped along U.S. 290 in Blanco and Hays Counties.
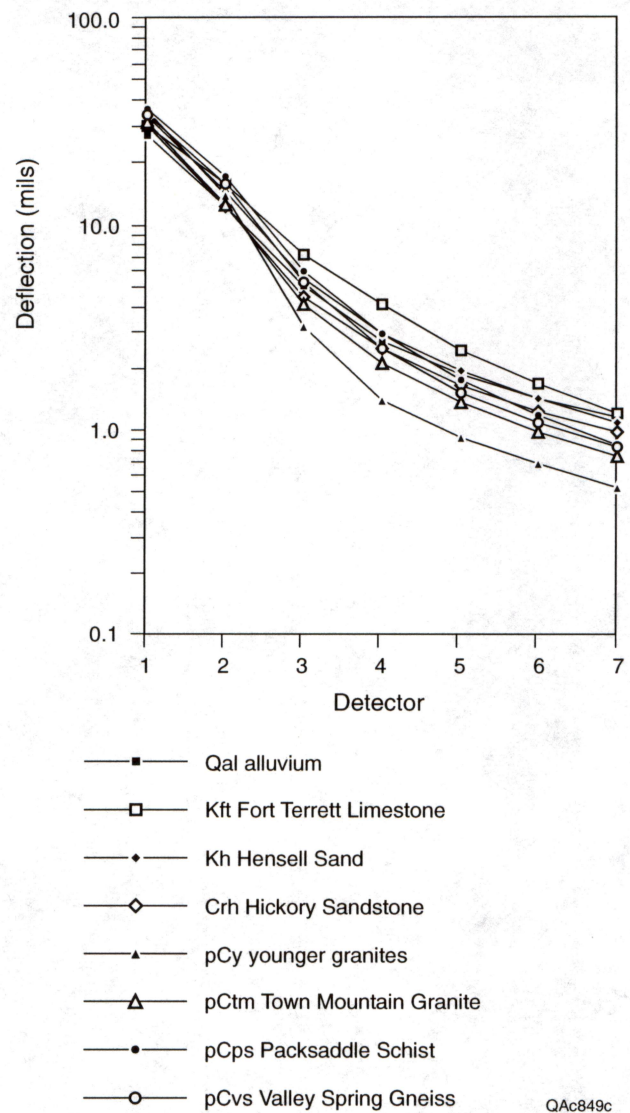
Figure 20. Average deflections for all rock units mapped along U.S. 290 in Blanco and Hays Counties.

(a)

(b)
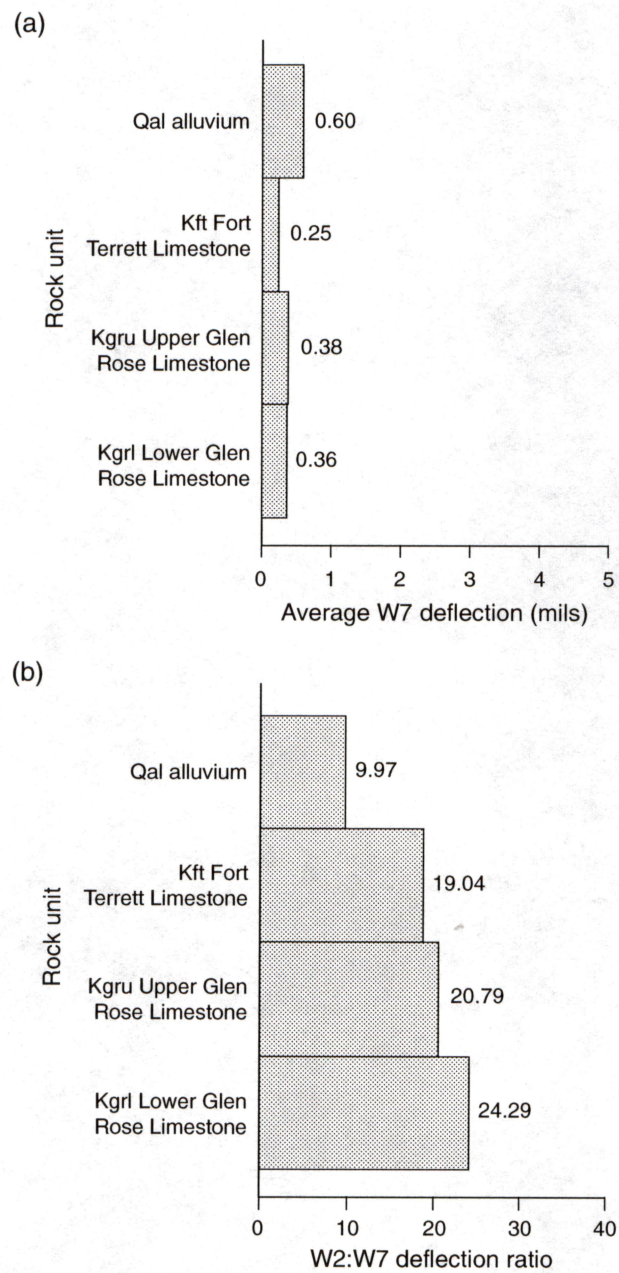
Figure 21. (a) Average W7 deflection and (b) W2:W7 deflection ratio by rock type along U.S. 290, Blanco and Hays Counties.

38

for Quaternary stream deposits is near 10, which is within the range of 7 to 12 observed for similar deposits in other regions.

Gulf Coastal Plains Sites

The Texas coastal plain, which slopes toward the Gulf of Mexico from the Edwards Plateau (fig. 3), is the largest and geologically youngest of the major physiographic regions. Bedrock types in this region are all Cenozoic sedimentary deposits that are variably lithified (table 1). This region has the highest county average W7 deflections in the state, ranging from 1.1 to more than 2.5 mils (fig. 1). The two sites studied in this region (sites D and E, fig. 3) are located on the central and south parts of the upper coastal plain.

Site E: Texas 71, Bastrop County

Site E is an 8-mi- (13-km-) long segment of Texas 71 between reference markers 590 and 598 on the central part of the upper Gulf Coastal Plains (fig. 3). Average W7 deflections for Bastrop County (between 1.1 and 1.5 mils) represent the low end of the range observed for all coastal plain counties (fig. 1). Geologic units mapped along this segment are old relative to deposits closer to the Gulf of Mexico (fig. 2; plate 1). They include Cretaceous clay and marl, Eocene mudstones, sandstones, and unconsolidated clay and sand, and unconsolidated Quaternary gravel, sand, and clay (fig. 22; appendix B).

Average deflections calculated from FWD measurements along both sides of the roadway at 17 locations (34 deflection series) are higher for the W3 to W7 detectors than they are for any other study site (table 3). Average W7 deflection is 1.49 mils, which is in the same range calculated for Bastrop County (fig. 1). There are large variations in deflections measured at individual detectors for some geologic units (W7 deflection is between 0.5 and 4 mils for the Hooper Mudstone, fig. 23) and relatively small variations in other geologic units (W7 deflection ranges from 0.9 to 1.5 mils for the Simsboro Sand).
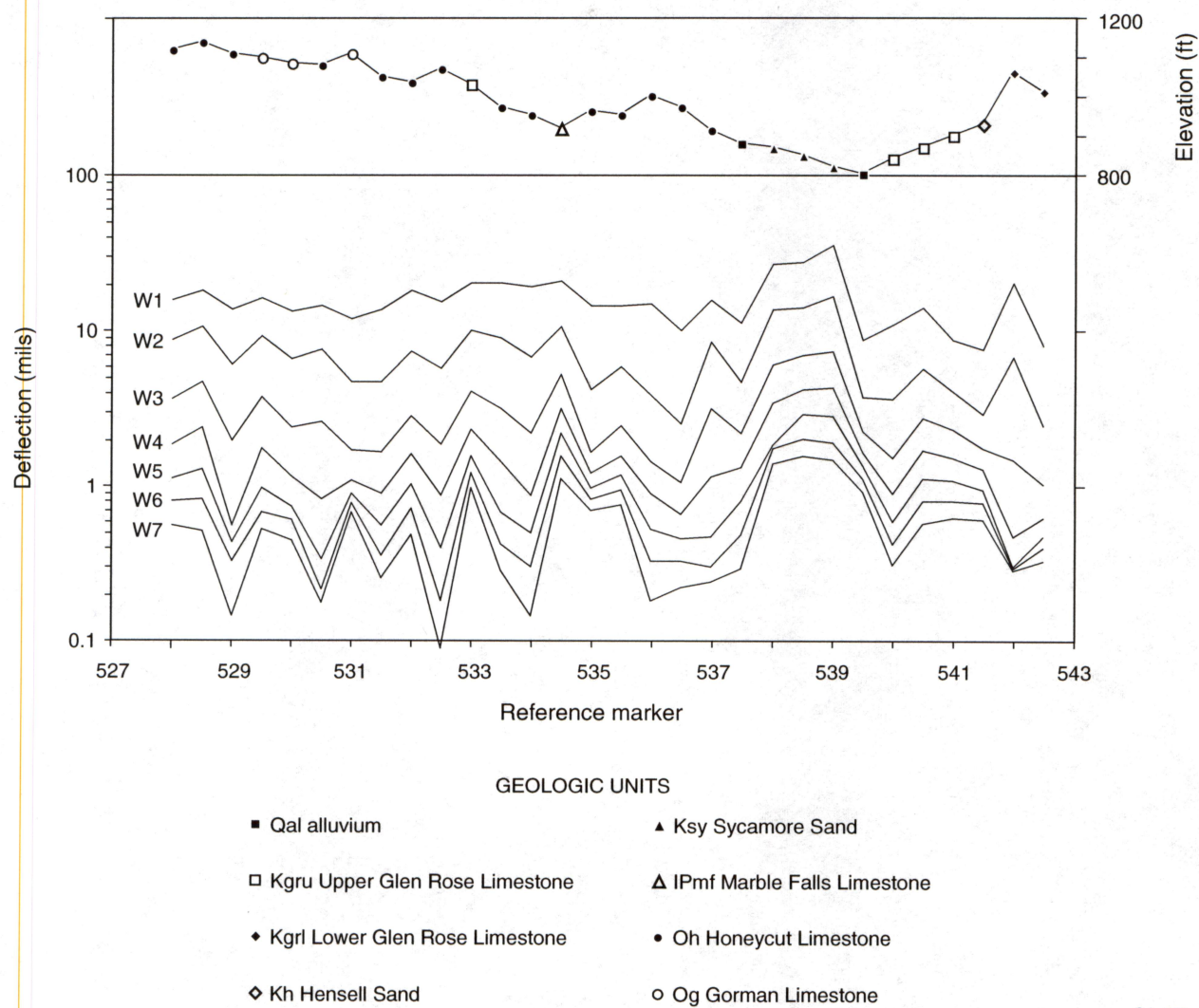
39
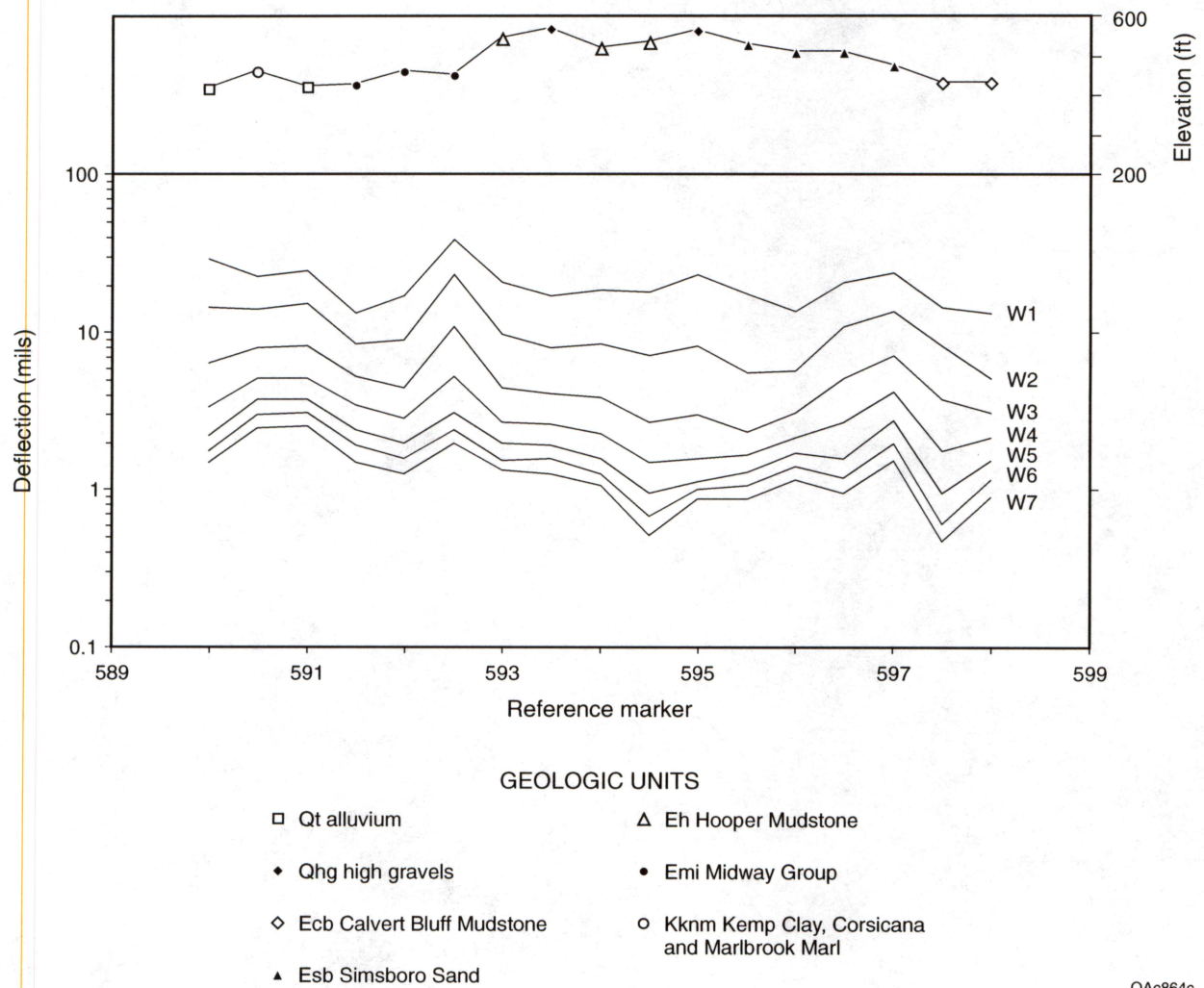
Figure 22. Geologic units, elevation, and W1 through W7 deflections along Texas 71 between reference markers 590 and 598, Bastrop County, southeast Texas.

40
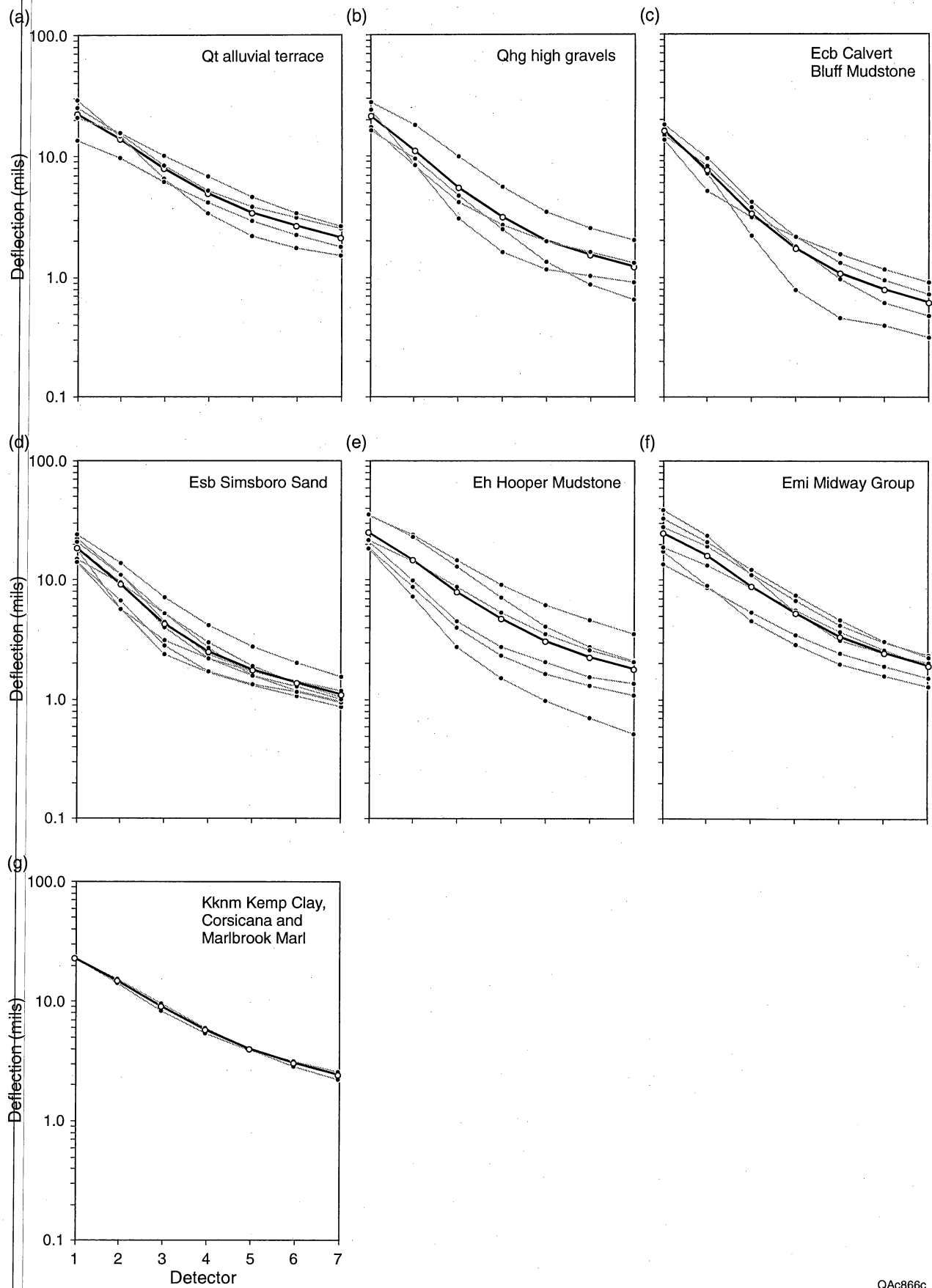
Figure 23. Average and individual deflections for rock types mapped along Texas 71 in Bastrop County.

41

Most geologic units have large average deflections relative to geologic units in other physiographic regions (figs. 24 and 25a). The largest W7 deflections, above 2 mils, were recorded at locations mapped as Cretaceous clay and marl units and Quaternary stream deposits. Intermediate W7 deflections of 1.1 to 1.9 mils were observed over the Midway Group, Hooper Mudstone, Simsboro Sand, and Quaternary gravel found at the highest topographic positions along the roadway (fig. 22). The smallest W7 deflections were measured over the Calvert Bluff Mudstone, which is the most rigid unit at site E.

Ratios calculated from average W2 and W7 deflections also suggest that the Calvert Bluff Mudstone is the most rigid of the geologic units mapped at this site (fig. 25b). The W2:W7 ratio for this unit is 15, well below that of the most rigid units in the Central Texas Uplift and Edwards Plateau regions, but comparable to those of similar lithified sedimentary rocks in the North-Central Plains. Ratios for all other geologic units at site E are below 10, indicating materials with low rigidity or deep bedrock (fig. 25b).

Site F: Texas 16, Jim Hogg and Zapata Counties

Site F is located in the Rio Grande Valley on the south part of the Gulf Coastal Plains (fig. 3). Average W7 deflections for the counties crossed by this segment of Texas 16 are moderate to high, ranging from 1.1 to 1.5 mils for Jim Hogg County and 1.6 to 2.0 mils for Zapata County (fig. 1). Geologic units mapped along this roadway are variably lithified Cenozoic sedimentary deposits that include Eocene sandstone and clay formations, Miocene to Oligocene mudstones, Pliocene clay, and younger Quaternary wind- and stream-deposited sediments (fig. 26; appendix B).

Average deflections calculated from FWD data from 89 locations between reference markers 758 and 804 are either the highest or second-highest values calculated for the 6 study segments (table 3). Average W7 deflection is 1.41 mils, a value that is within the deflection range reported for these counties (fig. 1). Individual deflections at all detectors are relatively high, particularly between reference markers 775 and 795, where Catahoula and Frio mudstones and Jackson Group sandstones are mapped (fig. 26). Ranges of individual deflections are large; despite differences in
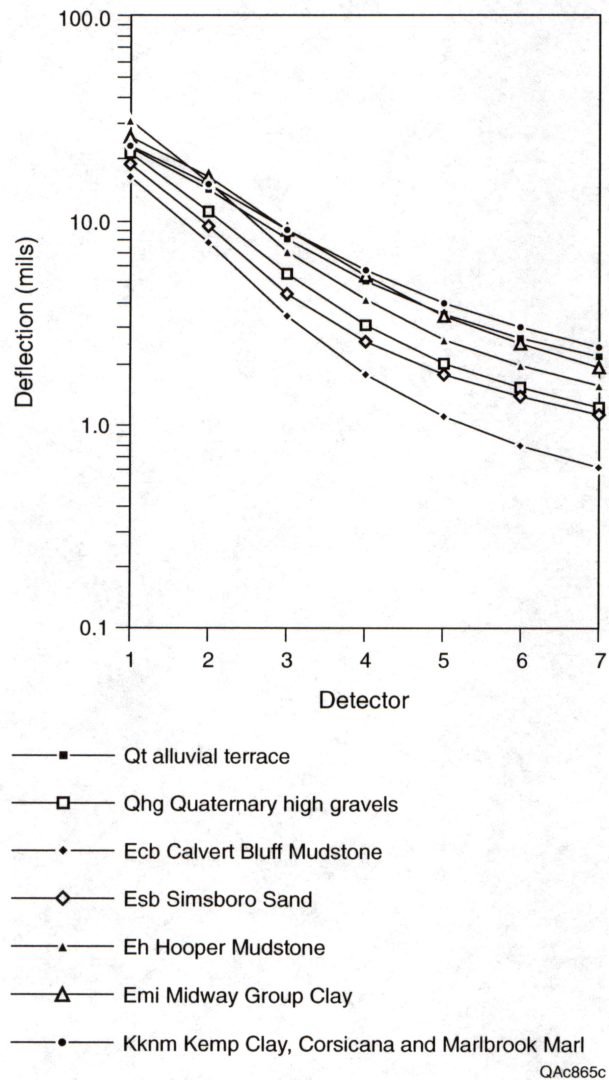
Figure 24. Average deflections for all rock units mapped along Texas 71 in Bastrop County.

(a)

Qt alluvium — 2.11
Qhg high gravels — 1.19
Ecb Calvert Bluff Mudstone — 0.60
Esb Simsboro Sand — 1.09
Eh Hooper Mudstone — 1.75
Emi Midway Group — 1.87
Kknm Kemp Clay, Corsicana and Marlbrook Marl — 2.34

Rock unit

Average W7 deflection (mils)

(b)

Qt alluvium — 6.71
Qhg high gravels — 9.84
Ecb Calvert Bluff Mudstone — 14.69
Esb Simsboro Sand — 8.37
Eh Hooper Mudstone — 9.06
Emi Midway Group — 8.16
Kknm Kemp Clay, Corsicana and Marlbrook Marl — 6.28

Rock unit

W2:W7 deflection ratio

QAc867c

Figure 25. (a) Average W7 deflection and (b) W2:W7 deflection ratio by rock type along Texas 71, Bastrop County.
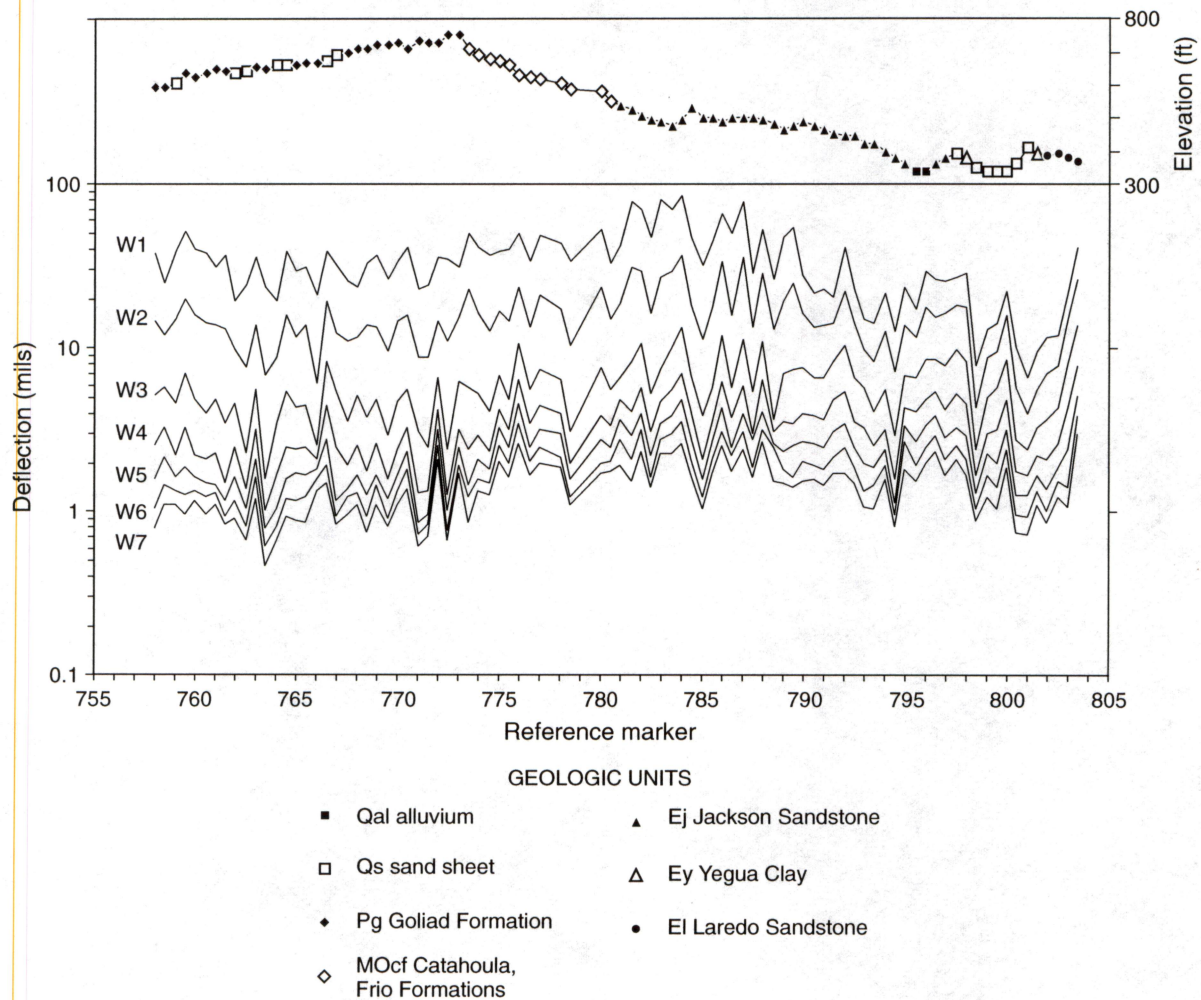
Figure 26. Geologic units, elevation, and W1 through W7 deflections along Texas 16 between reference markers 758 and 804, Jim Hogg and Zapata Counties, south Texas.

the average deflections for each geologic unit, many individual deflections collected over one rock type fall within a deflection range recorded for another rock type (fig. 27). W7 deflections measured over Jackson Group sandstones range from 0.8 to nearly 3.0 mils, a range that is similar to that measured for Catahoula and Frio mudstones and Laredo sandstones. Lower, but overlapping, W7 deflections are observed for the Goliad Formation (0.5 to 2 mils) and the Quaternary sand sheet (0.7 to 2 mils).

Average deflections for each geologic unit are relatively high at all offsets (fig. 28). The highest average W7 deflections (1.66 to 1.78 mils) are found over unconsolidated Quaternary stream deposits, Jackson sandstones, and Catahoula and Frio mudstones; the lowest average W7 deflections, just above 1 mil, are calculated for segments over areas where Quaternary windblown sands and the Pliocene Goliad Formation are mapped.

Ratios of W2 to W7 deflections occupy a narrow range between 7.9 and 13.1 (fig. 29b). These relatively low values are similar to ratios calculated over stream deposits in other physiographic regions, indicating that much of the coastal plains is underlain by materials of low rigidity. Ratios below 10, indicating the weakest material, were calculated for Quaternary stream deposits, the Yegua Clay, and the Laredo Sandstone. The Pliocene Goliad Formation (W2:W7 = 13) is the most rigid sedimentary deposit at this site.

Combined Site Response

Average FWD response for principal rock types can be examined by grouping individual geologic units into these basic types regardless of physiographic region. Principal rock types mapped in the Central Texas Uplift, North-Central Plains, Edwards Plateau, and Gulf Coastal Plains regions are (1) unconsolidated sedimentary deposits, (2) sandstones, (3) mudstones, (4) limestones, (5) granites, and (6) metamorphic gneisses and schists. Each geologic unit mapped at FWD sites along the six test segments can be classified as one of these principal geologic types.

W7 averages and W2:W7 ratios for each individual rock type define ranges of observed values for the principal rock types (fig. 30). FWD response along roadways built over igneous and

46
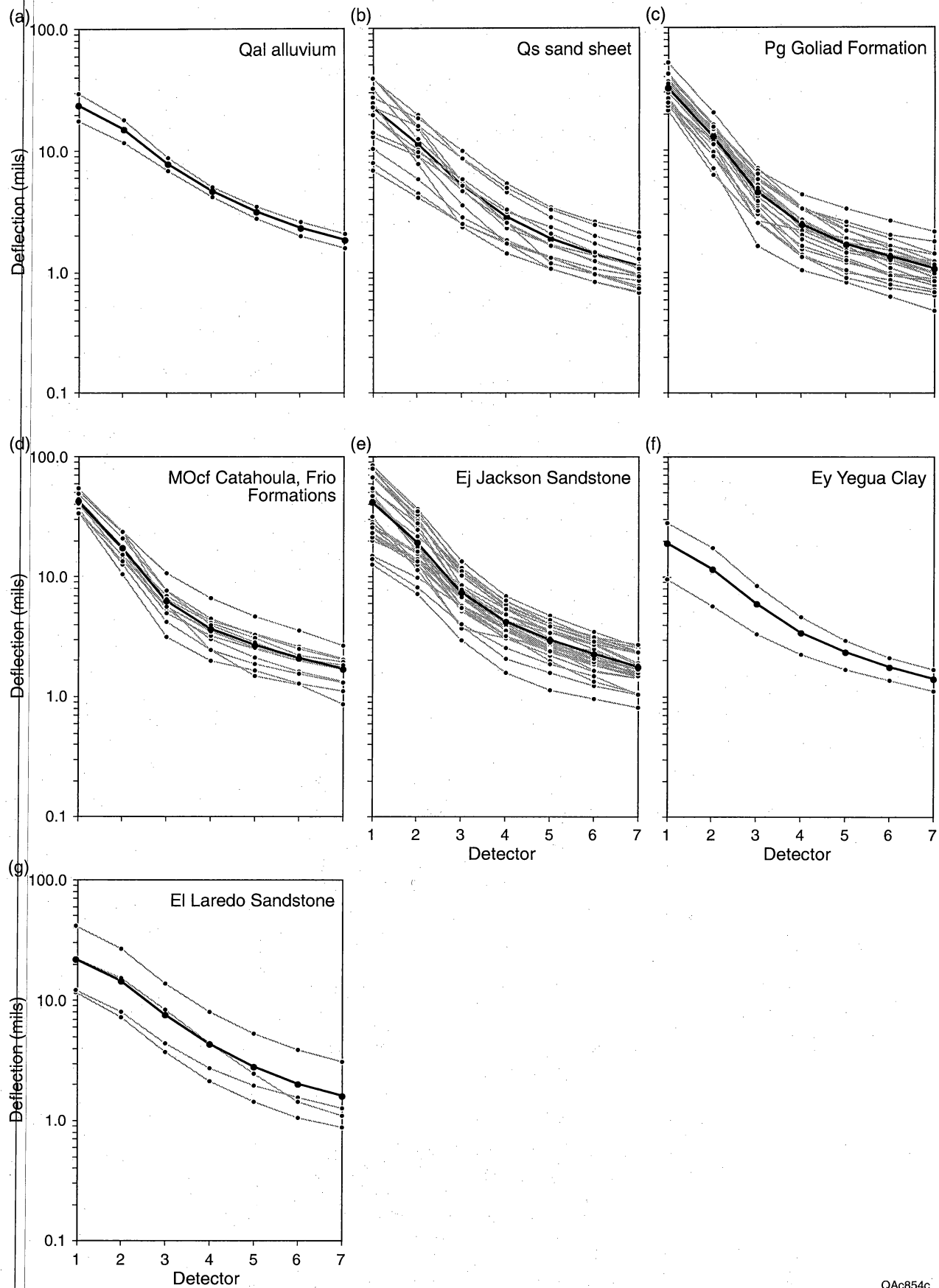
Figure 27. Average and individual deflections for rock types mapped along Texas 16 in Jim Hogg and Zapata Counties.
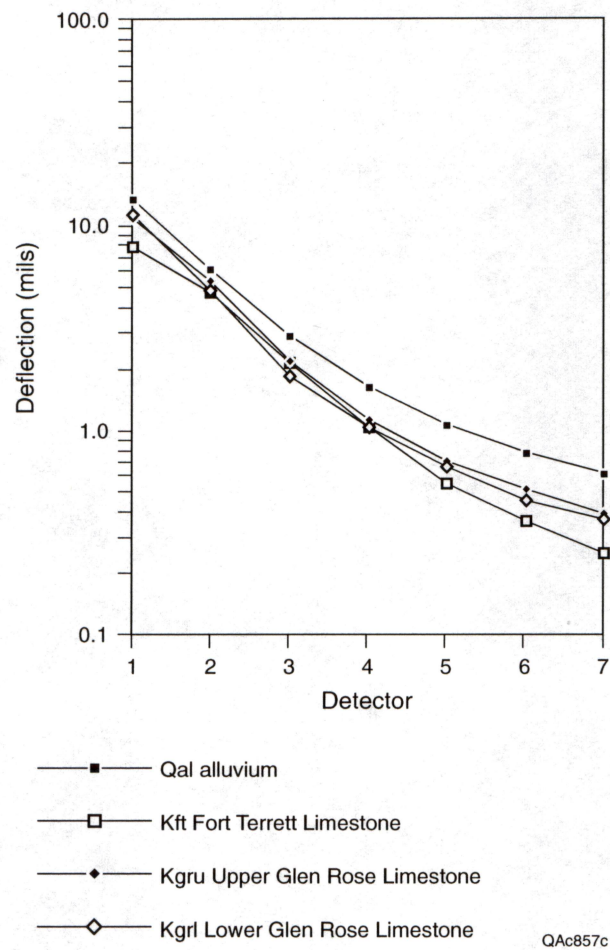
47
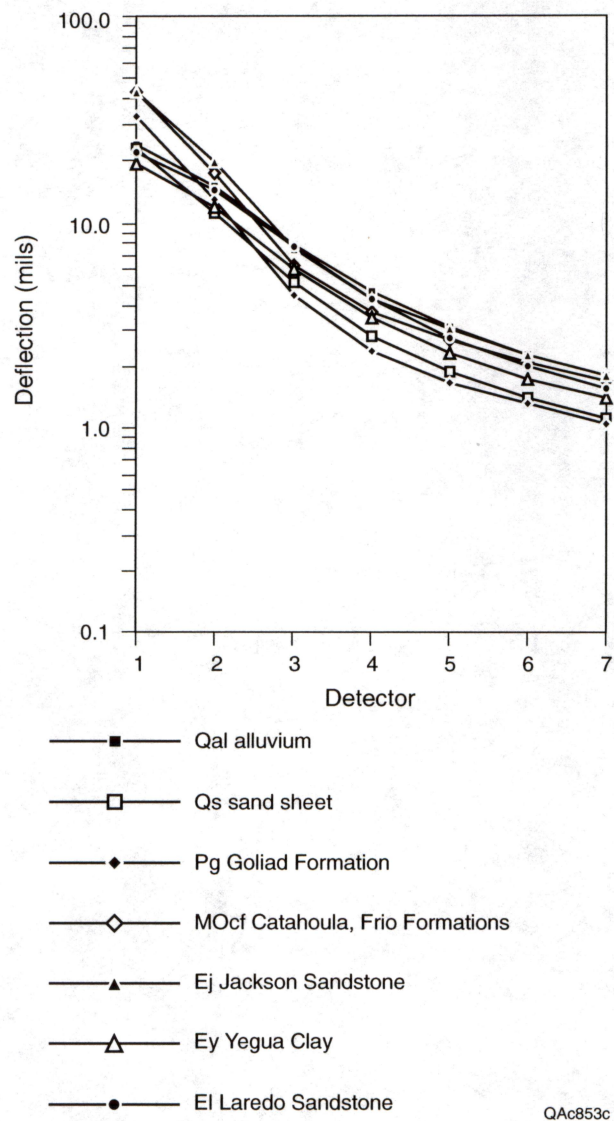
Figure 28. Average deflections for all rock units mapped along Texas 16 in Jim Hogg and Zapata Counties.
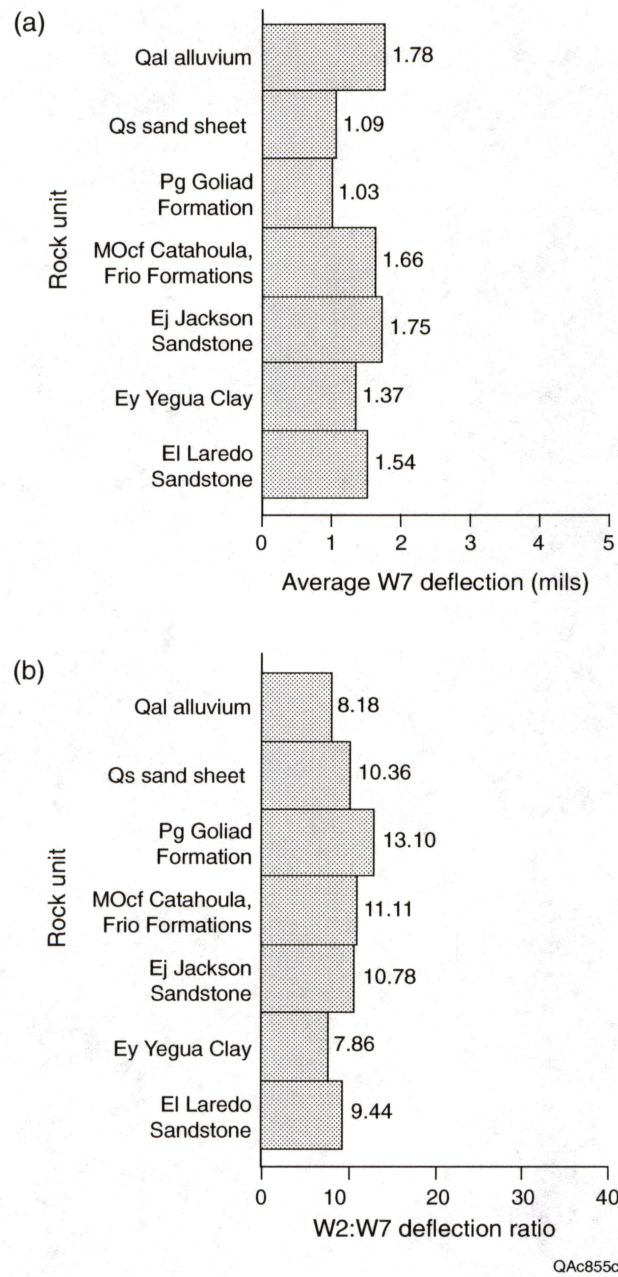
Figure 29. (a) Average W7 deflection and (b) W2:W7 deflection ratio by rock type along Texas 16, Llano and Gillespie Counties.
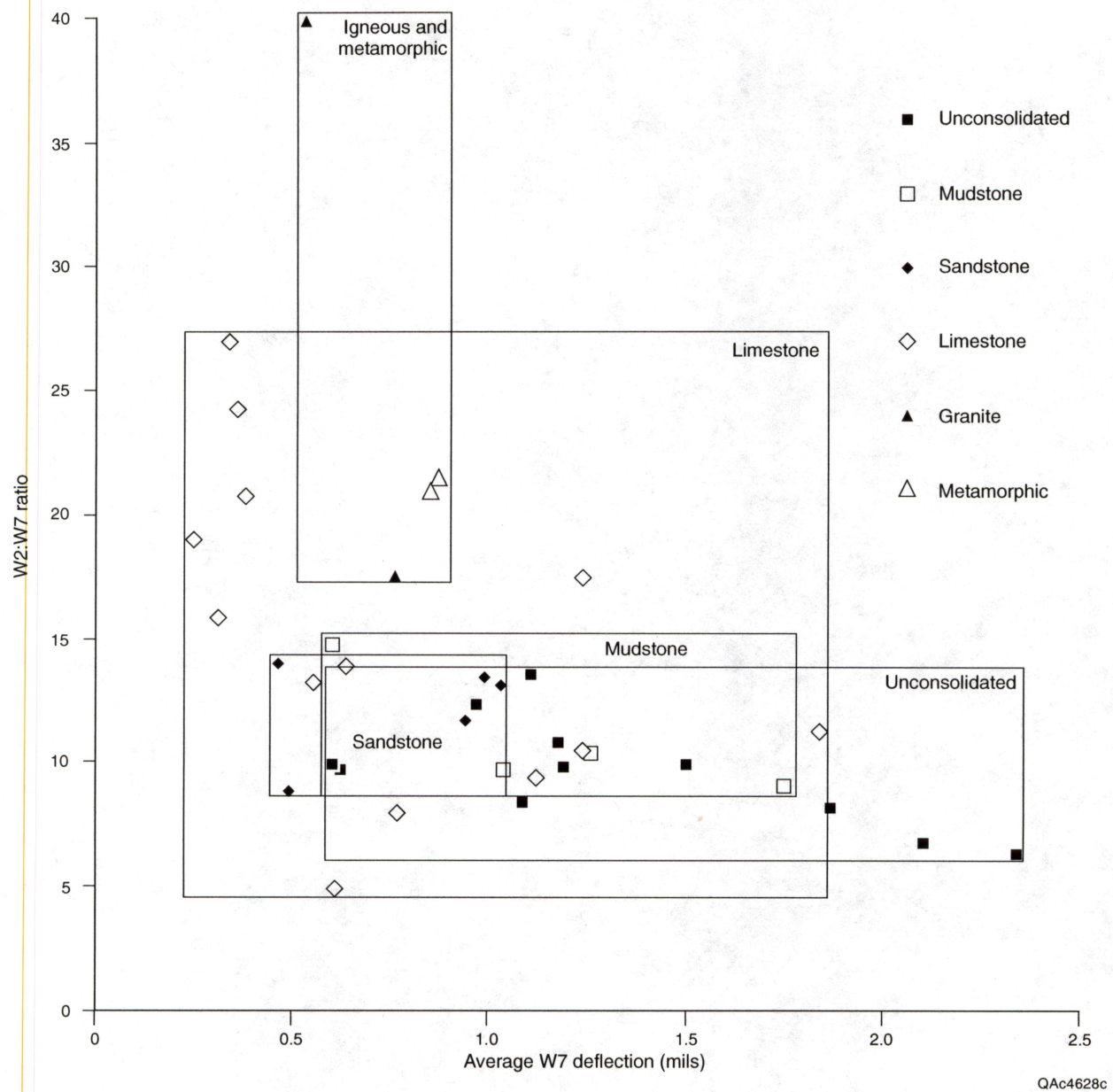
Figure 30. Average W7 deflection and W2:W7 deflection ratio for individual rock types mapped along the Texas 16, U.S. 290, and Texas 71 test sites.

metamorphic rock types such as granite, gneiss, and schist have low average W7 deflections (0.5 to 0.9 mils) and high to very high W2:W7 ratios (more than 17) compared to other rock types. Siliciclastic sedimentary units such as sandstone and mudstone have similarly low W2:W7 ratios between 9 and 15, but sandstone tends to have smaller average W7 deflections than does the less consolidated mudstone. Unconsolidated sediments, including Quaternary alluvium and older uncemented sand and gravel, exhibit a wide range of W7 deflections (0.6 to 2.3 mils) along with very low W2:W7 ratios (6 to 14) that are similar to those observed for lithified siliciclastic rocks. Although sandstone, mudstone, and unconsolidated sedimentary deposits have similar W2:W7 ratios, average W7 deflections, which are generally highest for unconsolidated deposits and lowest for sandstones, provide a basis for discriminating these types.

FWD response along highways underlain by limestone is perhaps the most variable of all the principal rock types (fig. 30). Some limestone units have the lowest observed W7 deflections (below 0.5 mils) and high W2:W7 ratios (15 to 27); other limestone units have W7 deflections as much as 1.8 mils and W2:W7 ratios as low as 5, values that are comparable to those of siliciclastic units. These higher W7 deflections and lower W2:W7 ratios probably indicate either common clay-rich units within larger sections of limestone, weathered limestone, or greater depth to bedrock.

BEDROCK DEPTHS FROM SEISMIC REFRACTION

We collected seismic-refraction data at two sites (fig. 1) to prove the concept of collecting refraction data in typical highway settings, to investigate the usefulness of the data in determining bedrock depth to support deflection analysis, and to optimize equipment and acquisition parameters to balance operational simplicity with the collection of interpretable data. Knowing bedrock depths at a given site enables one to address the ambiguity of whether bedrock type or depth is the source of the correlation between geologic unit and road deflection.

Pickle Research Campus Site

We acquired seismic-refraction data in September 1997 along Road D on the Pickle Research Campus (PRC) at The University of Texas at Austin (table 2). Road D is an asphalt-pavement road laid on an unknown thickness of road base over residual sediments and lower Cretaceous limestone of the Austin Group (Garner and Young, 1976).

Several seismic wave types are evident in a field record collected at PRC using the FWD as a seismic source (fig. 31). Types of ground motion detected by the geophones during the first 60 ms following impact of the FWD weight with the pavement include (1) high-amplitude, low-frequency, and slowly propagating surface waves (lower left of field record, less than 280 m/s propagation velocity); (2) a direct wave, which is the first recorded signal at geophones that are less than 4 m from the source; (3) a critically refracted arrival, representing the first recorded signal at geophones greater than 4 m from the source (3,000 m/s propagation velocity), and (4) a reflected wave that has a hyperbolic shape, arriving at approximately 20 ms at the source location and approximately 30 ms at the maximum offset. Spectral analyses of ground motion detected by near-source geophones indicate that the FWD produces an impulse with frequencies between about 20 and 200 Hz, which is a useful range for seismic-refraction and shallow-reflection investigations.

In refraction analysis, the direct arrival represents a compressional wave traveling from the source to the geophone without appreciable refraction through a surface layer. The surface layer has a wave velocity equal to the propagation velocity calculated from the direct wave's arrival time at each detector. The critically refracted wave represents a compressional wave that travels through the surface layer, is refracted along the interface between the surface layer and an underlying, higher velocity material (bedrock in this instance). The refracted wave travels at the velocity of the underlying material, generating wavefronts as it propagates along the boundary. The refraction-generated wavefronts subsequently reach the surface and are recorded by the geophones. To calculate the depth of the layer that refracts the compressional wave, we pick the arrival times of the direct and critically refracted waves, calculate an apparent velocity for the direct and refracted

52
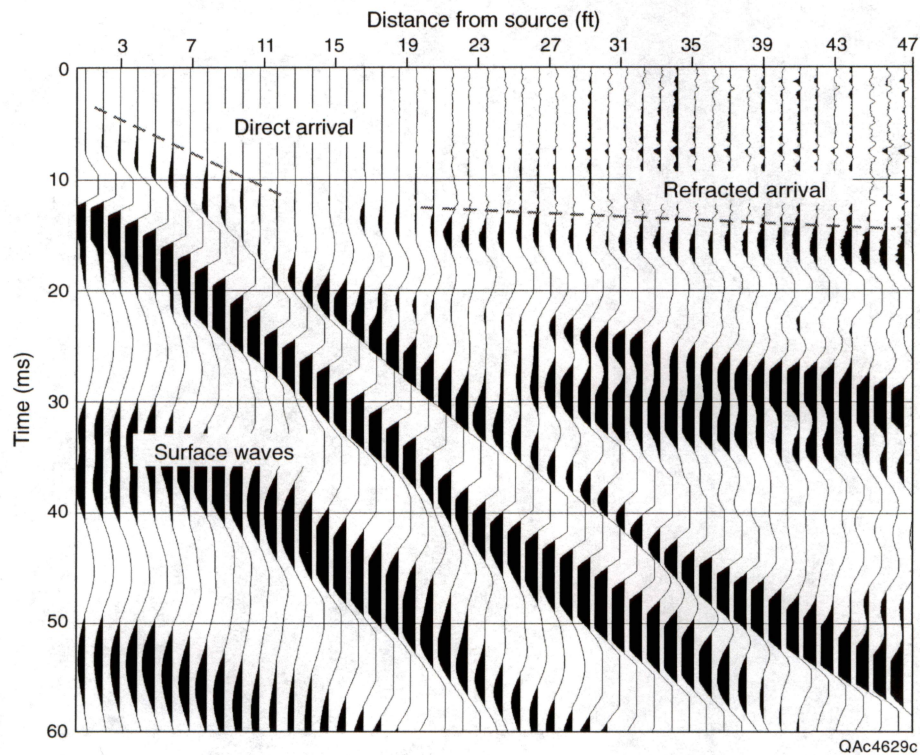
Figure 31. Seismic response recorded with a 48-geophone spread using the FWD as a seismic source. Visible phases include the direct arrival, a critically refracted arrival from the underlying rigid layer, long-wavelength, low-frequency surface waves, and reflected compressional waves. Data recorded on a flexible-pavement road on the PRC.

waves, and extrapolate the arrival time of the refracted arrival to a position beneath the source (zero offset). Because we were uncertain how well the beginning of the seismic record matches the impact of the FWD with the pavement, we did not calculate layer depths using the FWD source.

Refraction Experiment PRC SPH1

In this refraction test, both the soil-probe hammer source and the 48 geophones were located on the south shoulder of PRC Road D (fig. 4; tables 2 and 4). Displays of filtered and amplified seismic energy from impulses at the west and east ends and the center of the recording spread (fig. 32) reveal the presence of a slowly propagating direct arrival at geophones nearest the source and a faster, critically refracted arrival at geophones farther from the source. First-arrival times for each trace can be plotted against distance from the source and segregated into arrivals measured when the source was west of the geophone (arbitrarily assigned the forward direction, fig. 33) and when the source was east of the geophone (the reverse direction).

In the forward direction, arrivals can be grouped by offset range into two linear segments (fig. 33). The group located closest to the source (between 0 and about 6 m forward offset) is interpreted to be arrivals from the direct wave. Arrivals at greater offsets belong to the compressional wave that is critically refracted by a higher velocity layer at some depth beneath the surface, which may be bedrock or some other rigid layer. If a line is fit to these arrival times, the inverse of its slope (in m/s) is the apparent velocity of the critically refracted wave. Extrapolating this line to an offset distance of 0 gives the intercept time, which is used along with the direct and refracted velocities to calculate the depth of the refractor. Arrivals in the reverse direction can be interpreted similarly, but calculated velocities and intercept times may differ from those calculated in the forward direction.

Rather than qualitatively choosing arrival-time layer assignments by viewing a time-versus-distance plot (fig. 33), velocity-versus-distance and intercept-time-versus-distance relationships allow rigorous definition of layer assignments for forward- and reverse-propagation directions (figs. 34 and 35). By calculating best-fit velocities progressively (gradually increasing the offset

54

Table 4. Summary of refraction data collected at the Pickle Research Campus and the Jacksboro MLS site. Velocity, depth, and apparent dip calculated using the slope-intercept method (Palmer, 1986).

	Pickle Research Campus		Jacksboro MLS site
Forward direction	West to east		South to north
Shot sequence	PRC SPH1	PRC SPH2	Jacksboro SPH1
Source surface	Shoulder	Pavement	Pavement
Sensor surface	Shoulder	Shoulder	Pavement
Layer 1 velocity (m/s)			
Forward	499.5	602.2	584.5
Reverse	506.8	475.2	556.0
Calculated	503.1	531.2	569.9
Layer 2 velocity (m/s)			
Forward	3,795.6	3,475.6	2,083.7
Reverse	2,911.4	3,042.4	3,546.3
Calculated	3,294.5	3,244.4	2,620.6
Refractor intercept time (s)			
Forward	0.0089	0.0074	0.0066
Reverse	0.0087	0.0073	0.0109
Calculated layer 1 thickness (m)	2.26	2.00	1.92
Apparent refractor dip (degrees)	1.2 west	0.6 west	3.3 north
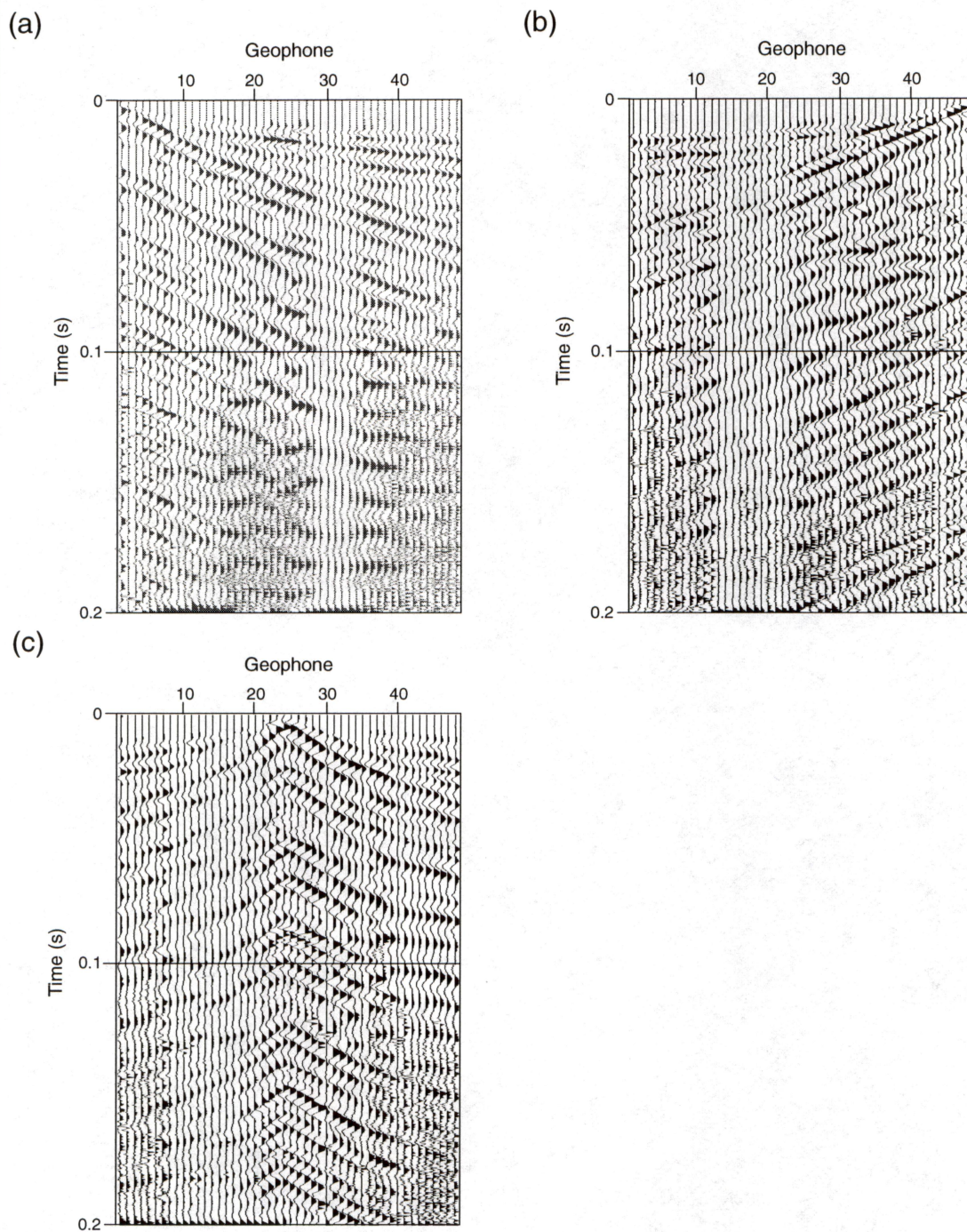
Figure 32. Field records from refraction test PRC SPH1 using a soil-probe hammer as a seismic source. Source was located on the shoulder of PRC Road D at the (a) west end, (b) east end, and (c) center of the recording spread. Records displayed with a 125-Hz low-cut filter and time-varying gain (20-ms window) applied. Geophone spacing is 0.3 m.

Figure 33. First-arrival times for refraction test PRC SPH1 for forward- (eastward-) and reverse-(westward-) propagating waves.

Figure 34. (a) Velocity and (b) intercept plots for forward data from refraction test PRC SPH1. Velocities and intercepts (black boxes) calculated from arrivals at geophones located between the source and progressively increasing source–receiver distances are used to pick the optimal velocity and offset range for arrivals assigned to the direct wave. Velocities and intercepts (open boxes) calculated from arrivals at geophones located between the maximum source–receiver distance and progressively decreasing source–receiver distances are used to pick the optimal velocity, intercept time, and offset range for arrivals assigned to the critically refracted wave.

58

(a)

(b)

Figure 35. (a) Velocity and (b) intercept plots for reverse data from refraction test PRC SPH1. Velocities and intercepts (black boxes) calculated from arrivals at geophones located between the source and progressively increasing source–receiver distances are used to pick the optimal velocity and offset range for arrivals assigned to the direct wave. Velocities and intercepts (open boxes) calculated from arrivals at geophones located between the maximum source–receiver distance and progressively decreasing source–receiver distances are used to pick the optimal velocity, intercept time, and offset range for arrivals assigned to the critically refracted wave.

59

range included in the calculation), the effect of changing the layer assignments can be quantified and the optimal offset range can be chosen (figs. 34a and 35a). Similarly, the effect of changing offset ranges on calculated intercept times can be assessed (figs. 34b and 35b). Ideally, cutoff distances between arrivals assigned to the direct wave and arrivals assigned to the critically refracted wave can be consistently chosen in this manner.

In the forward direction, calculated velocities for arrivals between the source and increasingly distant geophones (fig. 34a) increase to about 500 m/s by 1-m offset and remain near that velocity to an offset distance of 3 m. Including arrival times from more distant geophones in the velocity calculation causes the velocities to progressively increase with distance, suggesting that only arrivals between the source and 3 m belong to the direct arrival. This interpretation is confirmed by calculating zero-offset intercept times (fig. 34b), which begin increasing from the expected value of 0 s when arrivals from geophones at source–receiver distances greater than 3 m are included in the calculation. By assigning all arrivals at offsets of 3 m or less to the direct wave, a layer 1 velocity of 500 m/s is calculated (table 4).

To make layer 2 assignments in a two-layer setting such as that evident from the PRC SPH1 shot records and arrival times (figs. 32 and 33), velocity and intercept time can be calculated using arrival times from geophones between the maximum source–receiver distance and those progressively closer to the source. For PRC SPH1 forward data, calculated velocities reach a maximum when arrivals at geophones at distances greater than about 6 m are included in the calculation (fig. 34a). Calculated intercept times increase with increasing minimum source–receiver distance (fig. 34b), suggesting that arrivals at geophones less than about 6 m from the source belong to the direct wave or an intermediate refractor. Using arrival times from geophones at distances greater than 6 m results in a calculated apparent velocity of 3,796 m/s and an intercept time of 0.0089 s (table 4) for the forward data.

For seismic energy propagating from east to west (reverse data), time and distance plots (fig. 33) suggest a crossover distance separating direct from refracted arrivals of near 6 m. Calculated velocities for arrivals at geophones located nearest the source increase to 500 m/s by a

distance of 1 m from the source, remaining at that velocity to a maximum source–receiver distance of 5 m (fig. 35a). Intercept times, which should be zero for direct-wave arrivals, begin increasing as source–receiver distances increase beyond 5 m (fig. 35b). Non-zero intercepts for the reverse data suggest either a slight delay (<0.001 s) between the source impact and the onset of recording, or the presence of a very shallow, low-velocity refractor. The velocity calculated for layer 1 in the reverse direction is 507 m/s, only slightly higher than that calculated for the forward direction (table 4).

The apparent velocity of the critically refracted arrival reaches a plateau when arrivals from geophones beyond 7 m from the source are included in the velocity calculation (fig. 35a). Higher velocities calculated for greater threshold distances suggest that arrivals from deeper, higher velocity layers have been included in the analysis. Using 7 m as the cutoff distance, the apparent velocity of the critically refracted wave is 2,911 m/s. Its extrapolated intercept time is 0.0087 s (table 4).

To use the slope-intercept method (Palmer, 1986) to calculate refractor depth beneath the shoulder of Road D, we must know apparent velocities for the direct and critically refracted arrivals in the forward and reverse directions and the intercept times for the critically refracted arrivals. Using the values mentioned above, we calculate the true direct-wave velocity (layer 1) to be 503 m/s, the true layer 2 velocity to be 3,295 m/s, and the thickness of layer 1 to be 2.26 m (table 4). The interface between layers 1 and 2 has an apparent dip of 1.2° westward. Calculated depths to layer 2 are 2.27 m below at the west end and 2.21 m at the east end of the recording spread (fig. 36a).

Refraction Experiment PRC SPH2

The site and acquisition parameters are the same for this experiment as they were for PRC SPH1 (tables 2 and 4), except that the soil-probe hammer was offset from the receiver spread on the paved road rather than being on the unpaved shoulder (fig. 4). The geophones remained embedded in the shoulder.
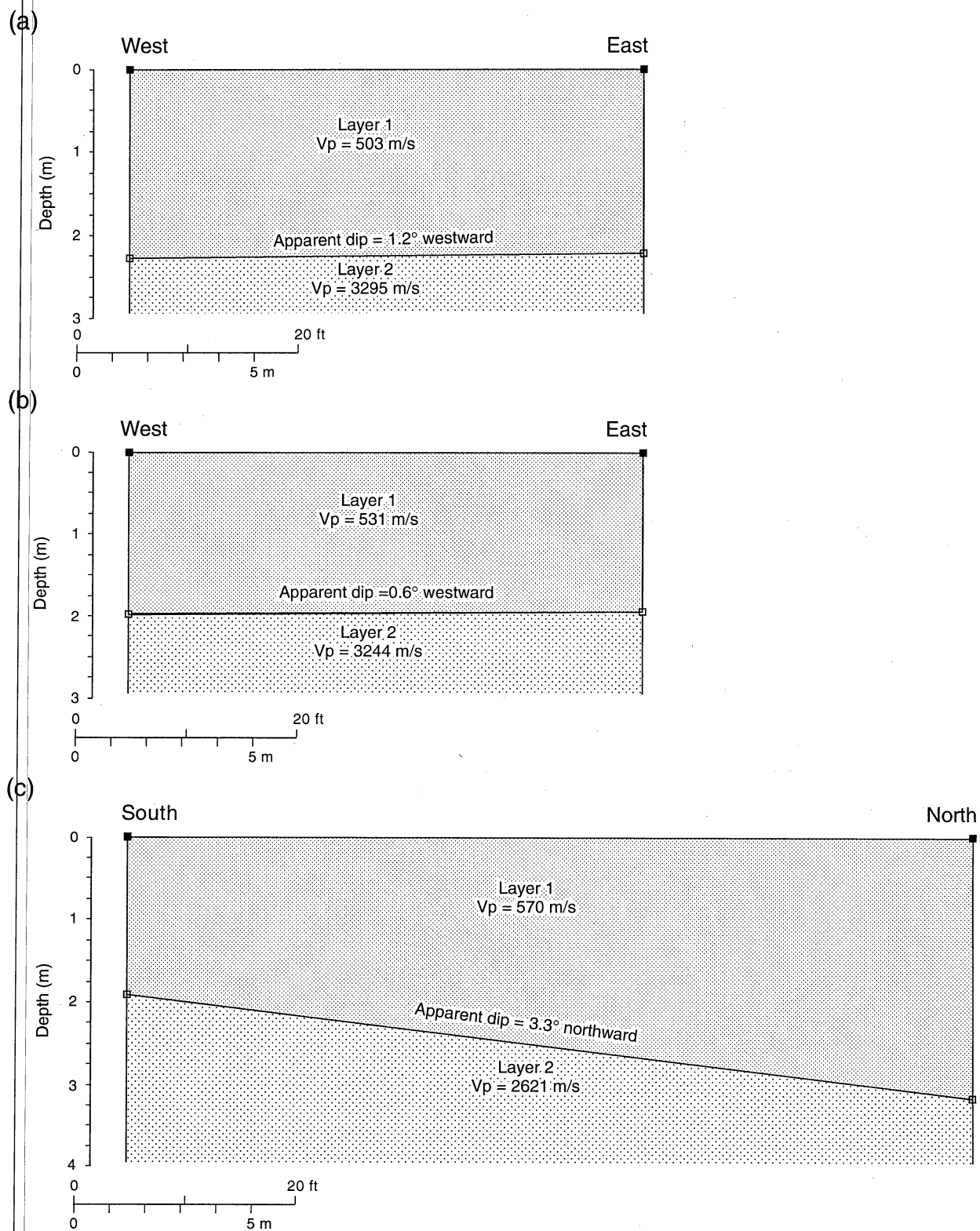
Figure 36. Calculated layer velocities and thicknesses and apparent dips of layer interfaces for refraction tests (a) PRC SPH1, (b) PRC SPH2, and (c) Jacksboro SPH1.

62

Filtered and amplified ground motion recorded by the geophones with the source located at the west end, east end, and center of the recording spread (fig. 37) is similar to that recorded for experiment PRC SPH1. Recorded wave types include surface waves and direct, critically refracted, and reflected compressional waves. The first ground motion reaches the geophones within 15 ms of the impact of the source on the pavement. These first arrivals in the forward- and reverse-propagation directions are assigned to the direct wave between the source position and a point about 8 m from the source, and to the critically refracted wave at source–receiver distances longer than about 8 m (fig. 38). A line extending through the arrivals assigned to the direct wave passes near the intersection of the axes, whereas a line extending through the critically refracted arrivals has a nonzero intercept time.

Apparent velocities and intercept times necessary for calculating layer velocities and thicknesses were determined using velocity and intercept plots. For forward data, in which the source is west of the recording geophones, apparent velocities remain near 500 m/s and intercept times near 0 s when geophones between the source and a distance as great as 6 m are included in the calculation (fig. 39a and b). Including geophones at greater distances causes the calculated apparent velocity and intercept time to increase, suggesting that the direct wave is the first arrival only out to a distance of about 6 m. By progressively increasing the minimum source–receiver distance, calculated apparent velocities increase from about 1,000 m/s using all geophones to about 3,500 m/s using geophones greater than 7 m from the source (fig. 39a). Intercept times are between 0.007 and 0.008 s where minimum distances are between 6 and 10 m (fig. 39b), suggesting that arrivals at 7 m and greater source–receiver distance can be attributed to the first critically refracted wave.

For reverse data, in which the source is east of the recording geophones, apparent velocities reach 500 m/s using arrival times measured at geophones between the source and a distance of 1.5 m (fig. 40a). Apparent velocities gradually increase when geophones beyond a 2-m source–receiver distance are included in the calculation. Intercept times calculated for the near-source geophones reach a minimum of near -0.001 s when geophones closer than 2 m from the

(a)

(b)
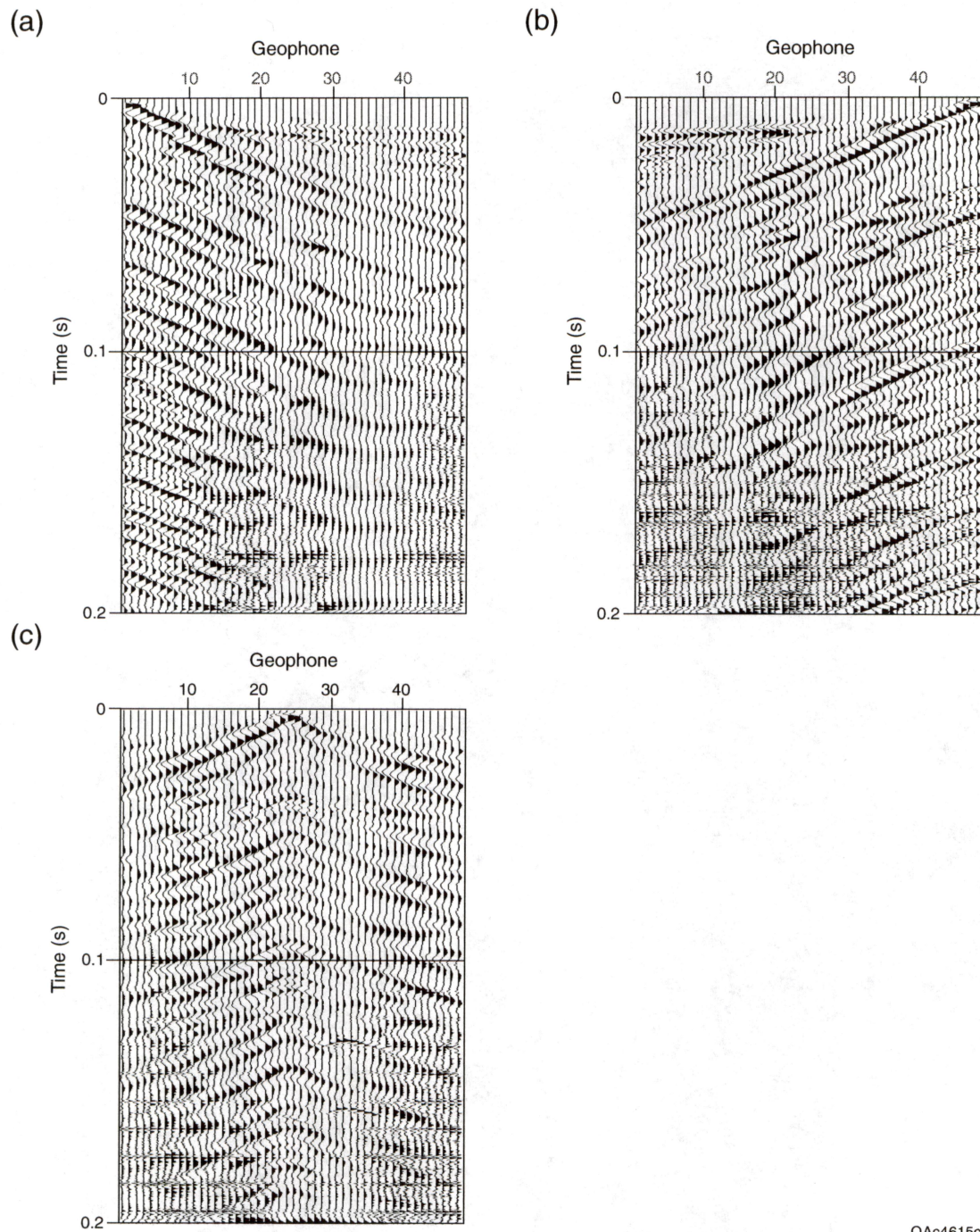
(c)

Figure 37. Field records from refraction test PRC SPH2 using a soil-probe hammer as a seismic source. Source was located on the pavement of PRC Road D at the (a) west end, (b) east end, and (c) center of the recording spread. Records displayed with a 125-Hz low-cut filter and time-varying gain (20-ms window) applied. Geophone spacing is 0.3 m.
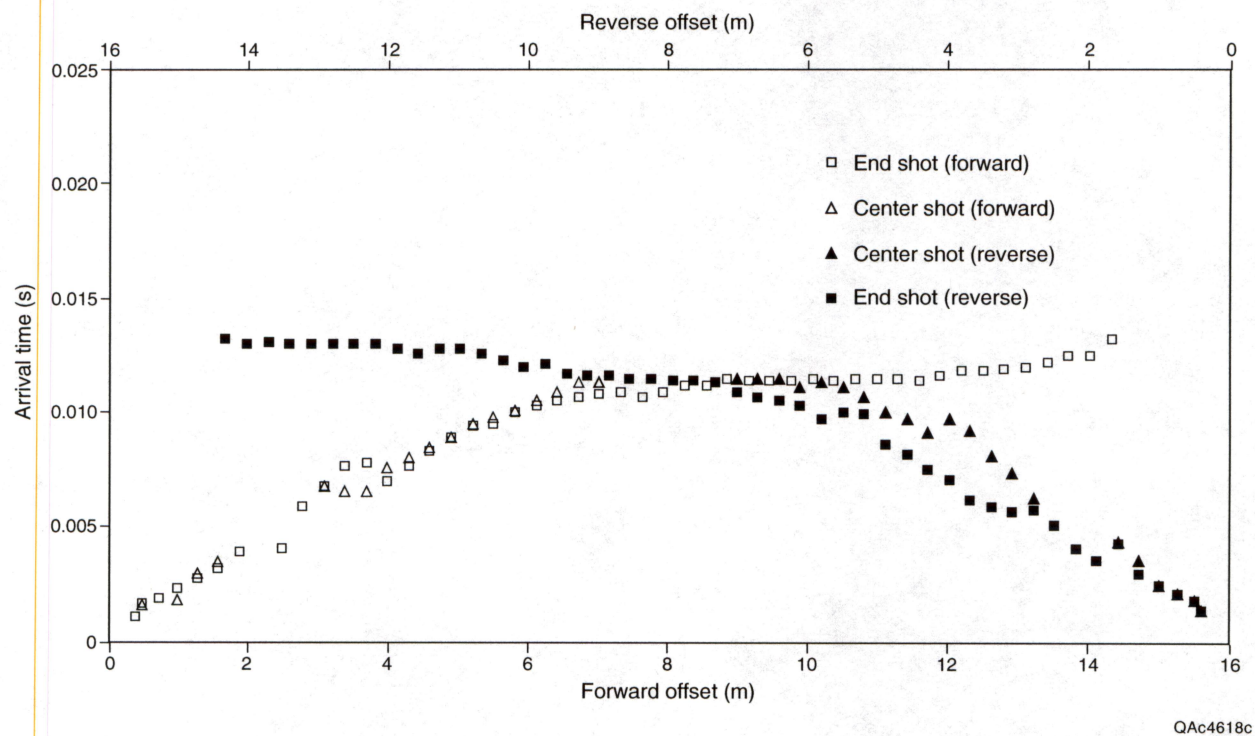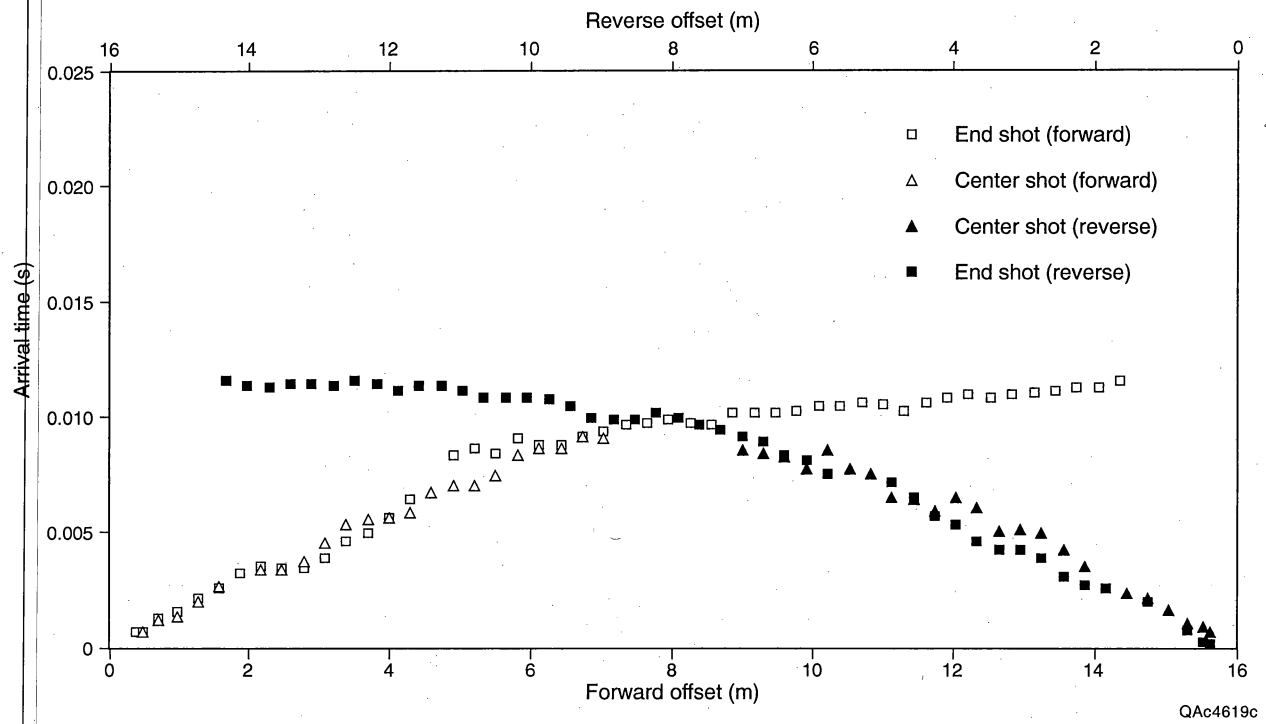
Figure 38. First-arrival times for refraction test PRC SPH2 for forward- (eastward-) and reverse-(westward-) propagating waves.
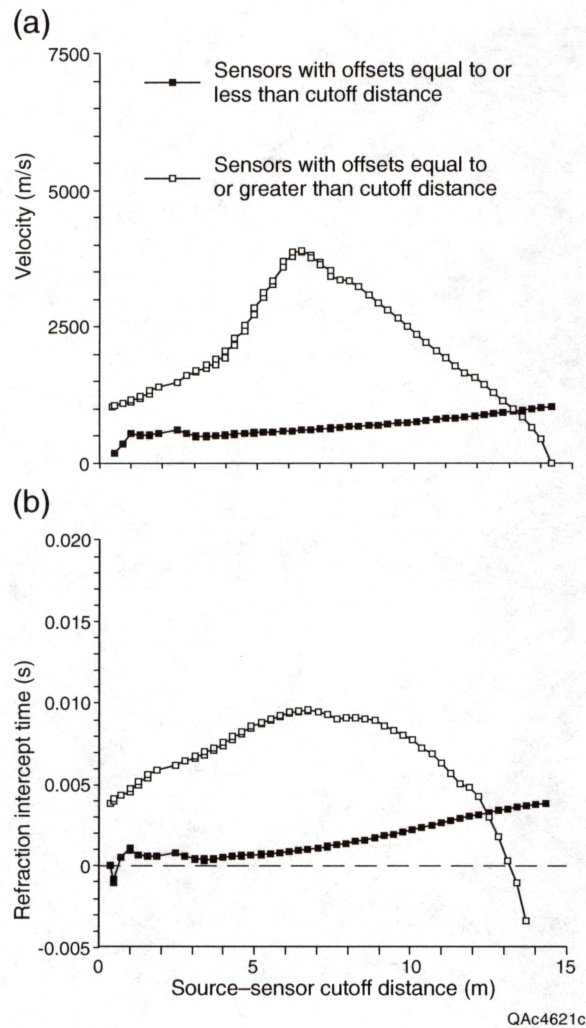
Figure 39. (a) Velocity and (b) intercept plots for forward data from refraction test PRC SPH2. Velocities and intercepts (black boxes) calculated from arrivals at geophones located between the source and progressively increasing source–receiver distances are used to pick the optimal velocity and offset range for arrivals assigned to the direct wave. Velocities and intercepts (open boxes) calculated from arrivals at geophones located between the maximum source–receiver distance and progressively decreasing source–receiver distances are used to pick the optimal velocity, intercept time, and offset range for arrivals assigned to the critically refracted wave.
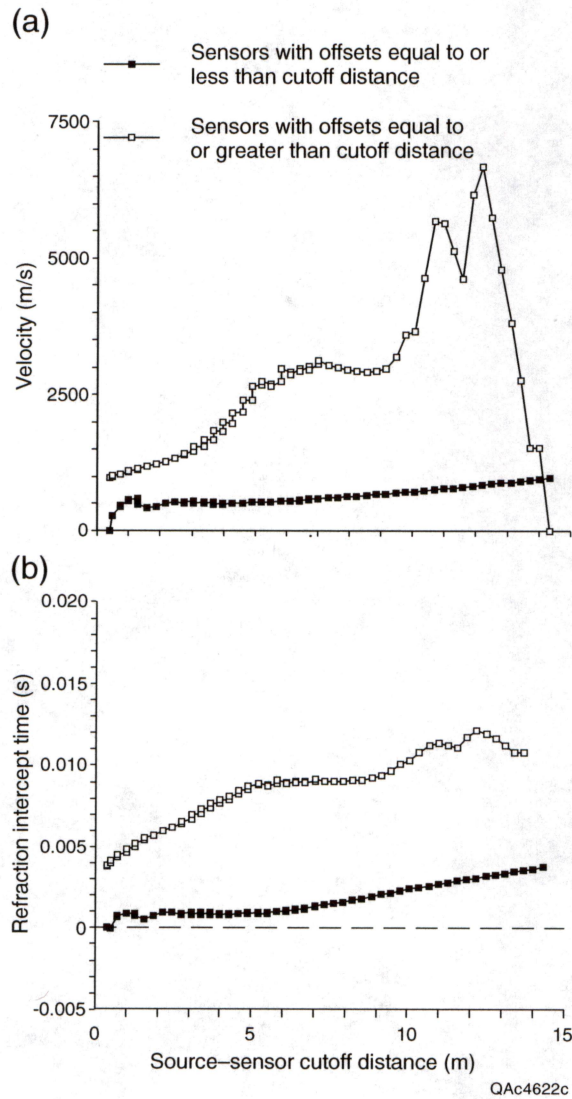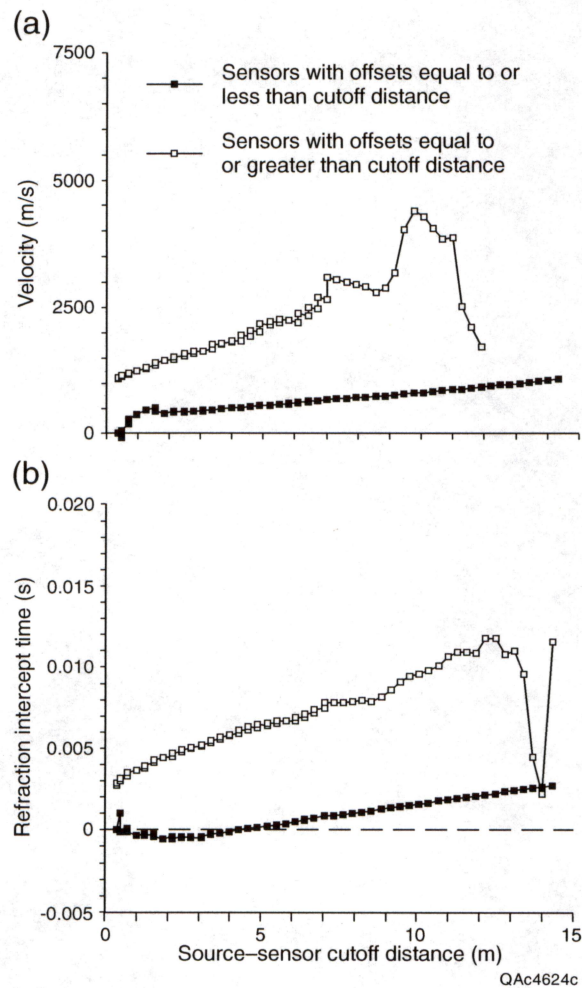
Figure 40. (a) Velocity and (b) intercept plots for reverse data from refraction test PRC SPH2. Velocities and intercepts (black boxes) calculated from arrivals at geophones located between the source and progressively increasing source–receiver distances are used to pick the optimal velocity and offset range for arrivals assigned to the direct wave. Velocities and intercepts (open boxes) calculated from arrivals at geophones located between the maximum source–receiver distance and progressively decreasing source–receiver distances are used to pick the optimal velocity, intercept time, and offset range for arrivals assigned to the critically refracted wave.

67

source are included (fig. 40b), suggesting either inconsistent arrival picks or a late recording onset. Using arrival times at all geophones, the calculated apparent velocity is near 1,000 m/s (fig. 40a). Apparent velocities and intercept times increase as the minimum source–receiver distance increases, reaching a minor plateau at about 3,000 m/s and between 0.007 and 0.008 s when geophones at distances greater than 7 to 9 m are included (figs. 40a and b).

The velocity calculated for the direct arrival is 531 m/s, which is the velocity of layer 1 (table 4). Because the interface between layer 1 and layer 2 has a small apparent dip to the west, the apparent layer 2 velocity is higher in the forward direction (eastward propagation) than it is in the reverse direction (westward propagation). Layer 2 velocity, which represents the propagation speed of the critically refracted wave, is calculated to be 3,244 m/s, similar to that obtained in experiment PRC SPH1 (table 4). Using the intercept times of 0.0074 s at the west end of the spread and 0.0073 s at the east end of the recording spread, depths to layer 2 are 1.99 m at the west end and 1.97 m at the east end (fig. 36b)

Interpreted Strata

Measured layer 1 compressional-wave velocities of about 500 m/s are within the 300 to 900 m/s range reported for dry, unconsolidated material (Press, 1966; Wylie, 1969), suggesting that layer 1 consists largely of road base and residual or surficial sediments above the bedrock contact. Higher velocities measured for layer 2, reaching nearly 3,250 m/s, are consistent with those expected for relatively soft limestone (Press, 1966) such as the Cretaceous Austin Chalk. The Austin Chalk is the mapped geologic unit at the site (Garner and Young, 1976) and is exposed in nearby ditches.

Jacksboro MLS Site

In May 1998, we acquired seismic-refraction data on U. S. Highway 281 south of Jacksboro, Texas (figs. 1 and 5; table 2). Data were acquired with seismic sources and geophones on the

southbound inner-lane pavement at a former location of TxDOT's MLS. Geologic maps of the site show the Pennsylvanian Ranger Limestone as the surface geologic unit (Hentz and Brown, 1987); a thin veneer of surficial sediments mantles the Ranger Limestone in fields adjacent to the highway. An FWD and the soil-probe hammer were both tested as on-pavement sources, but the FWD did not produce a sharp trigger impulse for the seismograph. This caused unacceptably large errors in establishing zero time.

Effect of Digital Filtering

Data quality is generally similar at the Jacksboro MLS and PRC sites (compare figs. 41d and 32a). Noise levels are somewhat higher at the Jacksboro site because of increased road traffic and poorer coupling between the ground and the geophones, but data quality is sufficient to detect direct and critically refracted arrivals. Accurate picking of arrival times is enhanced by digitally filtering and amplifying the recorded signals (fig. 41). Low-frequency and high-amplitude surface waves dominate the field record without filtering or amplification (fig. 41a), but direct and critically refracted arrivals are apparent in the record. Application of time-varying gain balances the amplitude along each segment of a geophone trace and makes first breaks easier to see (fig. 41b), yet low-frequency seismic noise visible in the early part of the record makes accurate picking of arrival times difficult. Applying a digital filter that removes seismic energy with frequencies below 125 Hz clarifies the field record, removes much of the low-frequency noise, and reveals the presence of a weaker, earlier arrival than the critically refracted arrival evident in the unfiltered record (fig. 41c). Balancing the amplitude of the filtered record using time-varying gain does not greatly aid the picking of first breaks, but does reveal the presence of reflected seismic energy later in the field record (fig. 41d). Filtered and amplified field records were used for refraction analysis at the Jacksboro MLS site, where vertical ground motion was detected after seismic impulses were generated at the south end, north end, and center of the recording spread (fig. 42).
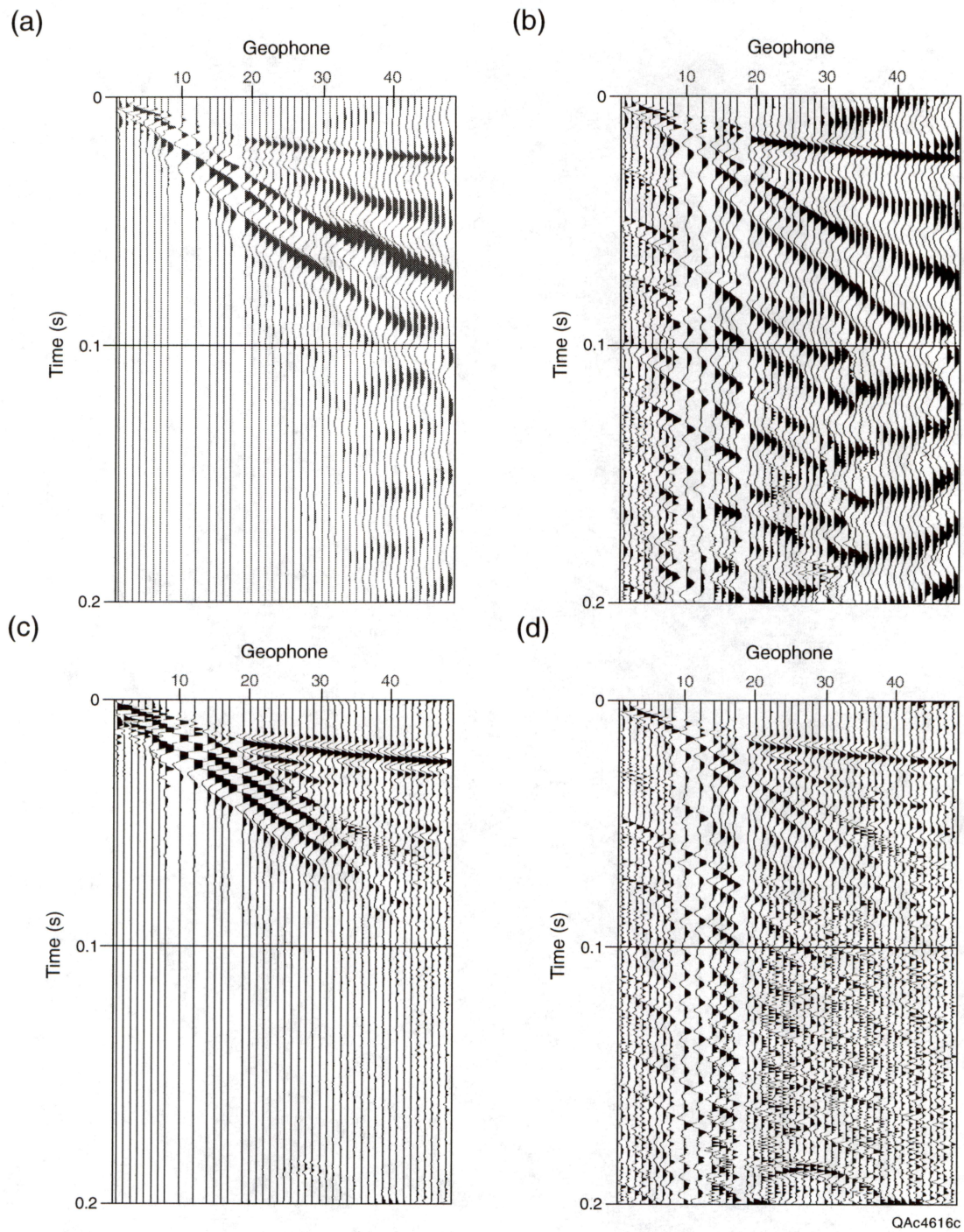
Figure 41. Effect of digital filtering and amplification on a field record from the Jacksboro MLS site using a soil-probe hammer as a seismic source. Record displayed with (a) neither digital filtering nor time-varying gain; (b) time-varying gain (20-ms window) but no digital filtering; (c) 125-Hz low-cut filter without time-varying gain; and (d) 125-Hz low-cut filter and time-varying gain (20-ms window) applied. Geophone spacing is 0.5 m.

70

(a)

(b)

(c)
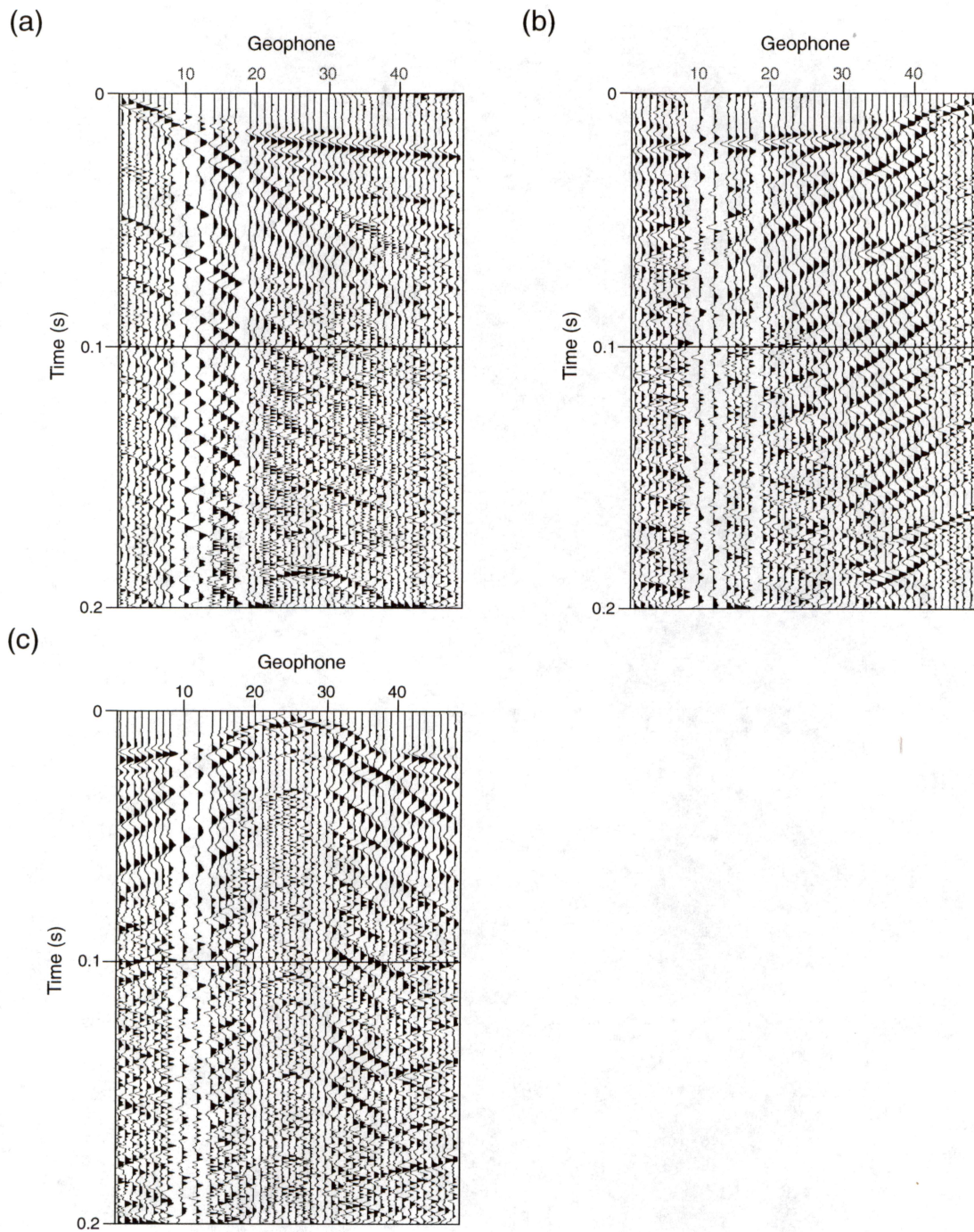
QAc4617c

Figure 42. Field records from refraction test Jacksboro SPH1 using a soil-probe hammer as a seismic source. Source and geophones were located on the pavement of U.S. Highway 281 at the (a) south end, (b) north end, and (c) center of the recording spread. Records displayed with a 125-Hz low-cut filter and time-varying gain (20-ms window) applied. Geophone spacing is 0.5 m.

Refraction Analysis

First-arrival times picked for the forward and reverse end shots and for the reverse part of the center shot form two groups, each with a linear trend (fig. 43). For the forward data, in which the seismic source was south of the recording geophones, near-source geophones (5 m or less from the source) record direct seismic waves that have an apparent velocity of about 585 m/s (table 4; fig. 44a) and intercept the time axis at 0 s (fig. 44b). Including geophones at longer source–receiver distances results in increasing apparent velocities and nonzero intercept times. The critically refracted wave is the first arrival at source–receiver distances greater than approximately 7 m. Including all geophones 7 m and farther from the source in the velocity and intercept calculation, the apparent velocity of the critically refracted wave is 2,084 m/s (fig. 44a; table 4) and its intercept time is 0.0066 s (fig. 44b).

For the reverse data, in which the source was north of the recording geophones, apparent velocity decreases as the maximum included source–receiver distance increases to about 6 m, remains relatively constant to a maximum included distance of about 9 m, and increases as geophones beyond a 9-m source–receiver distance are included (fig. 45a). Over this same distance range, intercept times decrease to near zero when arrival times at geophones at source–receiver distances less than 5 to 9 m are included (fig. 45b). The optimal maximum distance for arrivals attributed to the southward-propagating direct wave is 7 m, resulting in an apparent direct-wave velocity of 556 m/s (table 4).

As the minimum source–receiver distance decreases for reverse data, apparent velocity and intercept times reach a plateau when arrival times at geophones located at least 7 m from the source are included (fig. 45a and b). Using 7 m as the minimum source-receiver distance for inclusion in the calculation, apparent velocity of the arrivals attributed to the southward-propagating, critically refracted wave is 3,546 m/s and the intercept time is 0.0109 s (table 4).

True velocities derived from the forward and reverse data (table 4) are 570 m/s for the direct wave (layer 1) and 2,621 m/s for the critically refracted wave (layer 2). The interface between

72
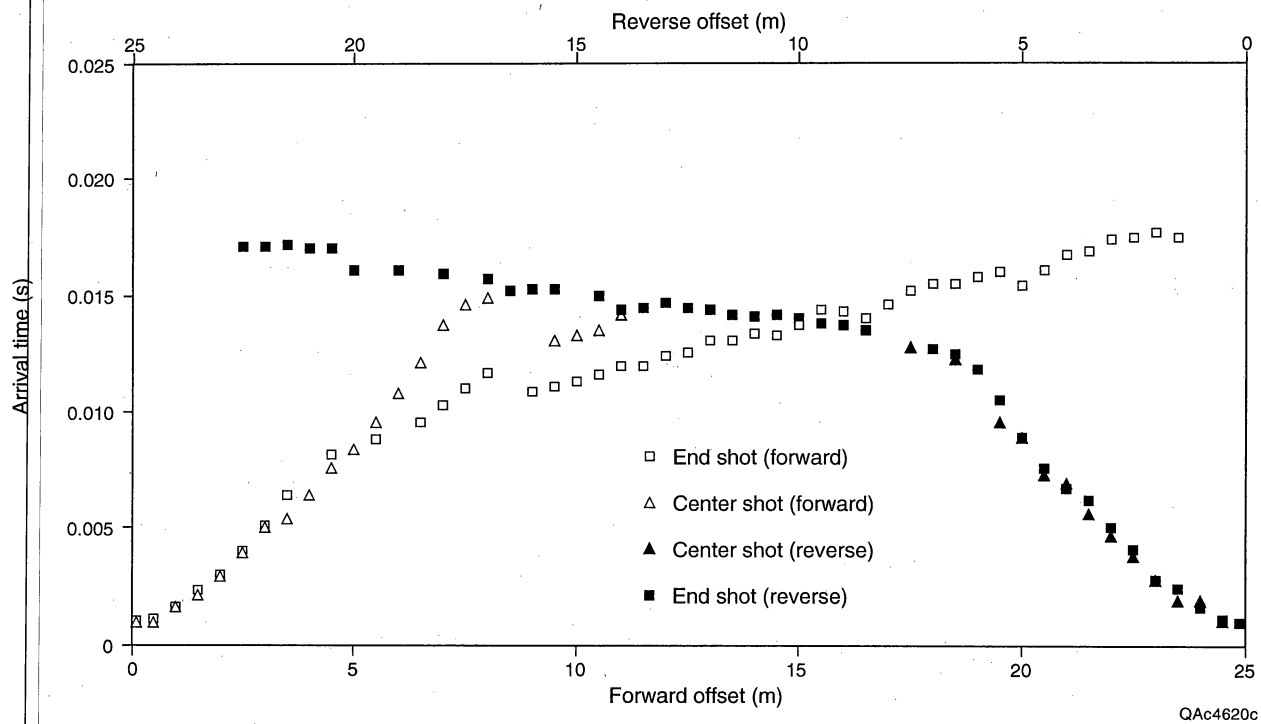
Figure 43. First-arrival times for refraction test Jacksboro SPH1 for forward- (northward-) and reverse- (southward-) propagating waves.

73

(a)

(b)
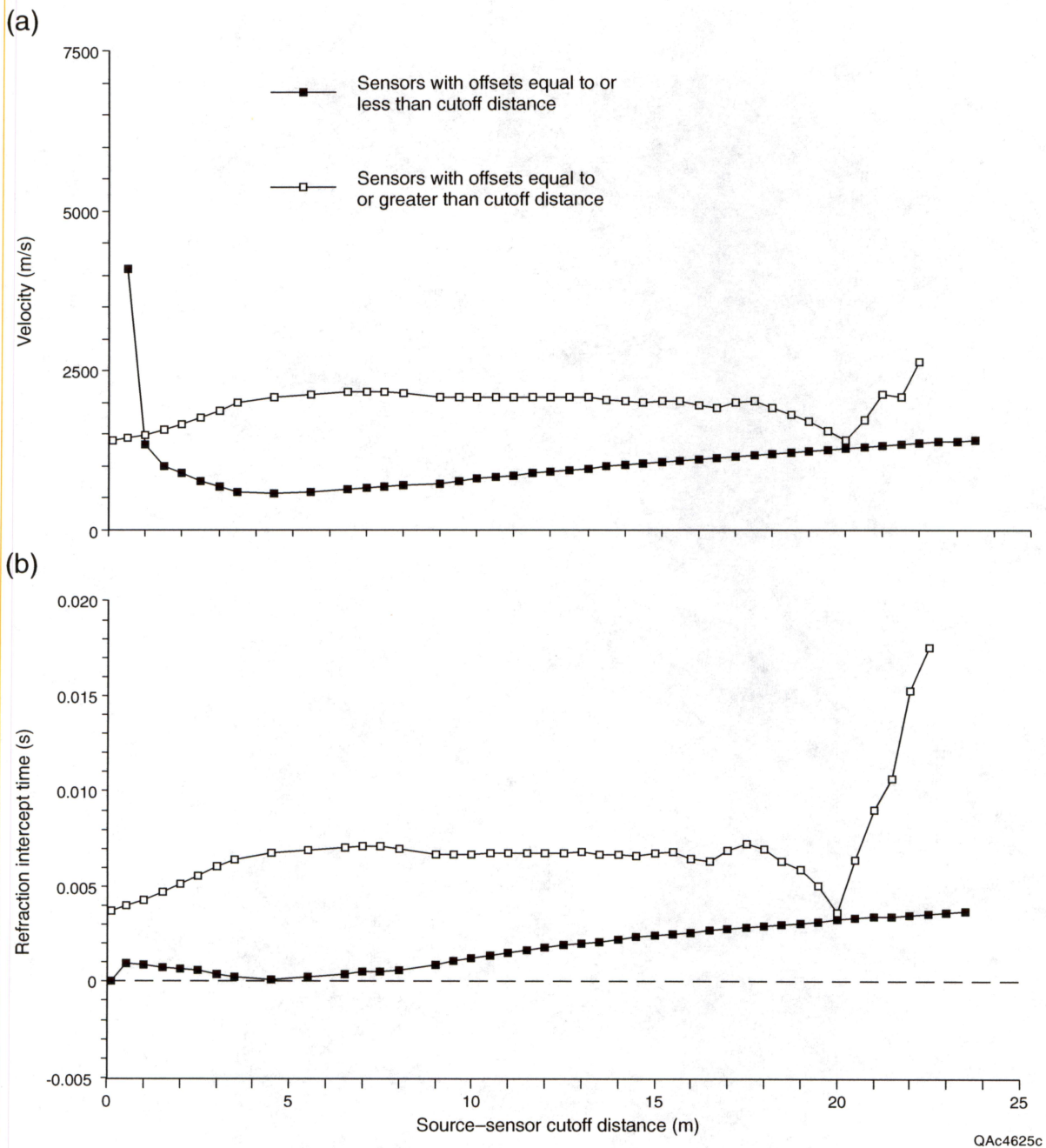
Figure 44. (a) Velocity and (b) intercept plots for forward data from refraction test Jacksboro SPH1. Velocities and intercepts (black boxes) calculated from arrivals at geophones located between the source and progressively increasing source–receiver distances are used to pick the optimal velocity and offset range for arrivals assigned to the direct wave. Velocities and intercepts (open boxes) calculated from arrivals at geophones located between the maximum source–receiver distance and progressively decreasing source–receiver distances are used to pick the optimal velocity, intercept time, and offset range for arrivals assigned to the critically refracted wave.
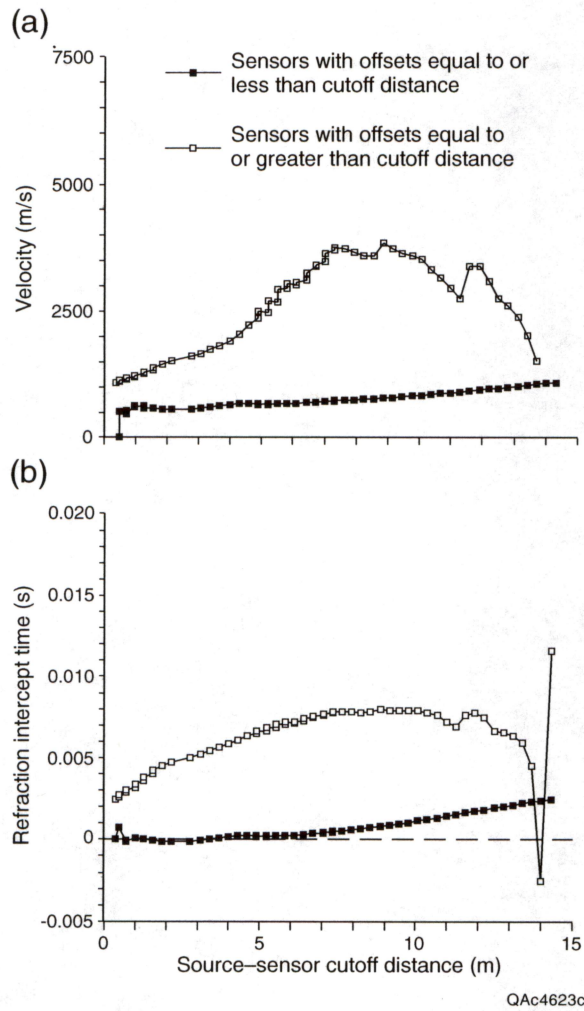
74
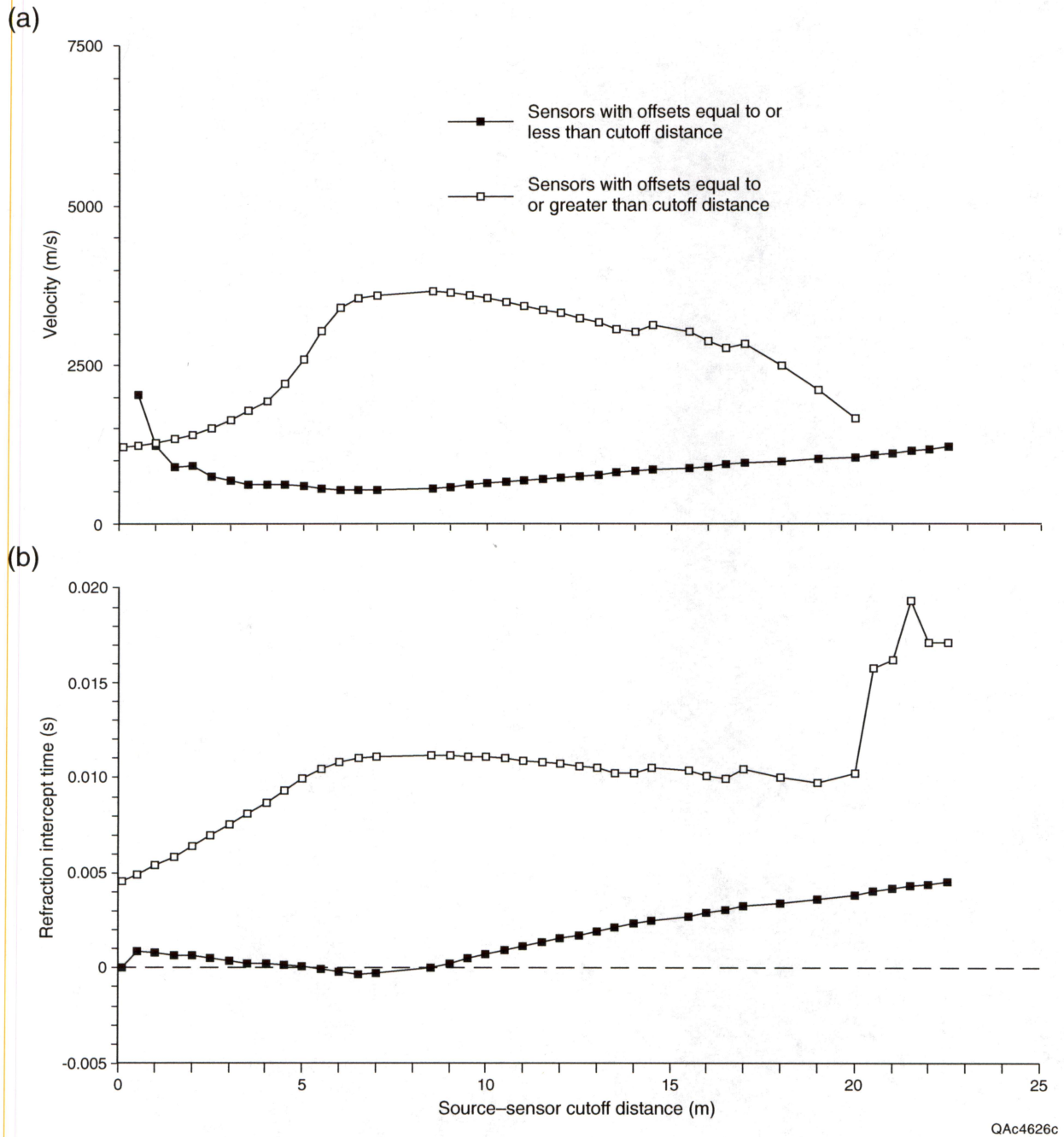
Figure 45. (a) Velocity and (b) intercept plots for reverse data from refraction test Jacksboro SPH1. Velocities and intercepts (black boxes) calculated from arrivals at geophones located between the source and progressively increasing source–receiver distances are used to pick the optimal velocity and offset range for arrivals assigned to the direct wave. Velocities and intercepts (open boxes) calculated from arrivals at geophones located between the maximum source–receiver distance and progressively decreasing source–receiver distances are used to pick the optimal velocity, intercept time, and offset range for arrivals assigned to the critically refracted wave.

layers 1 and 2 has an apparent dip of about 3° northward and a depth of 1.92 m calculated using the slope–intercept method (Palmer, 1986). Using the true velocities and the intercept times at each end of the recording spread, we obtain layer 2 depth estimates of 1.9 m at the south end and 3.2 m at the north end (fig. 36c).

Interpreted Strata

Layer 1 velocities at the Jacksboro site are relatively low, similar to those determined at the PRC site (table 4). These velocities are typical of dry, unconsolidated soil and sediment commonly found overlying more rigid bedrock in many geologic settings. At the Jacksboro site, layer 1 probably represents road base, underlying surface deposits, and perhaps weathered bedrock. Layer 2 velocities at the Jacksboro MLS site, though lower than those measured at the PRC site, are within the range reported for soft limestone (Press, 1966). This is consistent with the geologic map of the area, which shows the Pennsylvanian Ranger Limestone to be the bedrock unit (Hentz and Brown, 1987).

DISCUSSION

The relationship between bedrock and FWD response at long offsets that is suggested by average deflections by county is supported by more detailed analysis of FWD response along individual highway segments in four of the major physiographic regions of Texas. Although we can show that more rigid rock types such as limestones and igneous and metamorphic rocks have statistically lower deflections at the outermost detector than do less rigid sedimentary rock types, there is enough scatter in FWD deflections for a given rock type to make it difficult to predict rock type reliably from the outermost deflections alone. Better discrimination of rock types is obtained by comparing deflection ratios that tend to normalize road construction differences; in this study, W2:W7 ratios were highest for rigid rock types and lowest for materials with low characteristic stiffness, such as sandstones, mudstones, and unconsolidated sediments.

76

To develop a method that should help resolve the ambiguity of whether lower W7 deflections and higher W2:W7 ratios for highways over rigid rocks versus highways over soft rocks are due to differences in material properties of the mapped geologic units or to systematic differences in depth to bedrock among rock types, we collected seismic-refraction measurements at two sites in north and central Texas. These tests show that refraction data can be collected in highway settings, the FWD can serve as a seismic source, and estimates of bedrock depth and interpretations of bedrock type can be made using the refraction data. The success of this method will allow us to directly compare observed deflection, depth to bedrock, and mapped geologic unit and determine the relative influence of bedrock rigidity and bedrock depth on FWD response. It may be that bedrock rigidity accounts for the differences in average deflection calculated for the outermost FWD detector, and that site-to-site variations in bedrock depth over a given rock type account for the large variance observed for that rock type along a roadway.

Adaptation of the seismic-refraction method to highway settings shows promise in addressing the ambiguous influence of bedrock type and depth on highway deflections. We have demonstrated that (1) a small impulsive source and the FWD itself can be used as seismic sources on the shoulder and pavement of roads, and (2) direct-wave and critically refracted-wave arrivals, both necessary for velocity and depth calculations, are recorded by geophones placed in the shoulder or on the pavement. Arrival-time measurements acquired at two test sites have been successfully converted to estimates of compressional-wave velocities for the surface layer and underlying bedrock, apparent dip of the bedrock surface, and bedrock depth.

Difficulties encountered with the refraction method in a highway setting include deployment of the array of seismic detectors, operation of the seismic source, and accurate first-arrival picks on the seismic records. Geophones with attached spikes offer the best coupling with the surface, but can only be used on road shoulders where it may be difficult to insert the spikes fully into hard-packed material. Plate-mounted geophones can be laid rapidly and directly on pavement, but the surface coupling may be degraded. At the two sites tested, both geophone arrangements yielded acceptable data for refraction analysis. Further improvement in detector deployment may be

77

realized by using hydrophone arrays, in which seismic detectors are mounted at set intervals within a fluid-filled tube. The tube can then be rolled onto the pavement without needing to measure the geophone spacing at each site.

Because measurements might be made on roads and because calculations of true velocities and layer dips require source operation at both ends of the recording spread, the source chosen for refraction measurements should be nondestructive, rapidly operated, and easily moved. In our tests, the modified soil-probe hammer met these requirements, provided a reliable zero-time break for the seismograph to begin recording, and provided sufficient seismic energy for the relatively short source–receiver distances that are typical of most highway investigations. Longer arrays appropriate for bedrock depths greater than 4 or 5 m might require a stronger seismic impulse. The FWD provides a stronger seismic impulse and produces interpretable direct and critically refracted arrivals, but we have had difficulty obtaining a reliable zero-time break to begin seismograph recording. This is a problem that should be readily solved by using FWD-mounted electronic switches.

As is evident from the PRC and Jacksboro MLS data, accurate first-arrival picks are required to calculate bedrock depth accurately. Differing first arrivals may be interpreted by varying the display parameters of the seismic record, causing different bedrock depths to be calculated from the same record. At these two sites, using a digital low-cut filter to remove seismic noise below 125 Hz and a short-window (20 ms), time-varying gain produced the most interpretable seismic record. Records without these display adjustments might induce an interpreter to select later, stronger arrivals as a first arrival and inaccurately choose an arrival time for a geophone where seismic noise interferes with the first arrival.

IMPLEMENTATION

Results from this project suggest some possible implementations of the geology–FWD relationship and the demonstrated capabilities of the seismic refraction method:

1. Create a roadway data base with geologic unit, major rock type, average W7 deflection, and the observed range in W2:W7 deflection ratio as fields. This data base would allow users to enter a highway location and obtain mapped rock type for that location, as well as the expected influence that bedrock type has on FWD deflections. This would give the highway engineer a preliminary check on new FWD data and would provide an approximation of anticipated bedrock rigidity that would aid the deflection-series interpretation.

2. Use existing FWD data to define averages and ranges of FWD response for all mapped geologic units in the state, then use these data in the design and construction of new highway segments. Once a roadway alignment is known, the statistical FWD response for the geologic units mapped along the roadway can be used to suggest bedrock properties, control-test boring locations, and help make highway design decisions.

3. Collect FWD data at closely spaced intervals along roadways over geologic units that are susceptible to sinkhole development or other rapid lateral change in physical properties. W7 deflections should increase and W2:W7 ratios should decrease from a hard limestone substrate to sinkholes where limestone has been removed and voids filled with softer materials. This technique would also be useful in mapping alternating soft marls and hard limestones that are below the resolution of geologic maps in the Edwards Plateau region.

4. Modify the FWD to allow routine collection of deflections (as is currently done) and seismic-refraction data. While it is difficult to separate the influences of bedrock rigidity and bedrock depth with FWD data alone, tests with seismic-refraction equipment employing an FWD or other small, impulsive source suggest that bedrock depth and rigidity can be estimated from refraction data. These parameters, in turn, will allow better quantitative analysis of deflection series.

5. Use available FWD data, or combined FWD–refraction data, to improve geologic maps. This implementation will benefit all users of these maps, including those in transportation, construction, land-use planning, oil and gas exploration, mining, education, and materials

exploration. Deflections, bedrock depths, and seismic velocities of bedrock and overburden obtained from a combined FWD–refraction system would allow comparisons of observed values with expected values for mapped rock types, indicate areas where current mapping may need revision, and produce a better understanding of the distribution of geologic units over large areas of the state where surface exposures are limited.

CONCLUSIONS

The conclusions from this study of the relationship between bedrock type, depth, and FWD response are the following:

- FWD deflections at the outermost sensors correlate to mapped geologic units at the county average scale,

- at six test highway segments in four major physiographic regions, there is a statistical relationship between mapped geologic unit and FWD response,

- variance in FWD response within individual geologic units is large, making interpretation of geologic unit from FWD response alone uncertain,

- ratios of inner- and outer-detector deflections, such as W2:W7, partly normalize roadway construction differences and allow better rock-type discrimination than that obtained from W7 data alone,

- in general, highway segments constructed over relatively rigid bedrock units such as limestone, granite, and metamorphic rocks exhibit low average W7 deflections and high W2:W7 ratios, whereas highways constructed over softer bedrock units such as mudstone, sandstone, and unconsolidated sediments have high average W7 deflections and low W2:W7 ratios,

- from FWD data and mapped geologic units alone, we cannot determine whether the influence that bedrock type has on FWD response is due to bedrock rigidity or to systematic changes in bedrock depth among geologic units, and

80

- seismic-refraction data can be collected on or near roads to estimate bedrock depth and rigidity.

Continuing work on this project through the final project year will focus on developing and testing a seismic-refraction method optimized for data collection on roads and integrating seismic-refraction capability into existing FWD's. This will enable us to further quantify the relationship between mapped geologic units, bedrock rigidity, bedrock depth, and deflection series by acquiring FWD data and seismic-refraction data at sites that represent a variety of geologic and roadway types. The ultimate goal will be to determine the best way to obtain bedrock depth and rigidity information that will improve FWD analysis from geologic maps, FWD data, and seismic-refraction methods.

ACKNOWLEDGMENTS

REFERENCES

Barnes, V. E., Llano sheet: The University of Texas at Austin, Bureau of Economic Geology, Geologic Atlas of Texas, scale 1:250,000.

Brewton, J. L., Owen, F., Aronow, S., and Barnes, V. E., 1976a, Laredo sheet: The University of Texas at Austin, Bureau of Economic Geology, Geologic Atlas of Texas, scale 1:250,000.

Brewton, J. L., Owen, F., Aronow, S., and Barnes, V. E., 1976b, McAllen-Brownsville sheet: The University of Texas at Austin, Bureau of Economic Geology, Geologic Atlas of Texas, scale 1:250,000.

Brown, L. F. J., Goodson, J. L., Harwood, P., and Barnes, V. E., 1972, Abilene sheet: The University of Texas at Austin, Bureau of Economic Geology, Geologic Atlas of Texas, scale 1:250,000.

Bureau of Economic Geology, 1992, Geology of Texas: The University of Texas at Austin, Bureau of Economic Geology, scale 1:6,336,000.

Garner, L. E., and Young, K. P., 1976, Environmental geology of the Austin area; an aid to urban planning: The University of Texas at Austin, Bureau of Economic Geology Report of Investigations No. 86, 39 p.

Hentz, T. F., and Brown, L. F., Jr., 1987, Wichita Falls-Lawton sheet: The University of Texas at Austin, Bureau of Economic Geology, Geologic Atlas of Texas, scale 1:250,000.

Milsom, John, 1989, Field geophysics: New York, Open University Press, Milton Keynes, Geological Society of London Handbook, 182 p.

Palmer, Derecke, 1986, Refraction seismics: the lateral resolution of structure and seismic velocity, *in* Helbig, Klaus, and Treitel, Swen, eds., Seismic exploration: London, Geophysical Press, Handbook of Geophysical Exploration, v. 13, 269 p.

Press, Frank, 1966, Seismic velocities, *in* Clark, S. P., Jr., ed., Handbook of physical constants: The Geological Society of America Memoir 97, p. 195–218.

Proctor, C. V., Jr., Brown, T. E., McGowen, J. H., Waechter, N. B., and Barnes, V. E., 1974, Austin sheet: The University of Texas at Austin, Bureau of Economic Geology, Geologic Atlas of Texas, scale 1:250,000.

Telford, W. M., Geldart, L. P., Sheriff, R. E., and Keys, D. A., 1976, Applied Geophysics: Cambridge, Cambridge University Press, 841 p.

Wermund, E. G., Jr., 1996, Physiographic map of Texas: The University of Texas at Austin, Bureau of Economic Geology, scale 1:6,336,000.

Wylie, K. M., 1969, Seismic analysis: The Testing World, no. 22, p. 4–5.

APPENDIX A: TOPOGRAPHIC[1] AND GEOLOGIC[2] MAPS OF THE STUDY SITES

Site A: Texas 16, reference markers 220 to 264, Archer and Young Counties.

Topographic Maps	Reference Markers
Darnell Branch	220 to 228
Markley	229 to 236
Loving	237 to 239
Lake Eddleman	240 to 249
Graham	249 to 258
Ross Mountain	259 to 261, 264 to 265
Palo Pinto	262 to 263

Geologic Maps	Reference Markers
Wichita Falls–Lawton	220 to 261, 264 to 265
Abilene	262 to 263

Site B: Texas 16, reference markers 450 to 488, Llano and Gillespie Counties.

Topographic Maps	Reference Markers
Llano South	450 to 457
Oxford	458 to 466
Willow City	468 to 477
Fredericksburg East	478 to 487

Geologic Maps	Reference Markers
Llano	450 to 490

Site C: Texas 71, reference markers 528 to 542, Burnet County.

Topographic Maps	Reference Markers
Marble Falls	528 to 533
Round Mountain	533 to 534
Spicewood	535 to 543

Geologic Maps	Reference Markers
Llano	528 to 543

Site D: U.S. 290, reference markers 536 to 563, Blanco and Hays Counties.

Topographic Maps	Reference Markers
Monument Hill	535
Yeager Creek	536 to 543
Henly	544 to 553
Dripping Springs	554 to 560
Signal Hill	561 to 563

[1] U.S.G.S. 7.5-minute quadrangle map, 1:24,000 scale
[2] BEG geologic atlas map, 1° x 2°, 1:250,000 scale

Geologic Maps	Reference Markers
Llano	535 to 560
Austin	561 to 563

Site E: Texas 71, reference markers 590 to 598, Bastrop County.

Topographic Maps	Reference Markers
Webberville	590 to 592
Utley	593 to 596
Bastrop SW	597 to 598

Geologic Maps	Reference Markers
Austin	590 to 598

Site F: Texas 16, reference markers 758 to 804, Jim Hogg and Zapata Counties.

Topographic Maps	Reference Markers
McCambell Ranch	758 to 761
Armstrong Ranch	762 to 766
San Pablo Ranch	767 to 774
Randado	775 to 783
Escobas	784 to 792
Arroyo Huisache	793
Arroyo Veleño	794 to 802
Zapata	803 to 804

Geologic Maps	Reference Markers
Laredo	758 to 792
McAllen–Brownsville	793 to 804

APPENDIX B: AGE, LITHOLOGY, CONSTITUENTS, AND THICKNESS OF GEOLOGIC UNITS

Site A: Texas 16 between reference markers 220 and 264, Archer and Young Counties, Wichita Falls–Lawton (Hentz and Brown, 1987) and Abilene (Brown and others, 1972) geologic atlases.

Geologic unit	Symbol	Age	Major lithology	Minor lithology	Constituents[1]	Thickness (ft)	Notes
Alluvium	Qal	Quaternary	unconsolidated		sd, st, cl, gr	<30	
Markley	IPPm	Pennsylvanian–Permian	mudstone		st, cl		
Markley	IPPm-SS14	Pennsylvanian–Permian	sandstone	conglomerate	sd, gr	15 to 50	
Markley	IPPm-SS12	Pennsylvanian–Permian	sandstone	conglomerate, mudstone	sd, gr	30 to 60	
Markley	IPPm-SS11	Pennsylvanian–Permian	sandstone	conglomerate	sd, gr	10 to 30	
Markley	IPPm-SS10	Pennsylvanian–Permian	sandstone	conglomerate, mudstone	sd, gr	10 to 50	
Thrifty, Graham	IPtg	Pennsylvanian–Permian	mudstone		st, cl		
Ivan Limestone	IPi	Pennsylvanian–Permian	limestone			1 to 5	member of IPtg
Thrifty, Graham	IPtg-SS2	Pennsylvanian–Permian	sandstone	conglomerate	sd, gr	5 to 15	member of IPtg
Bunger Limestone	IPbu	Pennsylvanian–Permian	limestone			<4	member of IPtg
Gonzalez Creek Member	IPgc	Pennsylvanian–Permian	sandstone	shale, mudstone	sd, st, cl	10 to 50	member of IPtg

[1] gr=gravel; sd=sand; st=silt; cl=clay

Geologic unit	Symbol	Age	Major lithology	Minor lithology	Constituents	Thickness (ft)	Notes
Home Creek Limestone	IPhc	Pennsylvanian–Permian	limestone	sandstone, shale, conglomerate	sd, cl, gr	2 to 145	
Kisinger Sandstone	IPk	Pennsylvanian–Permian	sandstone	conglomerate	sd, gr	<140	member of IPhc
Ranger Limestone	IPr	Pennsylvanian–Permian	limestone	shale	cl	30 to 60	

Site B: Texas 16 between reference markers 450 and 488, Llano and Gillespie Counties, Llano geologic atlas (Barnes, 1981).

Geologic unit	Symbol	Age	Major lithology	Minor lithology	Constituents	Thickness (ft)	Notes
Alluvium	Qal	Quaternary	unconsolidated		gr, sd, st, cl	<35	
Fort Terrett Member	Kft	Cretaceous	limestone	dolomite		150 to 230	member of Ked
Hensell Sand	Kh	Cretaceous	unconsolidated	conglomerate	sd, st, cl, gr	<220	
Hickory Sandstone	Crh	Cambrian	sandstone		sd, st	275 to 470	
Younger granitic intrusives	pCy	Precambrian	granite				
Town Mountain Granite	pCtm	Precambrian	granite				age 1.0 by
Packsaddle Schist	pCps	Precambrian	schist				
Valley Spring Gneiss	pCvs	Precambrian	gneiss				

Site C: Texas 71 between reference markers 528 and 542, Burnet County, Llano geologic atlas (Barnes, 1981).

Geologic unit	Symbol	Age	Major lithology	Minor lithology	Constituents	Thickness (ft)	Notes
Alluvium	Qal	Quaternary	unconsolidated		sd, st, cl, gr	<35	
Glen Rose Limestone (upper)	Kgru	Cretaceous	limestone	dolomite, marl		220	
Glen Rose Limestone (lower)	Kgrl	Cretaceous	limestone	dolomite, marl		160	
Hensell Sand	Kh	Cretaceous	unconsolidated	conglomerate	sd, st, cl, gr	<220	
Sycamore Sand	Ksy	Cretaceous	unconsolidated	conglomerate	sd, st, cl, gr		
Marble Falls Limestone	IPmf	Pennsylvanian–Permian	limestone			385	
Honeycut Formation	Oh	Ordovician	limestone	dolomite		680	part of Ellenburger Group
Gorman Formation	Og	Ordovician	limestone	dolomite		425 to 490	

Site D: U.S. 290 between reference markers 536 and 563, Blanco and Hays Counties, Llano (Barnes, 1981) and Austin (Proctor and others, 1974) geologic atlases.

Geologic unit	Symbol	Age	Major lithology	Minor lithology	Constituents	Thickness (ft)	Notes
Alluvium	Qal	Quaternary	unconsolidated		sd, st, cl, gr	<30	
Fort Terrett Member	Kft	Cretaceous	limestone	dolomite		150 to 230	member of Ked

Geologic unit	Symbol	Age	Major lithology	Minor lithology	Constituents	Thickness (ft)	Notes
Glen Rose Limestone (upper)	Kgru	Cretaceous	limestone	dolomite, marl		220	
Glen Rose Limestone (lower)	Kgrl	Cretaceous	limestone	dolomite, marl		160	

Site E: Texas 71 between reference markers 590 and 598, Bastrop County, Austin geologic atlas (Proctor and others, 1974).

Geologic unit	Symbol	Age	Major lithology	Minor lithology	Constituents	Thickness (ft)	Notes
Fluviatile terrace	Qt	Quaternary	unconsolidated		gr, sd, st, cl		terraces along streams
High gravels	Qhg	Quaternary	unconsolidated		gr		
Calvert Bluff Formation	Ecb	Eocene	mudstone	sandstone, lignite	st, cl, sd	<1000	part of Wilcox Group
Simsboro Formation	Esb	Eocene	unconsolidated	mudstone	sd, cl, gr	<300	part of Wilcox Group
Hooper Formation	Eh	Eocene	mudstone	sandstone	st, cl, sd	<500	part of Wilcox Group
Midway Group	Emi	Eocene	unconsolidated		cl, st, sd		
Kemp, Corsicana, Marlbrook	Kknm	Cretaceous	unconsolidated		cl, st	600	Kemp Clay, Corsicana Marl, Marlbrook Marl

90

Site F: Texas 16 between reference markers 758 and 804, Jim Hogg and Zapata Counties, Laredo (Brewton and others, 1976a) and McAllen–Brownsville geologic atlases (Brewton and others, 1976b).

Geologic unit	Symbol	Age	Major lithology	Minor lithology	Constituents	Thickness (ft)	Notes
Alluvium	Qal	Quaternary	unconsolidated		cl, st, sd, gr		floodplain deposits
Sand sheet	Qs	Quaternary	unconsolidated		sd		eolian deposits
Goliad Formation	Pg	Pliocene	clay	sandstone, marl, caliche, limestone, conglomerate	cl, sd, gr	<600	
Catahoula and Frio Formations	MOcf	Miocene–Oligocene	mudstone	claystone, sandstone, tuff, clay	cl, st, sd		
Jackson Group	Ej	Eocene	sandstone	clay	sd, cl	360	
Yegua Formation	Ey	Eocene	clay	sandstone	cl, sd	400	
Laredo Formation	El	Eocene	sandstone	clay	sd, cl	620	

91

APPENDIX C: FWD DATA FOR STUDY SITES

Site A: Texas 16 between reference markers 220 and 264, Archer and Young Counties, Wichita Falls District.

County	Geologic[1] atlas sheet	Geologic unit	Elevation (ft)	Reference marker	Normalized FWD deflection (mils)						
					W1	W2	W3	W4	W5	W6	W7
Archer	WF-L	IPPm-SS14	1105	220.0	25.33	18.34	10.43	5.66	3.36	2.27	1.68
Archer	WF-L	IPPm-SS14	1055	220.5	8.17	5.88	3.17	1.62	0.95	0.63	0.53
Archer	WF-L	IPPm-SS14	1090	221.0	9.35	6.27	3.33	1.74	1.00	0.69	0.51
Archer	WF-L	IPPm-SS14	1060	221.5	14.08	10.52	6.96	4.33	2.68	1.78	1.41
Archer	WF-L	IPPm	1020	222.0	11.46	9.58	6.54	4.42	3.15	2.25	1.52
Archer	WF-L	Qal	1005	222.5	26.68	17.60	9.00	3.87	1.98	1.34	1.06
Archer	WF-L	IPPm-SS12	1045	223.0	16.42	11.70	6.52	3.59	2.10	1.29	0.90
Archer	WF-L		1040	223.5	14.74	10.20	5.49	2.62	1.34	0.87	0.61
Archer	WF-L	IPPm-SS12	1065	224.0	11.50	8.05	4.57	2.32	1.29	0.82	0.62
Archer	WF-L	IPPm-SS12	1095	224.5	12.15	7.71	4.05	2.22	1.44	1.05	0.74
Archer	WF-L	IPPm-SS12	1060	225.0	19.51	14.23	8.68	4.63	2.54	1.54	1.12
Archer	WF-L	IPPm-SS11	1020	225.5	13.37	9.01	5.16	3.01	1.92	1.43	1.21
Archer	WF-L	Qal	1015	226.0	12.49	7.17	3.32	1.89	1.29	1.04	0.89
Young	WF-L	IPPm	1018	228.0	19.59	7.75	2.18	0.82	0.59	0.50	0.38
Young	WF-L	IPPm	1035	228.5	37.66	22.18	11.43	6.57	4.45	3.29	2.56
Young	WF-L	IPPm	1065	229.0	24.92	11.67	4.78	2.47	1.73	1.37	1.00
Young	WF-L	IPPm	1065	229.5	17.95	9.17	4.54	2.56	1.67	1.18	0.90
Young	WF-L	IPPm-SS11	1100	230.0	40.52	22.96	9.86	4.45	2.46	1.67	1.20
Young	WF-L	IPPm-SS11	1115	230.5	29.34	16.72	8.31	4.68	3.09	2.23	1.66
Young	WF-L	IPPm-SS11	1100	231.0	15.33	8.94	4.26	2.11	1.24	0.86	0.64
Young	WF-L	IPPm	1100	231.5	32.55	16.92	7.93	4.13	2.68	1.92	1.47
Young	WF-L	IPPm-SS10	1105	232.0	30.63	20.12	10.95	5.92	3.55	2.48	1.94
Young	WF-L	IPPm-SS10	1110	232.5	46.12	22.57	9.47	4.38	2.51	1.77	1.24
Young	WF-L	IPPm-SS10	1115	233.0	27.62	13.45	5.46	2.91	2.05	1.61	1.33
Young	WF-L	IPPm-SS10	1150	233.5	24.42	11.05	4.19	2.10	1.40	1.05	0.75
Young	WF-L	IPPm-SS10	1125	234.0	22.33	13.32	6.99	3.73	2.46	1.83	1.45
Young	WF-L	IPPm-SS10	1150	234.5	19.24	9.08	3.36	1.49	1.03	0.81	0.63
Young	WF-L	IPPm	1160	235.0	28.35	12.76	4.15	2.00	1.33	1.01	0.80
Young	WF-L	IPPm-SS11	1205	235.5	28.43	18.28	8.29	3.06	1.95	1.50	1.16
Young	WF-L	IPPm-SS11	1265	236.0	20.45	10.23	3.67	1.50	0.94	0.73	0.60
Young	WF-L	IPPm-SS11	1290	236.5	34.79	16.22	6.24	2.99	1.80	1.22	0.88
Young	WF-L	IPPm-SS11	1290	237.0	24.69	14.30	6.51	2.75	1.39	0.83	0.61
Young	WF-L	IPPm-SS11	1290	237.5	20.89	14.05	8.08	4.59	2.93	2.02	1.54
Young	WF-L	IPPm	1290	238.0	11.67	8.23	5.26	3.44	2.53	1.93	1.51
Young	WF-L	IPPm	1295	238.5	17.25	11.27	6.00	3.43	2.32	1.72	1.23
Young	WF-L	IPPm	1295	239.0	15.59	11.30	7.25	4.58	3.09	2.21	1.70
Young	WF-L	IPPm	1275	239.5	8.83	6.04	3.66	2.28	1.54	1.10	0.81
Young	WF-L	IPPm-SS10	1275	240.0	15.31	10.23	5.42	2.54	1.28	0.84	0.57
Young	WF-L	IPPm-SS10	1290	240.5	12.54	8.90	5.57	3.38	2.17	1.49	1.09
Young	WF-L	IPPm	1260	241.0	18.66	12.29	6.59	3.65	2.26	1.57	1.20
Young	WF-L	IPtg	1255	241.5	15.12	10.99	6.99	4.50	3.02	2.16	1.58
Young	WF-L	IPtg	1230	242.0	19.23	13.67	8.22	4.75	2.89	1.95	1.42
Young	WF-L	IPtg	1210	242.5	21.75	14.50	7.75	3.83	2.33	1.57	1.25
Young	WF-L	IPtg	1215	243.0	15.89	12.25	8.11	5.09	3.24	2.09	1.45
Young	WF-L	IPtg	1200	243.5	15.93	10.25	5.68	3.12	1.99	1.40	1.02
Young	WF-L	IPtg	1200	244.0	20.79	11.47	5.95	3.46	2.32	1.64	1.29
Young	WF-L	IPtg	1165	244.5	12.62	6.77	3.46	2.02	1.36	1.04	0.78
Young	WF-L	IPtg	1175	245.0	9.33	5.54	3.35	2.19	1.61	1.17	0.86

[1] WF-L=Wichita Falls–Lawton; ABL=Abilene

County	WF-L sheet	Geologic unit	Elevation (ft)	Reference marker	W1	W2	W3	W4	W5	W6	W7
Young	WF-L	IPtg	1190	245.5	17.12	9.83	5.23	3.11	2.09	1.48	1.10
Young	WF-L	IPi	1175	246.0	22.37	12.93	6.79	3.86	2.50	1.72	1.24
Young	WF-L	IPtg	1190	246.5	19.38	10.00	4.70	2.62	1.90	1.50	1.23
Young	WF-L	IPtg	1220	247.0	13.65	5.94	2.82	1.56	1.03	0.69	0.48
Young	WF-L	IPtg	1190	247.5	12.48	6.94	3.57	2.00	1.31	0.99	0.81
Young	WF-L	IPtg	1130	248.0	31.28	15.19	6.53	3.73	2.64	1.94	1.55
Young	WF-L	IPtg	1090	248.5	17.33	9.23	4.39	2.63	1.89	1.47	1.14
Young	WF-L	IPtg	1075	249.0	9.35	5.59	3.65	2.62	1.98	1.52	1.14
Young	WF-L	IPtg	1060	249.5	21.87	13.05	6.84	3.84	2.60	1.93	1.49
Young	WF-L	IPtg	1060	250.0	13.67	6.50	3.85	2.87	2.15	1.65	1.25
Young	WF-L	IPtg	1030	250.6	6.87	5.20	3.58	2.38	1.68	1.22	0.94
Young	WF-L	IPtg		251.0	7.55	6.39	5.12	3.87	2.85	1.99	1.28
Young	WF-L	IPtg		251.5	16.63	9.10	3.96	2.00	1.24	0.77	0.43
Young	WF-L	IPtg-SS2		252.0	20.18	9.07	4.57	2.59	1.54	0.95	0.59
Young	WF-L	IPtg-SS2		252.5	9.48	3.22	1.23	0.59	0.39	0.26	0.21
Young	WF-L	IPtg-SS2	1040	253.0	8.72	3.34	1.40	0.89	0.60	0.41	0.28
Young	WF-L	IPtg-SS2	1065	253.5	13.65	6.36	2.92	1.57	0.88	0.57	0.33
Young	WF-L	IPtg	1030	254.0	19.75	11.53	5.70	3.02	1.81	1.08	0.70
Young	WF-L	IPtg	1030	254.5	21.62	9.62	2.57	0.97	0.74	0.59	0.46
Young	WF-L	IPtg	1080	255.0	13.48	5.02	1.65	0.96	0.71	0.57	0.42
Young	WF-L	IPtg-SS2	1130	255.5	14.00	7.12	3.51	2.30	1.74	1.21	0.91
Young	WF-L	IPbu	1150	256.0	38.96	20.79	8.88	5.15	3.49	2.61	1.84
Young	WF-L	IPgc	1120	256.5	26.58	13.76	5.68	3.65	2.79	2.17	1.69
Young	WF-L	IPgc	1140	257.0	14.38	4.96	1.65	0.93	0.56	0.42	0.38
Young	WF-L	IPgc	1170	257.5	20.77	10.53	4.18	2.20	1.40	1.08	0.76
Young	WF-L	IPtg	1090	258.0	25.90	12.87	6.14	3.40	2.36	1.67	1.22
Young	WF-L	IPtg	1170	258.5	9.68	4.69	2.51	1.64	1.18	0.91	0.65
Young	WF-L	IPhc	1050	259.0	11.33	6.32	3.00	1.94	1.46	1.16	0.95
Young	WF-L	IPhc	1040	259.5	12.72	4.74	2.24	1.36	0.96	0.71	0.51
Young	WF-L	IPhc	1050	260.0	20.68	9.65	5.13	3.33	2.25	1.48	0.99
Young	WF-L	IPk	1050	260.5	16.75	5.89	2.31	1.49	1.09	0.81	0.62
Young	WF-L	IPk	1060	261.0	7.21	2.86	1.36	0.96	0.72	0.53	0.36
Young	WF-L	IPhc	1055	261.5	8.33	3.76	2.11	1.32	1.01	0.78	0.62
Young	ABL	IPcc	1045	262.0	15.67	6.98	2.87	1.61	1.19	0.92	0.69
Young	ABL	IPcc	1075	262.5	18.04	8.04	2.71	1.13	0.73	0.54	0.36
Young	ABL	IPcc	1075	263.0	11.95	7.60	4.64	2.96	2.03	1.39	0.96
Young	ABL	IPcc	1095	263.5	18.83	9.69	4.02	1.75	0.91	0.54	0.34
Young	WF-L	IPr	1085	264.0	21.60	8.91	3.74	2.16	1.43	0.96	0.64

Site B: Texas 16 between reference markers 450 and 488, Llano and Gillespie Counties, Austin District.

County	Geologic[2] atlas sheet	Geologic unit	Elevation (ft)	Reference marker	——— Normalized FWD deflection (mils) ———						
					W1	W2	W3	W4	W5	W6	W7
Llano	LLN	pCps	1065	450.0	12.46	8.53	5.12	3.10	1.96	1.28	0.87
Llano	LLN	pCps	1065	450.5	31.43	18.04	7.40	3.35	1.73	1.17	0.87
Llano	LLN	pCps	1070	451.0	31.74	14.01	4.38	2.21	1.49	1.09	0.87
Llano	LLN	pCps	1080	451.5	39.21	16.94	4.41	1.45	0.71	0.59	0.40
Llano	LLN	pCy	1090	452.0	38.15	13.81	2.14	0.77	0.48	0.32	0.23
Llano	LLN	pCps	1090	452.5	43.35	21.48	7.07	3.38	2.05	1.38	1.18
Llano	LLN	pCy	1130	453.0	36.55	15.32	4.43	2.10	1.39	1.07	0.83
Llano	LLN	pCps	1150	453.5	45.29	19.12	6.14	3.00	1.66	1.00	0.68
Llano	LLN	pCps	1270	456.0	58.23	30.11	12.00	6.05	3.55	2.28	1.52
Llano	LLN	pCps	1310	456.5	56.29	24.43	7.57	3.87	2.24	1.53	1.12
Llano	LLN	pCps	1320	457.0	33.66	15.25	4.90	2.21	1.26	0.84	0.63

[2] LLN=Llano

93

Llano	LLN	pCps	1350	457.5	49.51	21.92	7.18	3.19	1.88	1.32	0.93
Llano	LLN	pCps	1390	458.0	37.32	17.49	5.60	2.87	1.78	1.24	0.91
Llano	LLN	pCvs	1390	458.5	46.97	23.85	8.79	4.22	2.44	1.64	1.25
Llano	LLN	pCvs	1360	459.0	40.06	17.10	5.29	1.99	0.91	0.58	0.39
Llano	LLN	pCvs	1310	459.5	10.83	3.63	1.46	0.91	0.57	0.41	0.28
Llano	LLN	pCvs	1270	460.0	40.86	18.53	5.81	3.16	2.08	1.49	1.12
Llano	LLN	pCvs	1270	460.5	18.28	7.57	2.99	1.62	1.01	0.77	0.55
Llano	LLN	pCvs	1230	461.0	19.85	8.65	2.98	1.71	1.19	0.94	0.71
Llano	LLN	pCvs	1200	461.5	36.86	15.26	4.42	2.11	1.33	0.96	0.65
Llano	LLN	pCvs	1210	462.0	34.72	14.37	5.01	2.37	1.33	0.80	0.60
Llano	LLN	pCvs	1160	462.5	46.25	22.70	7.47	2.74	1.27	0.76	0.65
Llano	LLN	pCtm	1150	463.0	46.98	18.82	5.37	2.20	1.26	0.99	0.85
Llano	LLN	pCtm	1190	463.5	39.09	15.35	4.67	2.67	1.88	1.42	1.16
Llano	LLN	pCtm	1220	464.0	42.91	20.81	7.61	3.82	2.28	1.55	1.14
Llano	LLN	pCtm	1180	464.5	32.69	12.36	4.17	2.51	1.72	1.36	1.03
Llano	LLN	pCtm	1240	465.0	34.01	14.28	4.92	2.61	1.56	1.01	0.78
Llano	LLN	pCtm	1270	465.5	41.81	16.03	4.88	2.76	1.72	1.26	0.93
Llano	LLN	pCtm	1280	466.0	21.45	7.42	2.36	1.18	0.73	0.47	0.34
Gillespie	LLN	pCtm	1340	468.0	39.17	16.64	5.42	2.44	1.51	0.94	0.67
Gillespie	LLN	pCtm	1290	468.5	31.36	13.92	4.45	1.80	1.12	0.85	0.71
Gillespie	LLN	pCtm	1290	469.0	26.50	10.37	3.57	1.72	1.10	0.84	0.68
Gillespie	LLN	pCps	1300	469.5	19.26	6.53	2.24	1.53	1.08	0.72	0.45
Gillespie	LLN	pCtm	1330	470.0	16.39	5.49	0.85	0.80	0.70	0.47	0.35
Gillespie	LLN	pCtm	1380	470.5	44.85	16.51	5.12	2.93	1.85	1.32	0.90
Gillespie	LLN	pCtm	1460	471.0	23.89	9.74	3.10	1.71	1.10	0.92	0.69
Gillespie	LLN	pCtm	1580	471.5	23.51	7.78	2.32	1.38	0.93	0.63	0.46
Gillespie	LLN	pCvs	1690	472.0	36.28	18.64	6.92	3.34	2.15	1.63	1.29
Gillespie	LLN	pCvs	1800	472.5	61.17	28.29	8.58	3.95	2.74	2.24	1.80
Gillespie	LLN	pCtm	1770	473.0	27.74	11.29	4.15	1.98	1.23	0.93	0.73
Gillespie	LLN	Kh	1820	473.5	47.20	21.55	10.07	5.92	3.80	2.65	1.86
Gillespie	LLN	Kh	1760	474.0	36.24	16.40	7.54	4.17	2.40	1.40	0.89
Gillespie	LLN	Crh	1745	474.5	33.14	12.79	4.04	2.31	1.49	1.16	0.91
Gillespie	LLN	Crh	1730	475.0	39.57	16.30	5.90	3.11	2.03	1.49	1.21
Gillespie	LLN	Crh	1730	475.5	21.58	10.67	4.36	2.57	1.87	1.47	1.12
Gillespie	LLN	Crh	1760	476.0	26.84	10.50	4.25	2.50	1.65	1.24	0.96
Gillespie	LLN	Crh	1750	476.5	35.63	13.85	4.38	2.15	1.38	0.96	0.73
Gillespie	LLN	Kh	1800	477.0	27.70	12.07	4.16	1.90	1.18	0.80	0.63
Gillespie	LLN	Kh	1840	477.5	22.95	9.56	3.95	2.29	1.52	1.12	0.86
Gillespie	LLN	Kh	1850	478.0	28.62	14.55	5.75	2.94	1.91	1.49	1.16
Gillespie	LLN	Kft	1880	478.5	27.32	15.08	8.06	4.84	3.08	2.09	1.53
Gillespie	LLN	Kft	1920	479.0	29.93	16.09	6.39	3.00	1.48	0.80	0.51
Gillespie	LLN	Kft	1930	479.5	36.32	17.93	7.75	4.81	2.89	2.29	1.67
Gillespie	LLN	Kh	1840	480.0	29.34	10.74	3.69	2.39	1.96	1.61	1.22
Gillespie	LLN	Kh	1780	480.5	13.87	4.71	2.46	1.72	1.32	1.14	0.94
Gillespie	LLN	Kh	1780	481.0	29.94	12.65	5.53	3.10	1.98	1.43	1.03
Gillespie	LLN	Kh	1720	481.5	22.77	7.80	2.34	1.21	0.67	0.48	0.39
Gillespie	LLN	Kh	1710	482.0	79.12	30.76	9.31	5.08	3.09	2.25	1.75
Gillespie	LLN	Qal	1660	482.5	28.21	12.73	5.24	2.80	1.91	1.46	1.18
Gillespie	LLN	Kh	1660	483.0	34.69	17.41	6.17	3.10	2.06	1.64	1.36
Gillespie	LLN	Kh	1640	483.5	44.70	19.70	6.83	3.58	2.23	1.54	1.13
Gillespie	LLN	Kh	1650	484.0	48.20	22.38	9.02	4.92	3.00	2.08	1.73
Gillespie	LLN	Kh	1690	484.5	64.28	30.17	9.12	4.59	3.11	2.52	1.96
Gillespie	LLN	Kh	1770	485.0	64.20	30.43	10.53	4.84	2.80	1.93	1.38
Gillespie	LLN	Kh	1780	485.5	39.42	14.31	4.55	2.66	1.78	1.37	1.07
Gillespie	LLN	Kh	1720	486.0	4.67	2.11	1.30	0.90	0.72	0.59	0.45
Gillespie	LLN	Kh	1710	486.5	30.38	9.87	4.08	2.73	2.04	1.60	1.33
Gillespie	LLN	Kh	1710	487.0	24.12	12.16	4.09	1.76	1.12	0.87	0.69
Gillespie	LLN	Kh	1690	487.5	7.49	4.23	1.92	1.14	0.77	0.55	0.42

Site C: Texas 71 between reference markers 528 and 542, Burnet County, Austin District.

County	Geologic[3] atlas sheet	Geologic unit	Elevation (ft)	Reference marker	Normalized FWD deflection (mils)						
					W1	W2	W3	W4	W5	W6	W7
Burnet	LLN	Oh	1120	528.0	15.79	8.66	3.68	1.86	1.15	0.81	0.56
Burnet	LLN	Oh	1135	528.5	18.14	10.57	4.77	2.40	1.31	0.82	0.51
Burnet	LLN	Oh	1110	529.0	13.63	6.05	1.98	0.57	0.44	0.33	0.15
Burnet	LLN	Og	1100	529.5	16.36	9.31	3.83	1.77	0.98	0.68	0.53
Burnet	LLN	Og	1085	530.0	13.48	6.68	2.43	1.17	0.75	0.61	0.45
Burnet	LLN	Oh	1080	530.5	14.59	7.52	2.62	0.83	0.34	0.21	0.18
Burnet	LLN	Og	1110	531.0	11.98	4.70	1.72	1.11	0.90	0.78	0.68
Burnet	LLN	Oh	1050	531.5	13.80	4.67	1.67	0.90	0.56	0.36	0.26
Burnet	LLN	Oh	1035	532.0	18.22	7.42	2.84	1.63	1.05	0.73	0.48
Burnet	LLN	Oh	1070	532.5	15.18	5.82	1.90	0.88	0.40	0.18	0.09
Burnet	LLN	Kh	1030	533.0	20.43	10.22	4.13	2.34	1.56	1.22	0.97
Burnet	LLN	Oh	970	533.5	20.48	9.06	3.22	1.47	0.69	0.42	0.29
Burnet	LLN	Oh	950	534.0	19.20	6.88	2.22	0.88	0.50	0.30	0.15
Burnet	LLN	IPmf	920	534.5	20.75	10.52	5.25	3.24	2.20	1.58	1.12
Burnet	LLN	Oh	960	535.0	14.35	4.24	1.69	1.23	0.99	0.83	0.70
Burnet	LLN	Oh	950	535.5	14.64	5.94	2.45	1.59	1.20	0.97	0.76
Burnet	LLN	Oh	1000	536.0	15.08	3.93	1.47	0.90	0.53	0.33	0.18
Burnet	LLN	Oh	970	536.5	10.17	2.55	1.06	0.67	0.46	0.33	0.22
Burnet	LLN	Oh	915	537.0	16.02	8.40	3.19	1.16	0.47	0.30	0.25
Burnet	LLN	Qal	880	537.5	11.43	4.75	2.25	1.33	0.80	0.49	0.30
Burnet	LLN	Ksy	870	538.0	27.09	13.61	6.02	3.47	1.87	1.77	1.42
Burnet	LLN	Ksy	850	538.5	27.40	14.29	7.00	4.21	2.94	2.06	1.59
Burnet	LLN	Ksy	820	539.0	35.96	16.85	7.51	4.34	2.83	1.93	1.50
Burnet	LLN	Qal	800	539.5	8.77	3.74	2.25	1.70	1.36	1.15	0.92
Burnet	LLN	Kh	840	540.0	11.02	3.69	1.53	0.91	0.60	0.43	0.31
Burnet	LLN	Kh	870	540.5	13.97	5.78	2.81	1.72	1.14	0.81	0.58
Burnet	LLN	Kh	900	541.0	8.76	4.15	2.33	1.54	1.09	0.80	0.62
Burnet	LLN	Kgrl	930	541.5	7.56	2.95	1.79	1.29	0.95	0.78	0.61
Burnet	LLN	Kgru	1060	542.0	20.25	6.90	1.48	0.48	0.30	0.29	0.28
Burnet	LLN	Kgru	1010	542.0	8.07	2.47	1.03	0.63	0.48	0.40	0.33

Site D: U.S. 290 between reference markers 536 and 563, Blanco and Hays Counties, Austin District.

County	Geologic[4] atlas sheet	Geologic unit	Elevation (ft)	Reference marker	Normalized FWD deflection (mils)						
					W1	W2	W3	W4	W5	W6	W7
Blanco	LLN	Kgrl	1260	536.0	9.26	3.56	1.21	0.74	0.52	0.40	0.34
Blanco	LLN	Kgrl	1250	536.5	13.05	5.73	2.78	2.12	1.43	0.89	0.72
Blanco	LLN	Kgrl	1220	537.0	9.21	3.26	1.14	0.60	0.40	0.31	0.23
Blanco	LLN	Qal	1180	537.5	10.42	4.62	2.22	1.25	0.86	0.64	0.52
Blanco	LLN	Kgrl	1180	538.0	11.78	4.63	1.73	1.04	0.78	0.58	0.45
Blanco	LLN	Kgru	1210	538.5	6.05	3.47	2.22	1.50	1.03	0.78	0.59
Blanco	LLN	Kgru	1230	539.0	11.27	5.67	2.52	1.38	0.87	0.65	0.46
Blanco	LLN	Qal	1120	539.5	15.85	7.56	3.45	1.94	1.25	0.90	0.68
Blanco	LLN	Kgru	1260	540.0	12.32	4.95	1.95	1.16	0.78	0.57	0.44
Blanco	LLN	Kgrl	1170	540.5	14.81	7.41	2.78	1.25	0.65	0.46	0.40
Blanco	LLN	Kgrl	1160	541.0	9.66	4.09	1.31	0.41	0.13	0.06	0.05
Blanco	LLN	Kgru	1220	541.5	14.78	4.86	1.60	0.94	0.71	0.56	0.49

[3] LLN=Llano; AUS=Austin
[4] LLN=Llano; AUS=Austin

County	Geologic atlas sheet	Geologic unit	Elevation (ft)	Reference marker	W1	W2	W3	W4	W5	W6	W7
Blanco	LLN	Kgru	1325	542.5	14.18	7.05	3.33	1.83	1.14	0.78	0.57
Blanco	LLN	Kgru	1330	543.0	14.27	8.08	4.27	2.55	1.67	1.20	0.84
Blanco	LLN	Kgru	1330	543.5	10.80	5.45	2.27	1.11	0.63	0.39	0.25
Blanco	LLN	Kgru	1360	544.0	11.26	5.10	2.14	1.20	0.81	0.65	0.48
Hays	LLN	Kgru	1360	546.0	9.25	4.60	1.65	0.75	0.54	0.43	0.33
Hays	LLN	Kgru	1380	546.5	8.67	4.53	2.23	1.45	1.09	0.86	0.67
Hays	LLN	Kgru	1340	547.0	7.09	2.69	0.70	0.34	0.26	0.21	0.18
Hays	LLN	Kgru	1320	547.5	9.42	4.30	1.45	0.44	0.15	0.09	0.07
Hays	LLN	Kgru	1360	548.0	12.58	5.97	2.27	1.14	0.77	0.55	0.43
Hays	LLN	Kgru	1300	548.5	8.74	3.91	1.28	0.60	0.43	0.34	0.30
Hays	LLN	Kgru	1320	549.0	9.97	5.19	2.58	1.66	1.28	1.05	0.87
Hays	LLN	Kgru	1330	549.5	13.26	6.56	2.52	1.25	0.73	0.48	0.29
Hays	LLN	Kgru	1300	550.0	9.04	3.39	1.22	0.63	0.47	0.29	0.22
Hays	LLN	Kgru	1290	550.5	12.90	7.05	2.82	1.31	0.78	0.59	0.50
Hays	LLN	Kgru	1300	551.0	12.10	5.66	2.04	0.79	0.34	0.18	0.11
Hays	LLN	Kgru	1280	551.5	7.44	3.29	1.28	0.76	0.54	0.43	0.36
Hays	LLN	Kgru	1290	552.0	15.00	7.87	3.15	1.37	0.73	0.53	0.41
Hays	LLN	Kgru	1245	552.5	10.91	4.87	1.84	1.08	0.74	0.53	0.40
Hays	LLN	Kgru	1210	553.0	11.21	6.83	3.88	2.42	1.61	1.11	0.80
Hays	LLN	Kgru	1190	553.5	17.08	8.01	2.83	1.15	0.62	0.40	0.29
Hays	LLN	Kgru	1200	554.0	6.76	3.25	1.31	0.58	0.30	0.18	0.14
Hays	LLN	Kgru	1200	554.5	4.45	2.30	1.04	0.61	0.45	0.34	0.29
Hays	LLN	Kgru	1165	555.0	11.45	6.06	2.53	1.31	0.78	0.50	0.32
Hays	LLN	Kgru	1155	555.5	10.88	6.81	3.48	1.84	1.15	0.78	0.55
Hays	LLN	Kgru	1190	556.0	10.60	5.97	2.37	0.86	0.30	0.13	0.07
Hays	LLN	Kgru	1260	556.5	7.39	4.57	2.28	1.04	0.42	0.17	0.05
Hays	LLN	Kgru	1240	557.0	11.08	6.77	3.21	1.60	0.91	0.73	0.59
Hays	LLN	Kgru	1210	557.5	9.08	4.89	1.93	0.98	0.70	0.62	0.52
Hays	LLN	Kgru	1249	558.0	5.65	3.21	1.48	0.69	0.35	0.23	0.16
Hays	LLN	Kgru	1245	558.5	10.94	3.95	1.55	0.85	0.49	0.33	0.25
Hays	LLN	Kgru	1240	559.0	18.29	9.47	3.23	1.01	0.33	0.21	0.14
Hays	LLN	Kgru	1250	559.5	11.44	5.79	2.41	1.25	0.82	0.60	0.47
Hays	LLN	Kgru	1240	560.0	8.42	4.53	2.01	1.06	0.68	0.51	0.40
Hays	LLN	Kft	1244	560.5	7.84	4.69	2.14	1.02	0.54	0.35	0.25
Hays	AUS	Kgru	1195	561.0	7.86	4.17	1.57	0.78	0.56	0.46	0.42
Hays	AUS	Kgru	1205	561.5	5.45	3.05	1.21	0.59	0.37	0.26	0.21
Hays	AUS	Kgru	1173	562.0	18.62	6.32	1.88	1.10	0.71	0.47	0.37
Hays	AUS	Kgru	1180	562.5	11.59	5.44	1.81	0.98	0.71	0.56	0.45

Site E: Texas 71 between reference markers 590 and 598, Bastrop County, Austin District.

County	Geologic[5] atlas sheet	Geologic unit	Elevation (ft)	Reference marker	Normalized FWD deflection (mils)						
					W1	W2	W3	W4	W5	W6	W7
Bastrop	AUS	Qt	415	590.0	28.96	14.45	6.49	3.37	2.21	1.76	1.50
Bastrop	AUS	Qt	415	590.0	13.53	9.59	6.15	4.14	2.94	2.23	1.80
Bastrop	AUS	Kknm	460	590.5	22.80	14.02	8.10	5.21	3.81	3.05	2.52
Bastrop	AUS	Kknm	460	590.5	22.14	15.12	9.35	5.88	3.86	2.79	2.17
Bastrop	AUS	Qt	420	591.0	24.85	15.16	8.37	5.18	3.79	3.08	2.53
Bastrop	AUS	Qt	420	591.0	20.77	15.41	10.14	6.80	4.62	3.36	2.63
Bastrop	AUS	Emi	425	591.5	13.49	8.61	5.29	3.43	2.44	1.91	1.50
Bastrop	AUS	Emi	425	591.5	27.92	18.93	11.12	6.60	4.16	3.01	2.35
Bastrop	AUS	Emi	460	592.0	17.07	8.89	4.48	2.84	1.99	1.57	1.27
Bastrop	AUS	Emi	460	592.0	18.57	13.17	8.50	5.53	3.65	2.57	1.89
Bastrop	AUS	Emi	450	592.5	38.57	23.67	10.95	5.29	3.13	2.42	1.99

[5] AUS=Austin

County	Geologic atlas sheet[6]	Geologic unit	Elevation (ft)	Reference marker	W1	W2	W3	W4	W5	W6	W7
Bastrop	AUS	Emi	592.5	450	32.51	20.93	12.19	7.33	4.57	3.03	2.24
Bastrop	AUS	Eh	593.0	541	20.99	9.68	4.42	2.69	2.01	1.53	1.35
Bastrop	AUS	Eh	593.0	541	34.65	23.83	14.35	9.07	6.04	4.52	3.49
Bastrop	AUS	Qhg	593.5	568	17.01	8.06	4.08	2.65	1.95	1.57	1.28
Bastrop	AUS	Qhg	593.5	568	26.98	17.51	9.69	5.43	3.39	2.47	1.97
Bastrop	AUS	Eh	594.0	520	18.60	8.63	3.91	2.28	1.60	1.28	1.07
Bastrop	AUS	Eh	594.0	520	35.57	22.93	12.87	7.03	4.02	2.69	2.07
Bastrop	AUS	Eh	594.5	530	18.18	7.24	2.72	1.48	0.96	0.68	0.51
Bastrop	AUS	Eh	594.5	530	21.29	14.27	8.59	5.28	3.50	2.56	2.04
Bastrop	AUS	Qhg	595.0	560	23.25	8.24	2.98	1.57	1.14	1.01	0.88
Bastrop	AUS	Qhg	595.0	560	15.93	9.33	4.58	2.41	1.31	0.85	0.63
Bastrop	AUS	Esb	595.5	525	17.78	5.65	2.38	1.66	1.31	1.06	0.87
Bastrop	AUS	Esb	595.5	525	14.86	9.28	5.15	3.01	1.88	1.35	1.03
Bastrop	AUS	Esb	596.0	510	13.91	5.70	3.12	2.17	1.71	1.40	1.18
Bastrop	AUS	Esb	596.0	510	22.18	11.24	4.45	2.39	1.70	1.39	1.19
Bastrop	AUS	Esb	596.5	510	20.73	11.03	5.16	2.66	1.58	1.18	0.95
Bastrop	AUS	Esb	596.5	510	14.05	6.67	2.80	1.69	1.33	1.15	0.94
Bastrop	AUS	Esb	597.0	475	23.91	13.69	7.15	4.11	2.74	2.01	1.53
Bastrop	AUS	Esb	597.0	475	18.56	9.54	3.97	2.20	1.59	1.27	1.00
Bastrop	AUS	Ecb	597.5	430	14.57	8.22	3.76	1.79	0.95	0.61	0.47
Bastrop	AUS	Ecb	597.5	430	16.65	7.08	2.20	0.78	0.46	0.40	0.32
Bastrop	AUS	Ecb	598.0	430	13.50	5.11	3.11	2.13	1.53	1.15	0.90
Bastrop	AUS	Ecb	598.0	430	18.05	9.53	4.16	2.13	1.30	0.93	0.72

Site F: Texas 16 between reference markers 758 and 804, Jim Hogg and Zapata Counties, Pharr District.

County	Geologic atlas sheet[6]	Geologic unit	Elevation (ft)	Reference marker	W1	W2	W3	W4	W5	W6	W7
Jim Hogg	LAR	Pg	593	758.0	37.85	14.47	5.15	2.57	1.59	1.05	0.78
Jim Hogg	LAR	Pg	592	758.5	24.45	11.79	5.81	3.32	2.15	1.48	1.11
Jim Hogg	LAR	Qs	608	759.0	38.91	14.74	4.64	2.24	1.64	1.33	1.09
Jim Hogg	LAR	Pg	636	759.5	51.71	19.96	6.92	3.26	1.86	1.26	0.96
Jim Hogg	LAR	Pg	625	760.0	39.73	15.63	4.82	2.22	1.62	1.33	1.18
Jim Hogg	LAR	Pg	637	760.5	37.81	14.09	4.05	2.12	1.48	1.22	0.97
Jim Hogg	LAR	Pg	650	761.0	31.37	13.54	4.92	2.31	1.45	1.30	1.09
Jim Hogg	LAR	Pg	645	761.5	36.29	12.99	3.43	1.49	1.15	0.93	0.84
Jim Hogg	LAR	Qs	635	762.0	19.07	9.90	4.55	2.46	1.63	1.17	0.91
Jim Hogg	LAR	Qs	642	762.5	24.18	7.68	2.27	1.38	1.03	0.80	0.67
Jim Hogg	LAR	Pg	655	763.0	35.43	13.87	5.57	3.15	2.10	1.61	1.19
Jim Hogg	LAR	Pg	650	763.5	23.62	6.90	1.58	1.00	0.79	0.61	0.46
Jim Hogg	LAR	Qs	660	764.0	19.36	8.80	3.45	1.67	1.04	0.81	0.66
Jim Hogg	LAR	Qs	658	764.5	39.10	15.82	5.38	2.45	1.59	1.20	0.94
Jim Hogg	LAR	Pg	660	765.0	29.49	11.74	4.31	2.41	1.70	1.17	0.88
Jim Hogg	LAR	Pg	665	765.5	31.38	13.88	4.52	2.45	1.70	1.24	0.86
Jim Hogg	LAR	Pg	665	766.0	21.16	6.08	2.56	2.12	1.81	1.59	1.33
Jim Hogg	LAR	Qs	670	766.5	38.57	19.34	8.20	4.47	2.77	1.92	1.51
Jim Hogg	LAR	Qs	690	767.0	31.61	12.30	5.50	2.50	1.16	0.93	0.83
Jim Hogg	LAR	Pg	695	767.5	25.50	10.83	3.60	1.93	1.38	1.21	0.95
Jim Hogg	LAR	Pg	712	768.0	23.23	11.74	5.09	2.55	1.68	1.29	1.10
Jim Hogg	LAR	Pg	710	768.5	32.57	13.57	3.73	1.80	1.27	0.94	0.75
Jim Hogg	LAR	Pg	720	769.0	37.11	13.49	4.82	2.61	1.68	1.47	1.11
Jim Hogg	LAR	Pg	720	769.5	26.14	9.57	2.92	1.59	1.20	0.91	0.82
Jim Hogg	LAR	Pg	725	770.0	33.35	14.45	4.74	2.44	1.66	1.34	1.11
Jim Hogg	LAR	Pg	710	770.5	41.36	15.86	5.58	3.26	2.35	1.85	1.38

[6] LAR=Laredo; MC-B=McAllen–Brownsville

Jim Hogg	LAR	Pg	732	771.0	22.65	8.66	3.11	1.30	0.87	0.71	0.62
Jim Hogg	LAR	Pg	730	771.5	24.15	8.81	2.49	1.33	0.96	0.83	0.69
Jim Hogg	LAR	Pg	730	772.0	35.89	14.72	6.60	4.25	3.20	2.57	2.08
Jim Hogg	LAR	Pg	750	772.5	34.49	10.92	2.44	1.28	1.01	0.77	0.66
Jim Hogg	LAR	Pg	750	773.0	31.19	15.46	6.31	3.22	2.50	1.95	1.72
Jim Hogg	LAR	MOcf	710	773.5	50.12	22.56	5.80	2.42	1.47	1.24	0.85
Jim Hogg	LAR	MOcf	690	774.0	41.04	16.33	5.31	2.97	2.09	1.57	1.32
Jim Hogg	LAR	MOcf	680	774.5	36.20	12.46	4.09	2.38	1.83	1.51	1.28
Jim Hogg	LAR	MOcf	673	775.0	38.67	16.60	6.77	4.25	3.25	2.56	2.05
Jim Hogg	LAR	MOcf	660	775.5	39.51	14.45	4.83	3.18	2.47	1.97	1.64
Jim Hogg	LAR	MOcf	630	776.0	50.34	23.38	10.57	6.47	4.60	3.49	2.61
Jim Hogg	LAR	MOcf	625	776.5	33.67	13.31	5.57	3.46	2.51	2.05	1.69
Jim Hogg	LAR	MOcf	615	777.0	48.38	20.65	7.48	4.42	3.19	2.45	2.01
Jim Hogg	LAR	MOcf	605	778.0	43.69	17.36	6.38	4.05	3.03	2.16	1.89
Jim Hogg	LAR	MOcf	590	778.5	33.57	10.41	3.06	1.97	1.60	1.25	1.09
Zapata	LAR	MOcf	580	780.0	53.23	23.18	7.54	3.91	2.76	2.00	1.74
Zapata	LAR	MOcf	550	780.5	32.88	14.92	5.58	3.41	2.50	2.04	1.79
Zapata	LAR	Ej	540	781.0	42.57	18.45	6.54	4.81	3.67	2.76	1.91
Zapata	LAR	Ej	525	781.5	77.57	30.89	8.40	4.16	2.97	2.08	1.55
Zapata	LAR	Ej	510	782.0	70.54	29.08	10.78	5.77	4.03	3.23	2.38
Zapata	LAR	Ej	495	782.5	47.39	16.21	5.24	3.06	2.19	1.62	1.43
Zapata	LAR	Ej	490	783.0	81.08	26.87	7.44	4.75	3.48	2.80	2.29
Zapata	LAR	Ej	480	783.5	68.91	29.00	10.06	5.55	3.85	3.01	2.31
Zapata	LAR	Ej	495	784.0	84.44	36.97	13.51	6.92	4.80	3.53	2.59
Zapata	LAR	Ej	530	784.5	46.79	18.27	6.75	4.15	2.88	2.09	1.69
Zapata	LAR	Ej	505	785.0	32.03	11.43	3.89	2.07	1.58	1.23	1.04
Zapata	LAR	Ej	505	785.5	45.01	17.81	5.75	3.62	2.69	2.08	1.72
Zapata	LAR	Ej	490	786.0	66.59	33.35	12.03	6.26	4.38	3.09	2.57
Zapata	LAR	Ej	500	786.5	49.23	15.99	5.73	3.80	2.49	2.24	1.78
Zapata	LAR	Ej	505	787.0	78.71	35.22	11.19	5.85	4.01	3.14	2.41
Zapata	LAR	Ej	503	787.5	28.59	13.50	5.41	3.02	2.77	1.89	1.62
Zapata	LAR	Ej	495	788.0	52.83	28.17	11.11	6.42	4.06	3.17	2.69
Zapata	LAR	Ej	485	788.5	25.85	13.09	3.68	3.08	2.59	2.46	1.55
Zapata	LAR	Ej	465	789.0	46.81	19.35	6.97	3.54	2.36	1.84	1.52
Zapata	LAR	Ej	475	789.5	54.11	24.58	7.49	3.49	2.55	1.65	1.42
Zapata	LAR	Ej	490	790.0	27.40	16.09	7.66	4.01	2.68	2.01	1.52
Zapata	LAR	Ej	475	790.5	21.71	13.43	6.70	3.84	2.63	1.92	1.58
Zapata	LAR	Ej	465	791.0	22.71	13.64	6.63	3.67	2.48	1.83	1.45
Zapata	LAR	Ej	455	791.5	20.10	14.18	8.23	4.90	3.10	2.17	1.72
Zapata	LAR	Ej	450	792.0	41.24	21.83	10.30	5.39	3.48	2.51	1.72
Zapata	MC-B	Ej	450	792.5	22.81	14.24	6.61	3.59	2.45	1.88	1.49
Zapata	MC-B	Ej	420	793.0	15.03	9.83	5.76	3.30	1.99	1.35	1.07
Zapata	MC-B	Ej	420	793.5	14.21	8.23	4.06	2.56	1.89	1.48	1.05
Zapata	MC-B	Ej	400	794.0	21.40	12.58	5.53	3.21	2.40	1.94	1.58
Zapata	MC-B	Ej	380	794.5	12.71	7.17	2.96	1.57	1.13	0.95	0.81
Zapata	MC-B	Ej	365	795.0	23.47	13.56	6.84	4.30	3.39	2.70	1.82
Zapata	MC-B	Qal	335	795.5	17.41	11.65	6.69	4.07	2.71	1.95	1.55
Zapata	MC-B	Qal	340	796.0	29.66	17.75	8.60	4.93	3.39	2.51	2.01
Zapata	MC-B	Ej	365	796.5	25.95	15.55	8.60	5.44	3.86	2.91	2.37
Zapata	MC-B	Ej	380	797.0	25.58	16.25	7.79	4.23	2.86	2.07	1.69
Zapata	MC-B	Qs	390	797.5	27.27	18.08	9.81	5.29	3.33	2.55	2.08
Zapata	MC-B	Ey	380	798.0	28.26	17.52	8.40	4.54	2.90	2.08	1.65
Zapata	MC-B	Qs	350	798.5	7.83	4.30	2.42	1.70	1.30	1.04	0.89
Zapata	MC-B	Qs	340	799.0	12.83	8.76	4.99	3.05	2.28	1.68	1.24
Zapata	MC-B	Qs	335	799.5	13.96	9.51	5.74	3.20	2.00	1.41	1.04
Zapata	MC-B	Qs	335	800.0	22.40	15.69	8.51	4.85	3.21	2.38	1.87
Zapata	MC-B	Qs	360	800.5	10.09	5.70	2.75	1.78	1.27	0.95	0.75
Zapata	MC-B	Qs	410	801.0	6.66	4.00	2.41	1.68	1.27	0.93	0.72

Zapata	MC-B	Ey	390	801.5	9.53	5.60	3.25	2.19	1.66	1.33	1.10
Zapata	MC-B	El	385	802.0	11.47	7.06	3.64	2.08	1.39	1.02	0.85
Zapata	MC-B	El	390	802.5	11.97	7.84	4.30	2.65	1.89	1.52	1.23
Zapata	MC-B	El	380	803.0	21.66	15.13	8.17	4.29	2.38	1.41	1.06
Zapata	MC-B	El	370	803.5	40.87	26.44	13.63	7.83	5.14	3.83	3.00